Design and analysis of Chaos-Based communication systems

by

Mohamed DAWA

MANUSCRIPT-BASED THESIS PRESENTED TO ÉCOLE DE TECHNOLOGIE SUPÉRIEURE IN PARTIAL FULFILLMENT FOR THE DEGREE OF DOCTOR OF PHILOSOPHY
Ph.D.

MONTREAL, "20 DECEMBER 2022"

ÉCOLE DE TECHNOLOGIE SUPÉRIEURE
UNIVERSITÉ DU QUÉBEC

BOARD OF EXAMINERS

THIS THESIS HAS BEEN EVALUATED

BY THE FOLLOWING BOARD OF EXAMINERS

Prof. Georges Kaddoum, Thesis supervisor
Department of Electrical Engineering, École de technologie supérieure

Prof. James Lapalme, Chair, Board of Examiners
Department of Industrial Engineering, École de technologie supérieure

Prof. Naïm Batani, Member of the Jury
Department of Electrical Engineering, École de technologie supérieure

M. Pascal Chargé, External Examiner
Departement of Electronics and Digital Technologies, Polytechnique University of Nantes

THIS THESIS WAS PRESENTED AND DEFENDED

IN THE PRESENCE OF A BOARD OF EXAMINERS AND THE PUBLIC

ON "13 DECEMBER 2022"

AT ÉCOLE DE TECHNOLOGIE SUPÉRIEURE

ACKNOWLEDGEMENTS

Firstly, I would like to thank my supervisor Professor Georges Kaddoum for the continuous guidance and support throughout this PhD. The expertise of Professor Georges Kaddoum in the field of study, his encouragement and advice have made this journey possible, with much more clarity.

Many thanks to the great people I met during this journey: lab mates, friends, coworkers outside of academia, that helped make this come to realization. Special thanks to my friend Dr. Zeeshan Sattar in whom I found a companion through the PhD journey and a true support in the most needed times. Many thanks to my friends Saber, Hamza, Oussama, and Bilal for their friendship and support. I will always cherish the moments that I shared with my lab mates Dr. Victor Evangelista, Dr. Vu, Dr. Long, Jung, Ibrahim, and Ali. Also, special thanks to my coworkers who grew to be my close friends during this PhD, including Yahia and Taina.

At last, the dearest of all, my family, who supported and encouraged me unconditionally, I extend my deepest gratitude. Words are not enough to express how much I'm in debt to my parents, my brother, my sister and her little Roukaya. Their love and warmth truly helped me going through this adventure.

Conception et analyse de systèmes de communication basés sur le chaos.

Mohamed DAWA

RÉSUMÉ

L'introduction du paradigme IoT pour façonner le futur réseau 5G, dans la mesure où des milliards de nouveaux dispositifs seront déployés avec des besoins différents en termes d'accès sans fil, est l'une des pierres angulaires de l'établissement de la norme 5G. Une grande partie du réseau IoT est constituée de dispositifs WSN et LOWPAN, connus comme des dispositifs aux ressources limitées en termes de calcul et d'autonomie. La nouvelle norme pour les appareils IoT, à savoir la norme 802.15.4aa, spécifie plusieurs méthodes d'accès à la couche physique pour les réseaux sans fil à faible débit utilisant des modulations telles que DSSS, FSK, MPSK et UWB. La plus grande partie déploie encore la modulation DSSS pour les WSNs étant donné ses excellentes performances en termes de sécurité et sa mise en œuvre simple.

Les modulations basées sur le chaos offrent de meilleures performances que la DSSS et ont été prises en compte dans la littérature en raison des excellentes propriétés statistiques des signaux chaotiques. Elles ont donc été considérées comme une alternative, notamment pour les dispositifs à faible capacité, comme c'est le cas dans les WSN et les LOWPAN. Le schéma non cohérent basé sur le chaos offre une excellente solution grâce à sa méthode de détection simple qui permet une transmission réussie même à travers des canaux très bruyants et des évanouissements par trajets multiples.

Dans la littérature, les performances TEB des schémas basés sur le chaos non-cohérent ne font pas l'objet d'une approche universelle, étant donné que chaque schéma est étudié séparément et que ses performances BER sont calculées à l'aide de simulations de Monte-Carlo ou de la fonction d'erreur pour chaque modèle. De plus, la limitation inhérente des systèmes non cohérents basés sur le chaos en termes de débit de données et d'efficacité spectrale a été abordée par l'introduction d'innombrables schémas de modulation. Cependant, la plupart des schémas proposés dans la littérature nécessitent des blocs de traitement du signal avancés pour la mise en œuvre de ces conceptions.

Dans ce contexte, la question du calcul du TEB est abordée dans le deuxième chapitre de cette thèse où les expressions du TEB de plusieurs schémas non cohérents basés sur le chaos sur le canal à évanouissement de Rayleigh à trajets multiples sont étudiées et une nouvelle métrique sous la forme d'une limite inférieure est introduite. Dans ce but, une transformation est appliquée à l'expression du TEB des schémas non cohérents basés sur le chaos pour remplacer la fonction d'erreur par une limite inférieure équivalente à la fonction exponentielle multipliée par le PDF du canal d'évanouissement, puis une anti-dérivée est calculée. On obtient ainsi une véritable expression théorique qui peut être utilisée pour calculer avec précision les valeurs du TEB sur la voie d'évanouissement Rayleigh à trajets multiples pour différents systèmes basés sur le chaos.

Dans la foulée, le troisième chapitre étend le travail effectué au chapitre deux à un modèle de canal plus généralisé, à savoir le canal à évanouissement de Nakagami-m à trajets multiples. La même méthodologie est appliquée aux modèles non cohérents basés sur le chaos afin de dériver une solution à forme fermée de l'expression du TEB. La nouvelle limite inférieure du TEB est ensuite calculée et comparée aux résultats de la simulation, et il est prouvé qu'elle offre une correspondance étroite avec de minuscules écarts de performance.

Le quatrième chapitre de la thèse est consacré à l'amélioration de l'efficacité spectrale de la conception DCSK de base. Puisque le schéma DCSK souffre de la transmission d'un signal de référence qui occupe la moitié du temps de transmission, nous optons pour une solution qui peut raccourcir ce temps. Nous combinons la conception DCSK avec le filtrage FTN pour réduire l'espacement entre les symboles transmis et, par conséquent, obtenir une meilleure utilisation du spectre. Les performances de la nouvelle conception introduite sont évaluées pour différents modèles de canaux et paramètres de système. En outre, les performances du système sont comparées aux conceptions de pointe en termes de BER et d'efficacité spectrale.

Mots-clés: 5G, Internet des Objets, DCSK, TEB, FTN

Design and analysis of Chaos-Based communication systems

Mohamed DAWA

ABSTRACT

The introduction of the IoT paradigm for shaping the future 5G network, as billions of new devices would be deployed with different needs in terms of wireless access, is one of the cornerstones in establishing the 5G standard. A large chunk of the IoT network consists of the WSN and LOWPAN devices, known as devices with limited computation and battery life resources. The new standard for IoT devices, i.e., 802.15.4aa specifies several physical layer methods of access for the Low-Rate Wireless Networks using modulations like DSSS, FSK, MPSK, and UWB. The more significant proportion still deploys the DSSS modulation for WSNs, given its excellent performance in terms of security and its simple implementation.

The chaos-based modulations offer better performances in comparison with the DSSS and were considered in the literature, given the excellent statistical properties of the chaotic signals. Hence, they were considered an alternative, especially for devices with low capabilities widely seen in WSNs and LOWPANs. The non-coherent chaos-based scheme specifically offers an excellent solution with its simple detection method that enables successful transmission even through very noisy channels and multipath fading.

In the literature, the BER performance of non-coherent chaos-based schemes lacks a universal approach in its establishment, given that every scheme is studied apart and its BER performance is computed using Monte Carlo simulations or through the error function for each model. Moreover, the inherent limitation of non-coherent chaos-based systems in terms of data rate and spectral efficiency has been tackled by introducing countless modulation schemes. However, most of the schemes proposed in the literature require advanced signal processing blocks to implement such designs.

In light of this, the issue of BER computation is tackled in the second chapter of this thesis, where the BER expressions of several non-coherent chaos-based schemes over the multipath Rayleigh fading channel are studied, and a new metric in the form of a lower bound is introduced. For this purpose, a transformation is applied to the BER expression of non-coherent chaos-based schemes to replace the error function with an equivalent lower bound to the exponential function multiplied by the PDF of the fading channel, and then an anti-derivative is calculated. This yields a true theoretical expression that can be used to accurately compute the BER values over multipath Rayleigh fading channels for different chaos-based systems.

As a follow-up, the third chapter extends the work done in chapter 2 to a more generalized channel model, namely the multipath Nakagami-m fading channel. The same methodology is applied to the non-coherent chaos-based models in order to derive a closed-form solution of the BER expression. The newly established lower bound to the BER is then computed and compared to the simulation results and proven to deliver a close match with tiny performance gaps.

The fourth chapter of the thesis is dedicated to the improvement of the spectral efficiency of the basic DCSK design. Since the DCSK scheme suffers from the transmission of a reference signal that actively occupies half of the transmission time, we opt for a solution that can shorten such time. We combine the DCSK design with the FTN filtering to reduce the spacing between the transmitted symbols and as a result obtain a gain in terms of spectrum usage. The performances of the newly introduced design are evaluated for different channel models and system settings. In addition, the system performances are compared to state-of-the-art designs in terms of BER and spectral efficiency.

Keywords: 5G, IoT, DCSK, BER, FTN

TABLE OF CONTENTS

Page

LIST OF TABLES

Page

LIST OF FIGURES

LIST OF ABBREVIATIONS

3GPP	3rd Generation Partnership Project
5G	Fifth Generation
AWGN	Additive White Gaussian Noise
BCJR	Bahl-Cocke-Jelinek-Raviv (BCJR) algorithm
BER	Bit Error Rate
BLE	Bluetooth Low Energy
BPSK	Binary phase-shift keying
CFO	carrier frequency offset
CI	Carrier Interferometry
COOK	Chaos on-off keying
CSK	Chaos Shift Keying
DCSK	Differential Chaos Shift Keying
DSSS	Direct-Sequence Spread Spectrum
ESD	Energy Spectral Density
FH-TDD-TDMA	Frequency Hop Time Division Duplex Time Division Multiple Access
FM-DCSK	Frequency-modulated Differential Chaos Shift Keying
FTN	Faster Than Nyquist
GFSK	Gaussian frequency-shift keying ,
IoT	Internet Of Things

IM	Index modulation
ISI	inter-symbol interference
LOS	Line-of-sight
LOWPAN	Low-Power Wireless Personal Area Networks
LTE	Long-Term Evolution
MIMO	Multiple-input multiple-output
WSN	Wireless sensor network
M2M	Machine to machine
MC-DCSK	Multi-Carrier Differential Chaos Shift Keying
NFC	Near Field Communication
OFDM	Orthogonal Frequency Division Multiplexing
PDF	Probability Density Function
PMA-DCSK	Permutation-Based Multiple Access Differential Chaos Shift Keying
PN-CG	Pseudo-Noise Code Generators
QCSK	Quadrature Chaos Shift Keying
RFID	Radio Frequency Identification
SNR	Signal-to-Noise Ratio

LIST OF SYMBOLS AND UNITS OF MEASUREMENTS

${}_2F_1(.)$	Gaussian hypergeometric function
Erfc	Complementary error function
Exp$(\cdot)$	Exponential function
$\Gamma(\cdot)$	Gamma function
$\mathbf{x}$	Vector
$\dot{\mathbf{x}}$	Vector first derivative
M^T	The transpose of matrix M
$\mathbb{R}$	Set of real numbers
$\mathbf{J_n}$	The Jacobian transform
ln$(\cdot)$	Natural logarithm
E$(\cdot)$	Expectation operator
Var$(\cdot)$	Variance operator
Q$(\cdot)$	Q-function
arctan$(\cdot)$	arctangent function

INTRODUCTION

The ever-expanding coverage offered by the successive generations of wireless communication is increasingly challenged by the ever-growing number of devices that need to join these networks to satisfy the different modern services offered to consumers. With the already limited resources in the spectrum, the obvious solution was to use spectral resources that were previously thought to be unusable such as the millimeter waves. The solution focused on using the spectrum around the higher frequencies offered more access flexibility while introducing new technological challenges related to the design and implementation of access methods. The traditional solution involves the optimization of the way the devices access the network in a manner to share the available resources. In this vein, several multiple access technologies have been introduced throughout the different generations of wireless access (i.e., 2G, 3G, 4G, and 5G) for optimal spectrum utilization. Several other approaches have been pursued in order to maximize the network's capacity in enabling vast numbers of devices to access the radio resources, namely multi-user technologies, multi-antenna transmissions, and higher cell density.

In this context, the 5G network enables a sub-network of interconnected devices labeled IoT from various aspects of life. The IoT network is a voluminous set of devices with different communication protocols coming together to offer new ways of exploiting data collection and enabling novel services. However, guaranteeing such access seriously constraints the new 5G network since the necessary resources for coverage in terms of spectrum and power are extremely high. In addition, the vast majority of the devices belonging to the IoT network (sensors and LOW-PAN) are often constrained by various restrictions such as battery capacity, hardware complexity, and the available spectrum.

The communication protocol plays a crucial role in optimizing the usage of the available resources for these devices (Otayf & Abbas, 2022). For this purpose, numerous proposals have been introduced over the decade to offer a unified approach to the communication of IoT

devices. From a physical layer perspective, the methods of access offered to IoT devices are diverse and dependent on the hardware limitations of each family of devices. However, the communication methods originate from the older generation of wireless access, suffering from the same limitations. The existing IoT communication protocols include Bluetooth Low Energy (BLE), EPCglobal, LTE-A, Z-Wave, 6LowPAN, NFC, and mainly IEEE 802.15.4 and IEEE 802.15.6 (Al-Fuqaha, Guizani, Mohammadi, Aledhari & Ayyash, 2015) were introduced to cover a variety of applications. Each one of these protocols deploys a different architecture for its physical layer communications depending on the limitations of the devices under consideration, the application's requirements, and the network restrictions.

For instance, the IEEE 802.15.4, widely used for WSN and M2M, uses the Direct-Sequence Spread Spectrum (DSSS) technique to enable access to the radio channel. In contrast, the BLE uses the Frequency Hop Time Division Duplex Time Division Multiple Access (FH-TDD-TDMA), and the orthogonal frequency division multiple access (OFDMA) is used for the LTE-A. The DSSS method, the primary enabler of physical layer communications in the 5G IoT standard IEEE 802.15.4, is based on encoding the transmitted messages by masking codes generated from one of the well-known Pseudo-Noise Code Generators (PN-CG) such as Maximum, Walsh-Hadamard sequences, Gold, and Kasami generators. Although these codes perform well for standard AWGN channels, their performance degrades significantly in the presence of multipath fading, which impacts the system's BER performances (Litvinenko & Aboltins, 2016). In this vein, chaos-based codes were shown to represent a good alternative for such scenarios, given their excellent statistical properties and the ability to combat the effect of fading channels. With low cross-correlation, an unlimited set of generated states, and enhanced security, chaos-based codes were shown to serve as a good alternative in the design of DSSS systems (Kaddoum, 2016a).

The use of chaos in communications is divided into two major categories, namely coherent and non-coherent designs. The coherent design is a DSSS method since it requires encoding

the transmitted information by a chaos-based code and is dependent on a synchronization process. The synchronization is the hardest part of this concept since it requires at least a second-order chaotic process which means that the chaotic system should at least be described by a two equations mathematical representation (Pecora, Carroll, Johnson, Mar & Heagy, 1997). Although the synchronization process is straightforward, the system's noise sensitivity represents a significant communication obstacle. The second branch of chaos-based systems, the non-coherent chaos-based systems, were shown to constitute a better alternative for communications since synchronization is not required anymore in order to establish a successful transfer of data. The best-known design for this category is the Differential Chaos Shift Keying (DCSK) (Kolumbán *et al.*, 1996) which is based on transmitting a chaotic reference sequence followed by its product with the binary data bit. The design of this scheme is very simple and requires no synchronization with the receiver. The reception is achieved by delaying the incoming stream of data by the length of the reference sequence, multiplying the reference by its delayed version, and then applying an ML detection. However, the main drawback of this design is the loss of half the transmission duration to transmit the reference signal. Over the last two decades, many DCSK-based systems have been introduced to solve this issue and to improve the system's overall performance based on coupling it with other signal processing transforms. In addition, its performances were studied extensively, especially the derivation of its BER expression over the AWGN and fading channels.

0.1 Problem statement

The BER performance of the DCSK system is often derived in its basic form using the system expectation and variance. Over the AWGN channel, the final BER expression is obtained by applying the complementary error function (*erfc*) to the squared expectation divided by the

variance of the system as follows,

$$BER = \frac{1}{2} erfc(\frac{2V}{E^2}) \tag{1}$$

For the basic DCSK design, the expectation and variance expressions are exclusively related to the chaos energy, the noise power, and the multiplication and delay procedures. However, in DCSK-based advanced designs, other transformations are introduced, and hence many other factors play a role in the derivation of the variance and expectation of the system. The process of theoretical derivation is explained in detail in (Kaddoum, Chargé & Roviras, 2009) for the AWGN and fading channels, where the transition from one to another is carried out by the integration over all the possible values of the fading channel coefficient while multiplying the BER expression for the AWGN case with the channel distribution. The evaluation of such metric is usually accomplished using calculation software running on a high-computation machine for every design based on the DCSK scheme. Since dozens of systems similar in design to the DCSK have been proposed in the literature over the last two decades, dozens of BER expressions have been introduced for their performance measurements. In addition, numerical simulation is usually the way forward when studying these systems and their behaviors in the presence of fading channels. For IoT devices with low computation capacities, running such simulations is impractical, given the amount of energy and time required for such evaluations (Zhai *et al.*, 2022; Cai & Song, 2020).

Besides, the inherent limitation of the DCSK scheme, represented by the loss of half the transmission time sacrificed to achieve a successful detection, constitutes a major drawback. The problem was addressed in countless schemes that introduced complementary signal processing transforms in order to solve this issue. The main idea shared between these designs was to introduce a transformation that can compensate for the loss occurring because of the transmission of the reference signal (Miao, Wang & Chen, 2022; Munirathinam, Aboltins, Pikulins & Grizans,

2021; Cai, Xu, Hong & Wang, 2021b; Maali, Boukhelifa, Mesloub, Sadoudi & Benssalah, 2019). This approach often resulted in adding extra blocks to the basic design and, as a byproduct, a higher complexity. However, these approaches may not be fit for devices with several restrictions in terms of hardware complexity, energy resources, and computational capacity.

0.2 Research Objectives

To address the aforementioned issues about (i) performance analysis of non-coherent chaos-based schemes and (ii) their inherent limitation of data-rate reduction, this thesis focuses on these two axes of research on non-coherent chaos-based modulations. The performance analysis of non-coherent schemes is explored for the cases of AWGN and fading channels. The Rayleigh and Nakagami-m channel models are considered for the fading channels' distributions. They are integrated with the BER expression for the AWGN channel in order to establish the system's performance over fading channels. Given the expression in Equation (1), directly obtaining a simplified final expression for the BER performance over fading channels is non-achievable. As a solution, a simplification of the problem can be applied using a transform that results in an easily integrable form. Our methodology consists of applying a bound to the expression in Equation (1) that can lead to a closed-form expression for the integral, better known as anti-derivative or primitive. An anti-derivative can be obtained by using an exponential form of lower bound that closely matches the *erfc* function. Moreover, since Equation (1) is a general form of BER that can express the performances of many non-coherent chaos-based schemes with a change of parameters, the newly developed lower bound would successfully match the BER performances of the given systems with a simple change of parameters, which are constant terms in the expression of the final anti-derivative.

The second axis of focus in this thesis is the improvement of performances of non-coherent chaos-based schemes by proposing new modulation designs. In non-coherent communications, using a reference signal constitutes a considerable bandwidth and data rate loss. Hence, reducing

the reference size or eliminating its impact is the principal methodology for improving such modulations. Previous works focused on compensating for the use of the reference sequence by deploying multi-carrier, multi-index communications, which lessens the impact of the loss caused by the transmission of the reference signal. While succeeding in compensating for the reference signal, most works caused the designs to grow much more complex and impractical for applications and devices with limited hardware capabilities. Our approach consists of an elementary signal processing transform using the basic matched filters to gain in terms of spectral efficiency. We apply the concept of Faster Than Nyquist signaling consisting of reducing the spacing between the transmitted symbols, which results in an overall reduction of the reference size and data-bearing signals used in non-coherent chaos-based communications (Ishihara & Sugiura, 2018; Zavjalov, Prokhorov & Chudnov, 2022).

0.3 Contributions and Outline

The thesis is structured as follows.

Chapter 1 presents a general overview of 5G networks, IoT protocols, and communication systems, followed by a literature review on chaos theory, chaos-based communications using non-coherent schemes, and the FTN theory.

In Chapter 2, the generalized lower bound on the BER of the DCSK, QCSK, and MC-DCSK systems over the multipath Rayleigh fading channel is presented. The DCSK, QCSK, MC-DCSK, and several other chaos-based schemes all share an *erfc* form of BER expression mathematically identical for all cases with a slight change in the weights related to the SNR in these expressions. In this chapter, we use the generalized form as a base for the derivations where we apply an exponential approximation to the *erfc* followed by a lower bound to the exponential function. We then calculate the anti-derivative by multiplying the resultant lower bound by the channel's PDF and integrating all possible values of channel coefficients. Afterward, we conduct a comparative

analysis between the newly obtained lower bound, the theoretical expression of the BER, and the results of the different systems simulations for different configurations of the multipath Rayleigh fading channel. Having a close match between the lower bound and the actual BER of the systems, we conclude that the approach is successful. It needs to be extended to more complex channel models to add generality to the study of non-coherent chaos-based schemes performances.

In chapter 3, we replace the multipath Rayleigh fading channel model with the multipath Nakagami-m fading channel to broaden the scope of analysis presented in chapter 2. Since the methodology presented in chapter 2 proved to be a success in establishing an integrable anti-derivative for the multipath Rayleigh fading channel case with an approximate match to the actual theoretical BER expression, we apply it to the multipath Nakagami-m fading channel as well. Here also, the different cases of system models DCSK, QCSK, and MC-DCSK are considered, where we use the generalized form of BER represented by the *erfc* with different SNR weights for each case. The remaining derivations are identical to the channel model in chapter 2, where we approximate the *erfc* by an exponential function, then apply a lower bound to it followed by a derivation of the closed-form anti-derivative. The chapter is then concluded by plotting the numerical results for the newly derived expression, which is also compared to the simulations of the different systems considered for this study. This chapter concludes with certainty the validity of the methodology used for deriving new easily computable closed-form lower bounds to BER of multiple non-coherent chaos-based systems that can further be used for implementation and optimization problems in future designs.

Chapter 4 tackles the issue of spectral efficiency related to non-coherent chaos-based schemes. In order to reduce the size of the reference used for these schemes, a new approach based on using the matched filters deployed in transmission below the limits set by Nyquist, namely FTN signaling (Lu, Li, Bai & Yuan, 2022), is applied. We apply the FTN concept to the

sinc filters, where we reduce the spacing between the transmitted chaotic symbols. The exact process is repeated for the receiver to enable a successful detection. Moreover, varying the FTN sampling parameter results in a new form of orthogonality that we use to introduce multi-user transmissions over the same radio channel. By considering various FTN sampling rates for different users, each user can transmit separately in an asynchronous mode over the same channel paths without using any extra resources or blocks for the design. Since the FTN signaling generally introduces new forms of inter-symbol-interferences, we derive the BER expression for the new proposed design. We also explore the variances of the interloping signals resulting from a multi-user FTN transmission. We then conduct a numerical analysis of the newly proposed design in terms of BER and spectral efficiency, and we explore its performances in the presence of different channel models and system configurations. A comparison with state-of-the-art non-coherent chaos-based schemes is also presented to highlight the gains obtained by the new design, especially regarding spectral efficiency and reduced complexity.

The thesis is finally concluded with a summary of the most important findings of this research work and an insight into possible future directions for research on non-coherent chaos-based schemes.

Author's Publications

The outcomes of the author's PhD research are the articles listed below published and submitted in IEEE journals.

M. Dawa, M.Herceg, and G. Kaddoum , Design and analysis of Multi-user Faster-Than-Nyquist-DCSK communication systems over Multipath fading channels, MDPI Sensors, Sept. 2022.

M. Dawa, G. Kaddoum and M.Herceg, A Framework for the Lower Bound on the BER of DCSK Systems over Multipath Nakagami-m Fading Channels, IEEE Transactions on Circuits and Systems II: Express Briefs, vol. 67, no. 10, pp. 1859 - 1863, Oct. 2020.

M. Dawa, G. Kaddoum and Z. Sattar, A Generalized Lower Bound on the Bit Error Rate of DCSK Systems Over Multipath Rayleigh Fading Channels, IEEE Transactions on Circuits and Systems II: Express Briefs, vol. 65, no. 3, pp. 321-325, March 2018.

CHAPTER 1

LITERATURE REVIEW

1.1 IoT in the context of 5G

The 5G mobile and wireless communication networks are intended to embody the vision of unlimited access to information through the connection of billions of IoT devices. As a result, it is established that the 5G technology will cope with many aspects of life like home, transportation, and work. The considerable amount of data collected by the different devices will result in a high traffic volume density, high connection density, and high mobility requirements (Ge, Cheng, Guizani & Han, 2014; Andrews *et al.*, 2014). Hence, the unlimited access is based on the network being scalable, energy smart, and very versatile to support the continuously growing number of connected devices. Therefore, the new standard should ensure ubiquitous connectivity for different devices in the network. Besides, wireless broadband connectivity and high throughput are highly needed to enable the new applications and use cases (ITU-R, 2015). Although 5G promises a better resolution of the inherent problems encountered by the previous generations of radio technology, the development of the new generation of mobile and wireless communication technologies addresses a good number of technological and common challenges (Hirzallah, Krunz, Kecicioglu & Hamzeh, 2021; 3GPP, 2017). The technological problems are related to cell sizes, access medium, and network traffic management. Moreover, more challenges in common with the previous standards, including the number of services offered to the heterogeneous networks, technologies, and devices operating systems, are also to be resolved. In addition, other issues can be listed, like the infrastructure, the services related to navigation and sensing, and the security and privacy issues related to the protection of personal data (Dutta & Hammad, 2020; Benchaabene, Boujnah & Zarai, 2017).

With currently over 21 billion connected IoT devices offering support to various sectors like consumer products (home utility devices, smartwatches, and many others), industrial machinery, infrastructure, fleet and logistics, and connected Markets, the number of IoT devices is expected to skyrocket to approximately 51 billion by 2025 which will create several challenges for the 5G network (Yinbiao *et al.*, 2014; Painuly, Sharma & Matta, 2021).

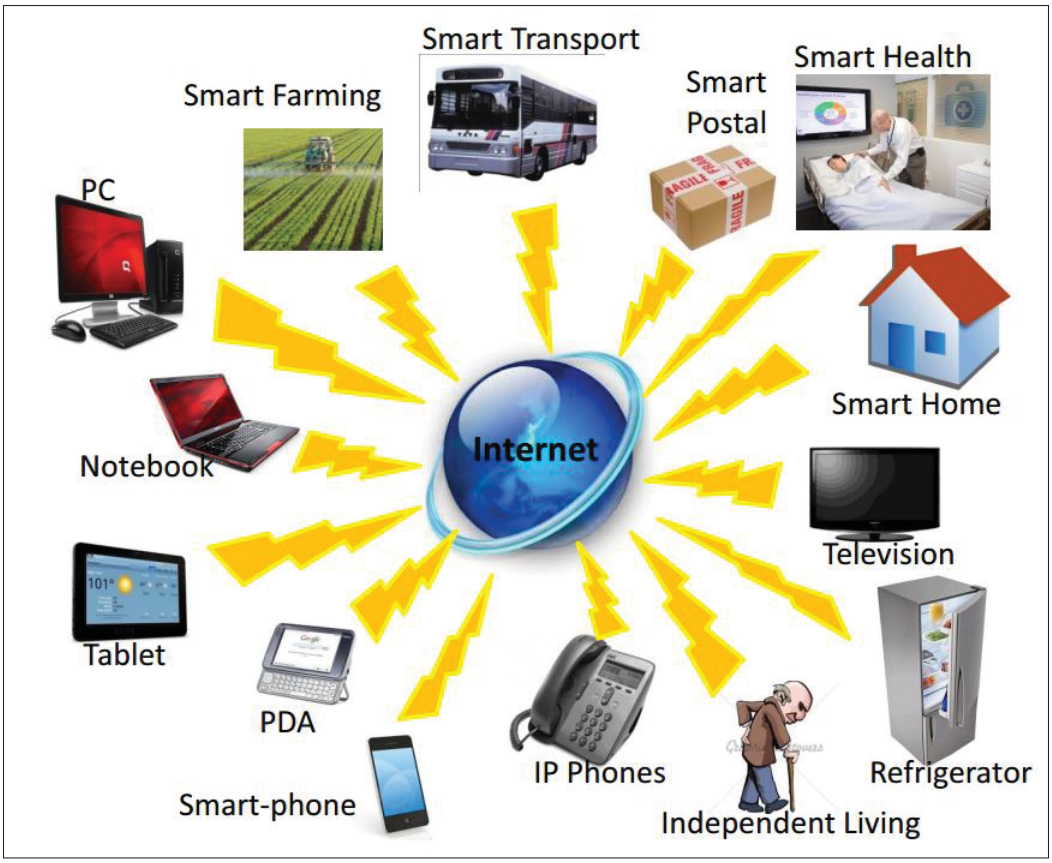

Figure 1.1 Overview of Environments Connected Through the 5G Network (Khan *et al.*, 2012)

Consequently, the interaction and cooperation between the different devices will create a huge volume of data that needs to be delivered with minimum delays. Therefore, the IoT network is viewed as the expansion of the internet through the interconnection of things (physical and virtual), as seen in Figure 1.1.

1.2 IoT communication protocols

Although many proposals exist about the architecture of IoT networks, most of them agree on a few basic sets that include the usual layers like physical, transport, and application layers. One generalized architecture can be considered and is composed of five layers of protocols, namely the perception layer, the network layer, the middleware layer, the application layer, and

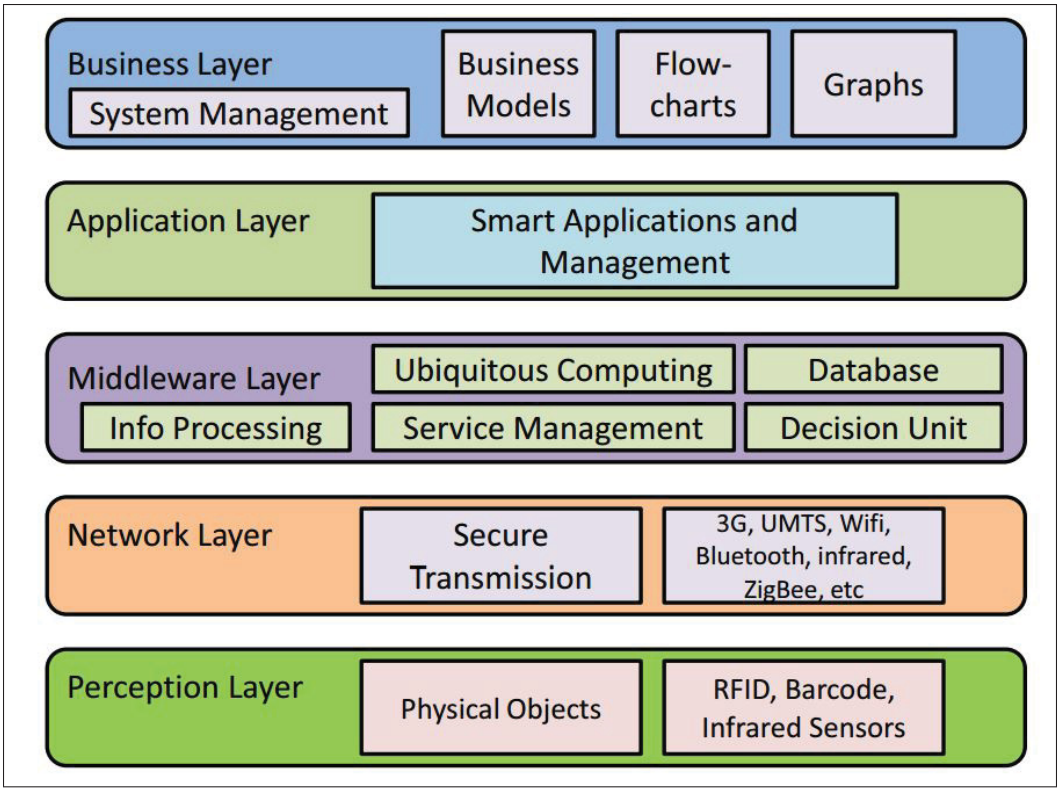

Figure 1.2 An Example of an IoT Stack Architecture (Khan *et al.*, 2012).

the business layer (Wu, Lu, Ling, Sun & Du, 2010; Khan *et al.*, 2012) as shown in Figure 1.2. The perception layer is also known as the device layer and is associated with the hardware devices. The devices include sensors, RFID tags, 2D barcodes, and embedded systems. The device layer is primarily responsible for collecting information from an environment or a system before passing it to the network layer.

The information retrieved by the perception layer is transmitted to the proper information processing system through a transmission medium. The transmission is carried out using wired or wireless technology, depending on the medium available in the device. The diagram in Figure 1.3 illustrates another representation of the IoT architecture from a design perspective.

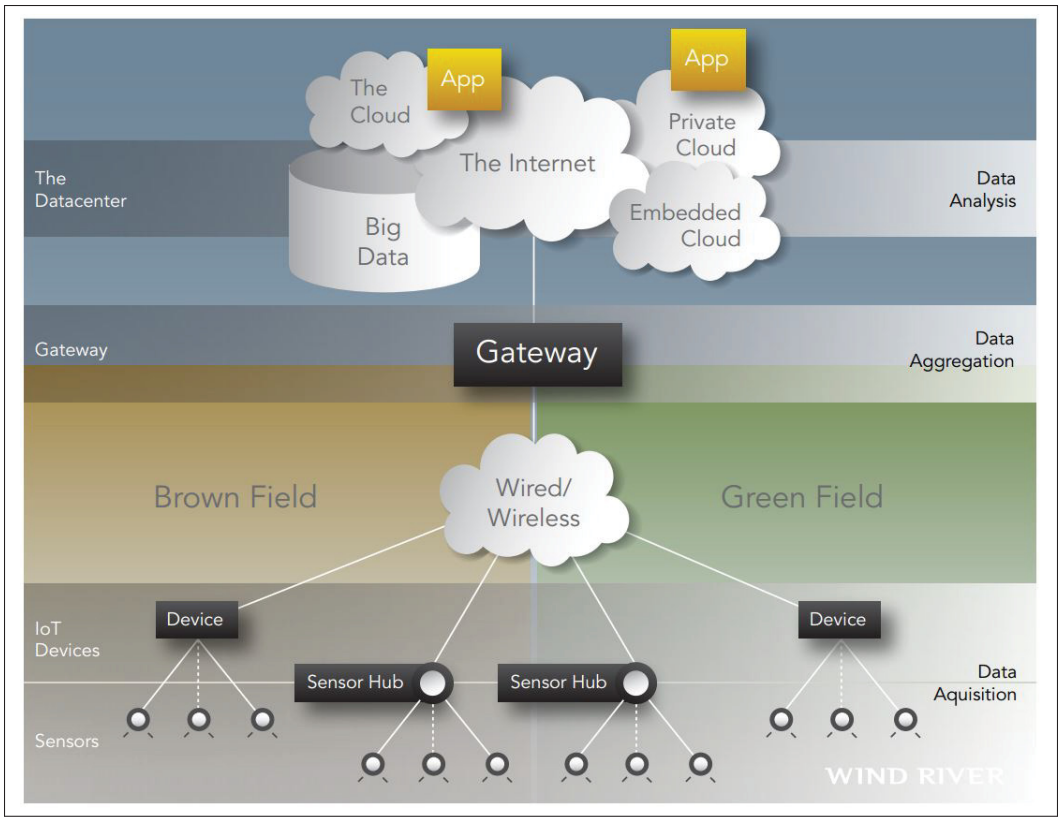

Figure 1.3 IOT Network (win, 2015).

1.3 Physical layer methodologies for IoT communications

The work on communication models for IoT devices has been one of the most intensive in the last decades. With a wide range of IoT devices covering several applications, the communication models have been diversified. The norm 802.15.4 specifies several physical layer access methods depending on the family of devices and the specific application being targeted. Moreover, few other communication protocols are used for particular types of transmissions. The 802.15.4 offers communication over three channel bands at 868 MHz, 915 MHz, and 2.4 GHz with a width of 20 kbps, 40 kbps, and 250 kbps consecutively (802.15.4-2015, 2016).

The 802.15.4 defines various physical layer schemes depending on the application under consideration. The DSSS is used the most often in combination with BPSK or O-QPSK. Moreover, FSK, OFDM, UWB, and Gaussian frequency-shift keying (GFSK) are also used. On the other hand, other IoT communication protocols use similar approaches for their physical

layer access. The BLE for instance uses the FHSS-GFSK as its access method while the Zigbee uses the same physical layer approaches as the 802.15.4. The LTE-A offers access to high-end devices with its sophisticated OFDM-based access that allows for higher data rates.

1.4 Overview of nonlinear dynamics and chaos theory

This section introduces the fundamentals of nonlinear systems conjointly to the relation between chaos theory and nonlinear dynamics.

1.4.1 Non-linearity: origins and characteristics

A nonlinear system is mathematically introduced through state equation representation, similar to the representation of any linear system. The only exception in the mathematical representation of a nonlinear system is introduced through a dynamic looping function instead of the constant matrix used for the linear case. Equation (1.1) defines the state equations for linear and nonlinear systems for continuous-time signals.

$$\text{Linear}\begin{cases} \dot{x}(t) &= Ax(t), \\ y(t) &= Cx(t). \end{cases} \qquad \text{nonlinear}\begin{cases} \dot{x}(t) &= f(x(t)), \\ y(t) &= h(x(t)). \end{cases} \tag{1.1}$$

A is the state matrix, C is the observation matrix, and $\mathbf{y}$ is the output vector. For the nonlinear system $f : R^n \rightarrow R^n$ and $h : R^n \rightarrow R^n$ are two non-linear functions. The system's evolution in nonlinear dynamics is introduced through the determination of the equilibrium points since the usual method valid for linear systems is very complex to compute. An equilibrium point for a given nonlinear system is obtained when the condition in Equation (1.2) is satisfied,

$$f(x^*) = 0. \tag{1.2}$$

A nonlinear system can have multiple equilibrium points; thus, their representation in the phase space allows the observation of the system evolution for all data entries. A limit cycle is

observed in the phase space representation of a nonlinear system for continuous-time data only and is independent of initial conditions. The limit cycle revolves around the equilibrium points in the phase space for all data entries.

Contrariwise, for a discrete nonlinear dynamical system the representation in the phase space results in a cycle of order K which is the generalization of the limit cycle representation and where all stable and unstable equilibrium points are included (Abraham-Frois, 1998). Figure 1.4 illustrates an example of a K=3 order cycle representation for a nonlinear system with three equilibrium points x^{*i}, i=1,..,3. Cycles of order K are specific descriptions of nonlinear periodic behaviors, unlike the non-periodic behavior, which is represented by an invariant closed curve. Another non-periodic behavior with very distinct aspects in nonlinear phase space representation is observed under some special conditions and referred to as chaos.

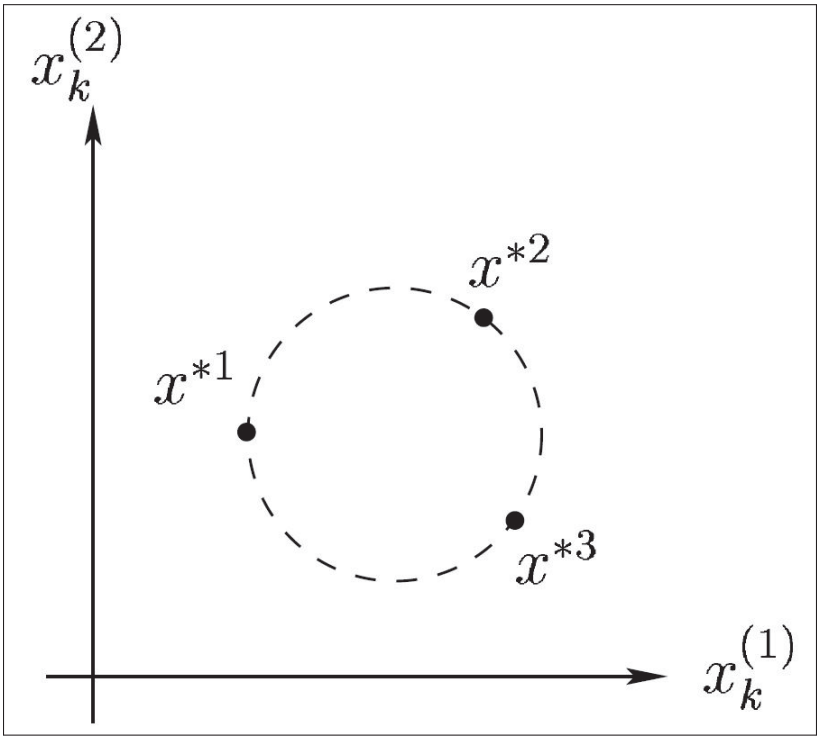

Figure 1.4 A Representation of K=3 Cycle.

1.4.2 Chaotic behaviors

The designation of chaos is related to a specific behavior observed in some nonlinear dynamical systems. In the literature, the chaotic behavior of a nonlinear system is a qualitative study of the unstable aperiodic comportment of the system. Although a very deterministic set of equations rules a nonlinear system, in aperiodic behaviors, the system never undergoes the same state and continues to manifest the effect of some perturbation. Therefore, the aperiodic behavior combined with an extreme sensibility to initial conditions is what is called chaos.

1.4.2.1 Definition of chaos

The term chaos is used in the literature to describe very complicated behaviors that seem random. In contrast, it is the direct opposite of what is believed since chaotic phenomenons are observed in nonlinear dynamics ruled by precise dynamic equations (Hilborn, Coppersmith, Mallinckrodt, McKay *et al.*, 1994). There is no specific definition for chaos in the literature studies, but all agree on some characteristics to define a chaotic system. The most notable trait is the sensibility to initial conditions. Here, we present two definitions of chaos which mathematically reveal the specific characteristics of the phenomena (Zhang, Shi & Chen, 2013), (Kirchgraber & Stoffer, 1989).

Definition 1. Let (χ, δ) be a metric space and $f : V \subset \chi \to V$ is a nonlinear function.

$$x_{k+1} = f(x_k). \tag{1.3}$$

The dynamical system given in Equation (1.3) is considered chaotic in the sense of Devaney (Devaney, Keen & Alligood, 1989) if the following conditions are satisfied:

1. f is topologically transitive in V
2. f is sensitive to initial conditions in V
3. The set of periodic points of f is dense in V

Definition 2. Let (χ, δ) be a compact metric space, $f : \chi \to \chi$ is a map and S is a subset of χ with two points at least.
S is called a scrambled subset of f if any couple of points a,b in S satisfies the condition in Equation (1.4).

$$\lim_{n\to\infty} inf\delta(f^n(a), f^n(b)) = 0 \quad \lim_{n\to\infty} sup\ inf\delta(f^n(a), f^n(b)) > 0, \tag{1.4}$$

f is considered chaotic if it is constituted of countless scrambled subsets S.
One metric can be used to measure the sensibility of a chaotic system to initial conditions, which indicates the amplification of the effect of the initial conditions for a given dynamic system. The mathematical quantity is called Lyapunov exponent (Arnold & Wihstutz, 1986). For the system given in Equation (1.3) and for two close initial conditions x_0 and $x_0^{'}$, the maximal Lyapunov exponent is given by

$$\lambda(x_0) = \lim_{n\to\infty} \frac{1}{n} \sum_{i=0}^{n-1} ln|f^{`}(x_i)|, \tag{1.5}$$

where λ is the convergence criterion considering the two initial conditions, ln is the logarithmic operator, and $f^{`}$ is the first derivative of f. If the sign of λ is positive then the system is considered chaotic. The generalization for maps with dimensions that exceed one is as follows,

$$\lambda(x_i) = \lim_{n\to\infty} \frac{1}{n} ln|\lambda_i(J_n, \ldots, J_0)| \ \ , i = 1, \ldots, n, \tag{1.6}$$

where λ_i is the i^{th} eigenvalue of the matrices product between the Jacobians J_n. The Jacobian $J_i, i = 1, \ldots, n$ is the result from the linearization of f for the initial condition x_n. For a dynamical system to be considered chaotic, at least one of its Lyapunov exponents should be positive.

1.4.2.2 Examples of chaotic maps

Many chaotic maps were considered for communication systems in the literature, whether for chaos synchronization, non-coherent communications, or cryptography. The recurrently used maps are the logistic map, the Hénon map, the Chebyshev map, and the Lorenz map. The aforementioned chaotic maps were studied in (Tse & Lau, 2003), and their statistical properties were presented. The chaotic maps that are widely studied in chaos-based communications are mathematically described as follows

- Logistic map

$$x_{n+1} = \theta x_n(1 - x_n), \quad \theta \in [0, 4]. \tag{1.7}$$

- Hénon map

$$\begin{aligned} x_{n+1} &= -\alpha x_n^2 + y_n + 1, \\ y_{n+1} &= \beta x_n. \end{aligned} \tag{1.8}$$

- Lorenz map

$$\begin{aligned} \dot{x}(t) &= \sigma\big(y(t) - x(t)\big), \\ \dot{y}(t) &= \rho\, x(t) - y(t) - x(t)\, z(t), \\ \dot{z}(t) &= x(t)\, y(t) - \beta\, z(t). \end{aligned} \tag{1.9}$$

Where $\theta, \alpha, \beta, \sigma$ and ρ are parameters specific to each map.

1.5 Chaos based communication schemes

The application of chaos theory in communications resulted in two major approaches for wireless chaos-based communications: coherent and non-coherent. The coherent method of transmitting data emphasizes synchronizing chaotic maps in the transmitter and the receiver and then starting the data exchange using the appropriate modulation technique (Kaddoum, 2016a). For non-coherent modulation, the basic concept is to correlate the transmitted chaotic signal with its delayed or truncated version in order to allow its detection.

1.5.1 Applications of chaos theory in communications

The application of chaos to communications is mainly related to its characteristics of unpredictability, randomness, and many other attributes needed in signal processing. At first, chaotic behaviors picked the interest of researchers in image processing for secure image coding through the encryption of frames using chaotic keys. The application of chaos for image processing proved the possibility of its application in other related signal processing-based fields, including communications. Since chaos is generated by specific deterministic systems, its deployment is relatively easy. Thus many domains in communications had sought to include chaotic behaviors in their models in order to secure the transfer of data much further. As a result, many encryption algorithms, modulation schemes, and even wired communication technologies have included chaotic behaviors in their development.

A chaotic signal is, by nature, very unpredictable and resembles noise. Hence, using such signals to encrypt data results in an advanced level of data protection. The methodology for using chaotic behaviors is the main difference between the different technologies. While data encryption uses chaotic signals to secure data through chaotic key generation, modulation uses the chaotic signal to transmit data through chaotic carriers. The way chaotic modulation is implemented resembles spread spectrum techniques since it allows the mitigation of multipath effects and transforms the transmitted signal into a wide-spectrum signal, which adds more privacy to the transmission. On the other hand, wired communications use chaos as a means to generate nonlinear optical carriers (Silva & Young, 2000).

1.5.2 Non-coherent modulations

The works on non-coherent chaos-based communication are derived from the standard model invented by G.Kolumban et al. in (Kolumbán *et al.*, 1996). The basic concept is to transmit a chaotic signal and a reference signal for transmitted symbols and use a delay combined with a correlation in the receiver to retrieve the message. The particular design proposed for non-coherent communications holds a vast amount of possibilities for designing new modulation

schemes since the detection layouts are countless and continuously evolving with the different generations of wireless communications and the use of different signal processing techniques.

1.5.2.1 Basic architectures

Without a doubt, the most basic scheme for non-coherent chaos-based communication is proposed in (Kolumbán *et al.*, 1996) for the first time and named differential chaos shift keying (DCSK). The main reason for proposing a non-coherent scheme was to bypass the major issues related to chaos synchronization and the matched filter approach. The idea is to transmit a chaotic reference followed by the information signal where the information is the reference signal itself if '1' is transmitted and the opposite value if '0' is transmitted. At the receiver, using a delay block, the information is multiplied by the reference and then correlated over a reference duration in order to determine the transmitted bit via the sign of the correlation output. The transmitted signal for the i^{th} bit duration is given in Equation (1.10),

$$e_{i,k} = \begin{cases} x_{i,k} & \text{for } 1 < \mathrm{k} \leq \beta, \\ s_i x_{i,k-\beta} & \text{for } \beta < \mathrm{k} \leq 2\beta, \end{cases} \tag{1.10}$$

where $s_i \in \{+1, -1\}$, β is the spreading factor, T_c is the time chip, and $2\beta T_c$ is the period of the signal. The signal x_k is the k^{th} sample and $x_{k-\beta}$ is the β delayed version of the same chaotic signal. Figure 1.5 illustrates the basic design of the DCSK system.

For transmission, the carrier of the signal $e_{i,k}$ can be either AM or FM modulated. The use of reference in the transmitted signal allows the DCSK to be very robust to the channel noise, thus reducing the error level in detection. Therefore, it was proven that the DCSK is very competitive with the other modulation techniques. The only drawback of the system remains the wasted reference transmission time which reduces the data rate to half in the transmission process.

In order to solve the data rate issue related to the DCSK architecture, another basic scheme is proposed in the literature. The enhanced design, named Quadrature Chaos Shift Keying

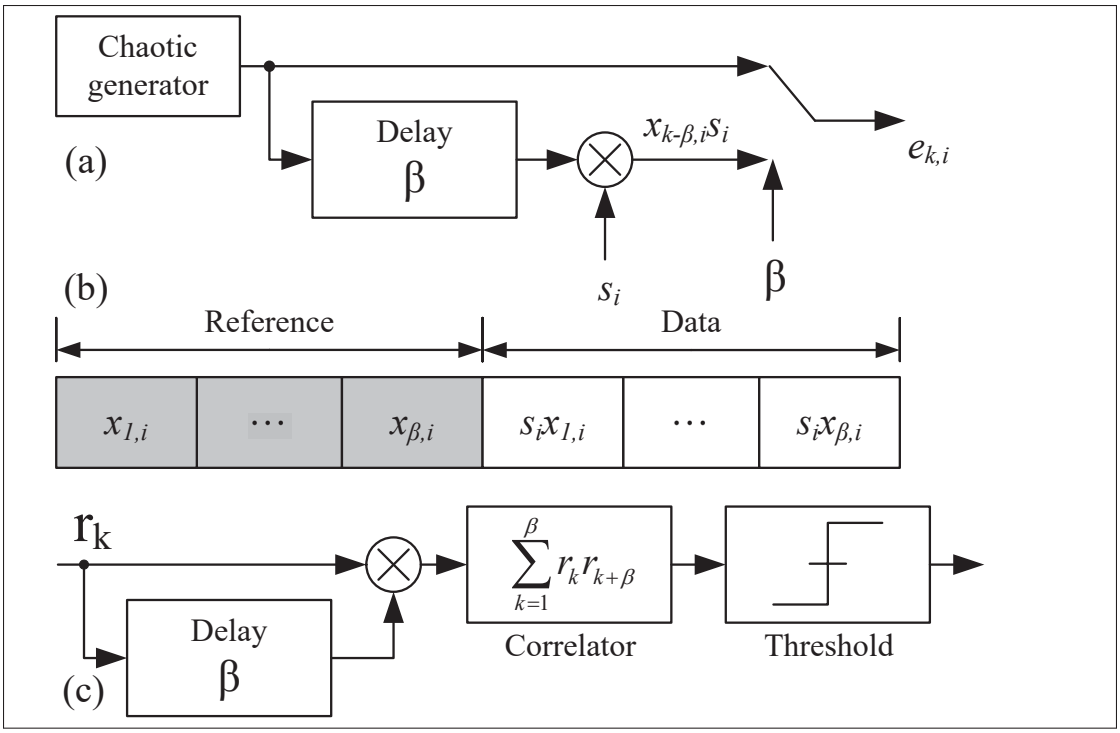

Figure 1.5 Basic Scheme of the DCSK System (a), the Transmitter (b), Symbol Composition (c) and the Receiver (Kolumbán *et al.*, 1996).

(QCSK), allowed the elimination of the reference effect on data rate through the use of an orthogonal carrier to transmit another bit of data (Galias & Maggio, 2001). The similarity in designs between QCSK and DCSK resembles that of QPSK and BPSK. In the upgraded design, a second waveform is generated using a Hilbert transformation to ensure its orthogonality to the main signal generated by the simple DCSK scheme. In the QCSK design, only one reference signal is transmitted in the first half of the period while orthogonal carriers modulate the two data bits in the second half. Figure 1.6 illustrates the architecture for QCSK modulation and detection.

The QCSK transmitted signal is as follows,

$$e_{i,k} = \begin{cases} x_{i,k} & \text{for } 1 < \mathrm{k} \leq \beta, \\ s_i x_{i,k-\beta} + s_{i+1} x_{j,k-\beta} & \text{for } \beta < \mathrm{k} \leq 2\beta, \end{cases} \tag{1.11}$$

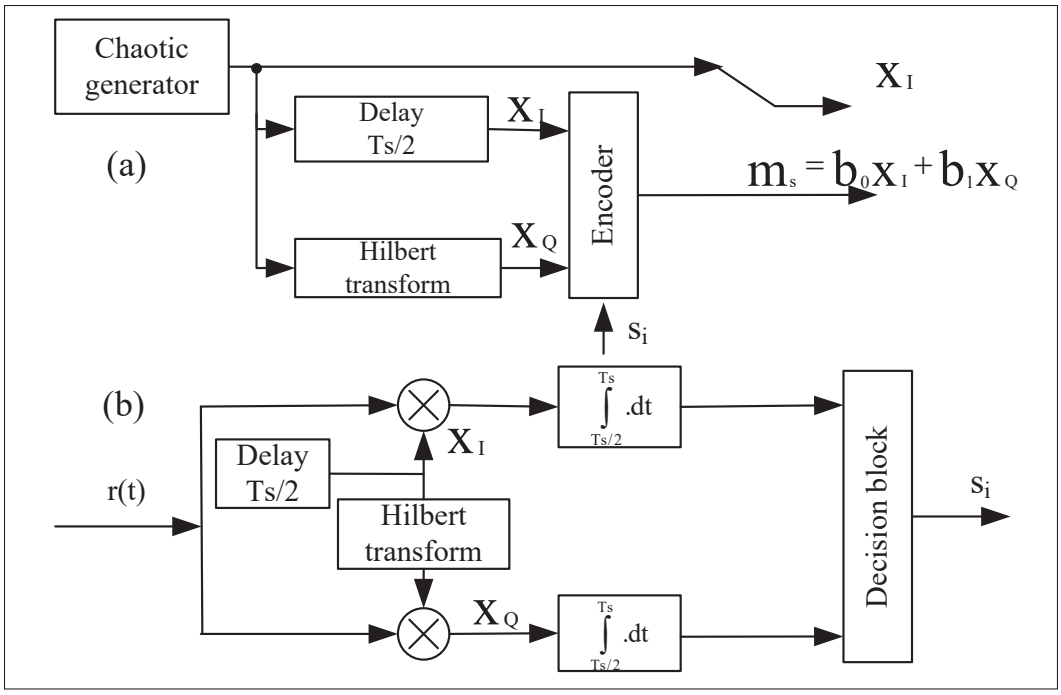

Figure 1.6 Architecture of the QCSK (a), the Transmitter and (b) the Receiver.

where $x_{i,k-\beta}$ is the reference signal and $x_{j,k-\beta}$ is the orthogonal reference generated by the Hilbert filter. As shown in Figure 1.6, a Hilbert transform is used in the receiver to generate the orthogonal chaotic carrier. After that, the signal is multiplied by the originally received signal and its locally generated orthogonal version and then integrated over half of the time period. The output of the integrators is fed to the decision block to estimate the received bit.

A simpler architecture of a non-coherent chaos-based communication scheme is studied in the literature, known as chaos on-off keying (COOK). The proposed scheme allows a reduction of the transmission's energy by a half magnitude. The central concept of COOK is to transmit a chaotic signal when the bit is '1,' and no signal when '0' is to be transmitted. Using the COOK scheme, the receiver's architecture is even simpler than the DCSK but suffers from noisy channels' effects and optimal decision threshold issues.

1.5.2.2 Advanced non-coherent modulation schemes

While DCSK, COOK, and QCSK were the starting points for non-coherent chaos-based communications, many other modulation schemes were proposed over the years. The newly invented models included advanced signal processing techniques like multi-carrier modulation, spread spectrum, and multi-user strategies.

The Permutation-Based Multiple Access DCSK (PMA-DCSK) system is one of the proposed models that offer multiple access over a non-coherent architecture (Lau, Cheong & Tse, 2002). While the PMA-DCSK keeps the same architecture as DCSK, it increases its efficiency using simple permutation techniques, adding an additional security feature to the basic model. The multi-user system is based on applying an additional transformation to the transmitted DCSK signal before sending it through the channel. The transformation applied to the transmitted signal differs for each user in the network. Transforming the signal eliminates the similarity between the reference and the data signals. If we consider F_i and s_i respectively as the transformation and transmitted bit associated with the i^{th} user for the l^{th} period, the overall transmitted signal block for the different N users is then given as follows,

$$u_l = \sum_{i=1}^{N} F_i(s_l^{(i)}). \tag{1.12}$$

To decode the message, each user applies the inverse transformation and then decodes following the DCSK decoding algorithm to recover the bits. Figure 1.7 presents the modulation and the demodulation architectures for the PMA-DCSK system. the transformation F_i is a permutation matrix used to enable multiple access for the different users.

Another advanced non-coherent scheme named Multi-Carrier multi-user DCSK (MC-DCSK) can be cited regarding its high efficiency, and originality (Kaddoum *et al.*, 2013c). The system uses OFDM modulation to increase efficiency and offer multi-user access. The principle of the proposed scheme is to generate a single chaotic reference for each user to serve as a reference and transmit it over a given frequency. Afterward, the data signals are transmitted over the

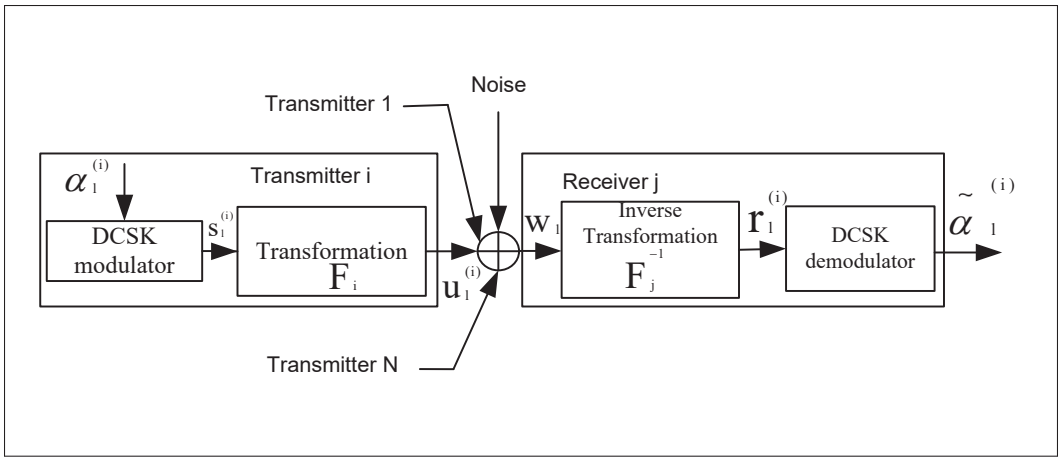

Figure 1.7 Architecture of the PMA-DSCK Transmitter-Receiver.

other orthogonal frequencies. Similarly to DCSK, the chaotic reference signal in the receiver is recovered from the first frequency and then used to decode the data transmitted over the other frequencies. The process is replicated for the different users to allow simultaneous multiple access. The Figure 1.8 illustrates the design of the MC-DCSK system for a single user.

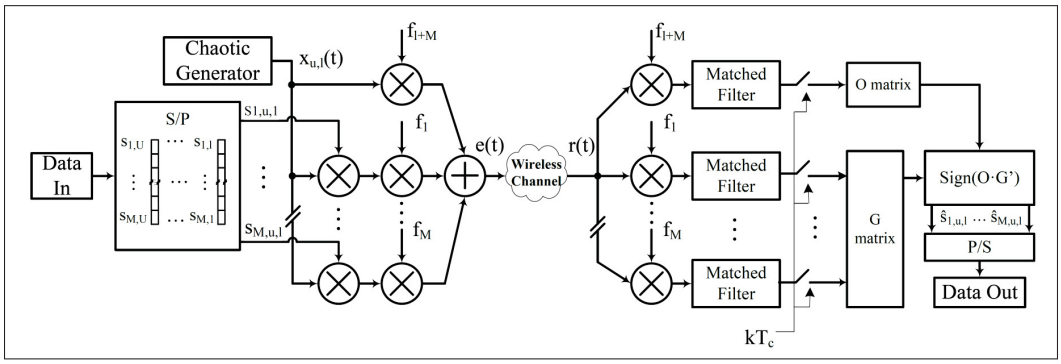

Figure 1.8 Design of the MC-DCSK System for One User (Kaddoum *et al.*, 2013c).

Equation (1.18) describes the transmitted signal for the l^{th} bit duration.

$$e(t) = x(t)cos(2\pi f_1 t + \phi_1) + \sum_{i=2}^{M} s_i x(t)cos(2\pi f_i t + \phi_i), \tag{1.13}$$

The use of multi-carrier techniques and multi-user access strategies allows this system to have a high spectral and energy efficiency since the slices of time used for reference transmission can be negligible when the number of carriers is essential (more than 20 carriers).
Many other non-coherent chaos-based modulation schemes have been proposed in the literature. The simplest scheme is the FM-DCSK, which introduces a scheme identical to the PMA-DCSK except for the transformation F_i being the FM (Kolumbán, Kis, Jákó & Kennedy, 1998). Numerous extensions and enhancements of FM-DCSK were proposed in order to solve problems related to bit energy, data rate, and spectrum efficiency in the basic FM-DCSK model (Chen, Wang & Chen, 2010) (Chen, Xu & Wang, 2008) (Abdullah, 2012). A literature review on the other extensions of DCSK is presented in (Kaddoum, 2016a), where detailed advancements in non-coherent chaos-based communication schemes are presented.

1.6 Multi-user access techniques

The non-coherent chaos-based communication systems have been the subject of study to extend the access offered to one user by the basic DCSK design to simultaneous multiple users access. For this purpose, several signal processing techniques have been proposed to add the desired additional dimension of multiple-user access varying from basic multi-antenna usage to OFDM and index modulation. The four typical dimensions used for elaborating multiple access schemes namely frequency, time, space, and code, were explored in the literature, to deliver new chaos-based schemes that can offer multi-user transmissions. The focus was, however, tilted towards exploring the frequency and code dimension through a plenitude of signal processing approaches (Kramer, 2008).

1.6.1 Frequency-based multiple access

The use of FDMA derivatives was introduced in (Kaddoum *et al.*, 2013b) by combining the design of the DCSK system with a multi-carrier technique. The design enabled the use of multiple carriers to transmit multiple data streams on a limited bandwidth for the same

user by transmitting the reference of DCSK over a specific carrier and data to correlate with the reference on the remaining carriers. The design principle is shown in Figure 1.9, where a separate bandwidth for every user is associated and used to transmit single-user data. The design is upgraded in (Kaddoum, 2016b) to enable the use of the time dimension as well with the introduction of OFDM. The design used an OFDM symbol's edge and center spectrum to transmit the references for the different users, and transmit the users' data over the remaining shared spectrum. The issues related to the use of OFDM are addressed in later works with

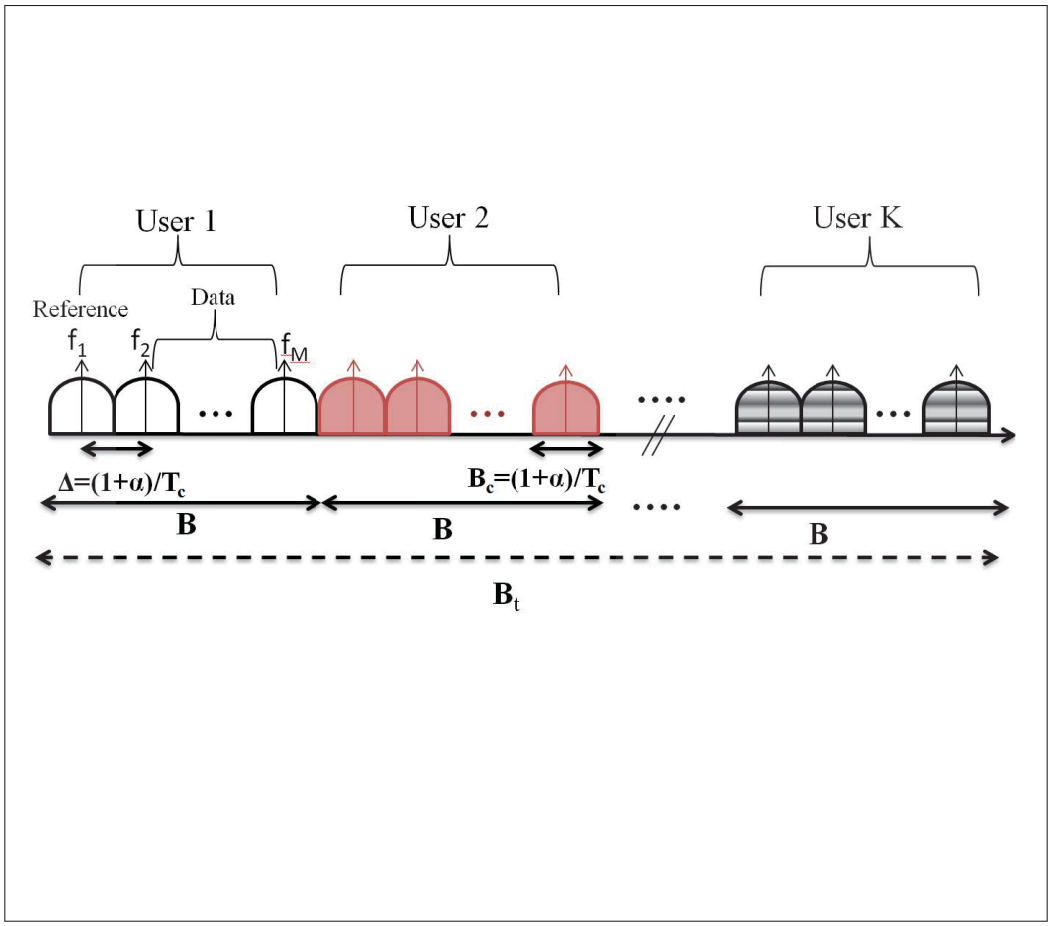

Figure 1.9 MU-MC-DCSK Bandwidth Separation (Kaddoum *et al.*, 2013b).

the objective of perfecting such designs. In (Mobini & Zahabi, 2019), the design is extended using a multi-variable approach for optimal power allocation. Furthermore, a deep learning algorithm is used to implement an optimal demodulator in (Zhang, Zhang, Jiang & Wu, 2020b),

to reduce the interferences resulting from the use of the OFDM. In (Liu, Zhang & Wu, 2020a), the carrier frequency offset (CFO) issue is tackled using precoding to the chaotic carriers before transmission. Carrier Interferometry (CI) spreading codes are used in (Liu, Zhang & Chen, 2018) to reduce the PAPR related to the use of OFDM. The Multiuser OFDM-DCSK is studied in (Wang, Hao, Wang, Zhang & Lei, 2019) to address the non-linearity introduced by the power amplifiers. The channel state information required for detecting OFDM transmitted signals is eliminated in (Liu, Zhang, Wu & Bian, 2020b), where the properties of the chaotic sequences and the frequency hopping resulting from the OFDM are used instead. Lately, a deep learning approach was used in (Zhang, Zhang, Jiang & Wu, 2022) to improve secrecy by not transmitting the reference, unlike the regular OFDM-DCSK.

1.6.2 Code Based Multiple Access

The use of code-based designs to introduce highly performing chaos-based schemes inspired numerous researchers to introduce a good number of transforms to enable such architectures. CDMA was the key inspiration for code-based modulation and it made its way through to chaos-based applications in (Li, Dai & Xu, 2004). The extension of the code-based multiple access to chaos-based systems allowed the extensive exploration of this dimension with various new designs. In (Zhang, Cui & Zhang, 2015), the DCSK design is combined with CDSK and Walsh codes to obtain better BER performances and a higher data rate than the regular DCSK with reduced interference due to the use of the Walsh codes. The introduction of index modulation for chaos-based designs in (Xu & Wang, 2016) where index modulation is combined with the DCSK design to introduce a new level of coding applied directly to the data-bearing signals, which significantly improves the data rate of the system without extra consumption of the spectrum. The design is improved in (Herceg, Vranješ, Kaddoum & Soujeri, 2018) where a different approach to applying IM is applied and enhances the system's energy and spectral efficiency. The enhanced spectral efficiency is achieved by transmitting the reference signal in the same frame duration as the data signal by taking advantage of a commute IM that ensures the orthogonality of the signals. In (Cai *et al.*, 2019) a multi-carrier M-ary differential IM-based

DCSK is introduced with an improved BER through the multi-level modulation and a new noise reduction capability which offers the possibility of the variable quality of service. The authors in (Liu, Zhang, Wu & Bian, 2019) combine IM with OFDM to reduce the PAPR through carrier interferometry that ensures orthogonality between the different carriers. The differential permutation indexing is used in (Liu, Chen & Chen, 2021) to enable a more optimized frame structure and, as a result, enhances the spectral efficiency of the DCSK system. A parallel IM-DCSK is introduced in (Chen, Chen, Fang, Chen & Kong, 2022), where the data-bearing signal is encoded using IM to decode the interference caused by the multipath channel. Thus, the design eliminates the effects of channel taps with high, very high delay spreads mainly encountered in severe fading scenarios.

1.7 Faster Than Nyquist Transmission

Modern digital communications are built based on the assumptions formulated by Nyquist in his works about models for baseband transmissions over band-limited channels. In his work, Nyquist defines a particular set of criteria for a choice of modulation, among which the separation between the transmitted signals would be critical for successful decoding. However, the separation would only consist of criteria to ensure orthogonality between the transmitted waveforms; hence, time overlap is allowed as long as the orthogonality is respected. The Nyquist rate limit for a pulse of period T consists of transmitting 2W pulses per second to obtain a rate of $\frac{1}{T}$, which would ensure no introduction of ISI.

By definition, a Nyquist pule *h(t)* is a time-domain function that follows the criterion listed as,

$$h(nT) = \begin{cases} 1 & n = 0 \\ 0 & n \neq 0 \end{cases} \tag{1.14}$$

which translates to the following in the frequency domain,

$$\frac{1}{T}\sum_{-\infty}^{+\infty} H(f+\frac{k}{T}) = 1 \tag{1.15}$$

where H is the Fourier transform for the pulse *h(t)*.

The Faster than Nyquist concept is based on the derivations presented by Mazo in (Mazo, 1975) where he proved that reducing the sampling rate to a limit that guarantees successful decoding can be considered if it respects the conditions on symbols separation in QAM modulation (Yatsukova, Ovsyannikova, Makarov & Cu, 2022). If we consider a signal carried out using a linear modulation, having the following expression,

$$s(t) = \sqrt{E_s}\sum_{n} a_n h(t - n.\rho T), \tag{1.16}$$

The a_n are independent binary bits, E_s is the pulse energy and T is the period. The term h represents the shape of the pulse with unitary energy, and ρ is a sampling parameter representing the acceleration in sampling rate in FTN when $\rho < 1$. In regular Nyquist transmissions, the parameter ρ must respect the limit value $\rho = 1$ to ensure that the h pluses are orthogonal to each other. Hence, reducing the value of the sampling parameter automatically results in interferences between the transmitted pulses. The minimum Euclidean distance for BPSK $a_n = \{+1, -1\}$ symbols given in Equation (1.16), with the filter h being the sinc function, is shown in (Ringh, 2013) to be derived as

$$\begin{aligned} d^2_{min} &= \min_{s_1(t)\neq s_2(t)} < s_1(t) - s_2(t), s_1(t) - s_2(t) > \\ &= \min_{s_1(t)\neq s_2(t)} \int_{-\infty}^{\infty} |s_1(t) - s_2(t)|^2 dt \\ &= \min_{c_n\neq 0} \frac{4T}{2\pi\rho} \int_{-\pi\rho}^{\pi\rho} |\sum_{n=N_1}^{N_2} c_n e^{-i\theta n}|^2 d\theta \end{aligned} \tag{1.17}$$

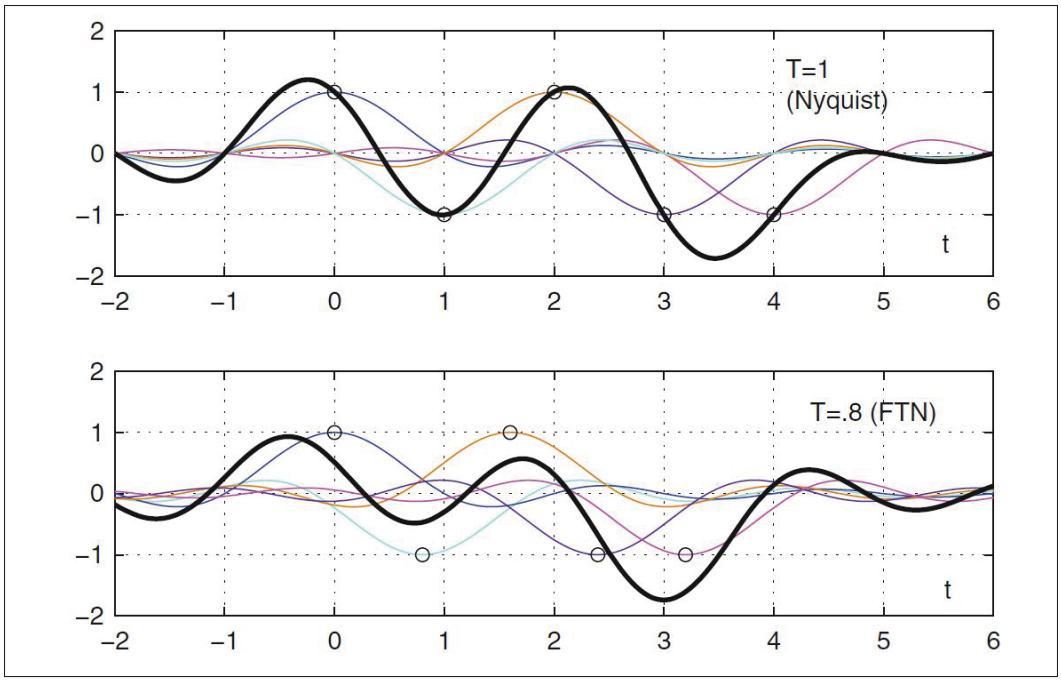

Figure 1.10 Comparisons of FTN Signaling to Regular Nyquist Transmission (Anderson *et al.*, 2013).

where c_n is the difference between the transmitted symbols a_n defined as $c_n = \frac{a_n^{(1)} - a_n^{(2)}}{2}$, N_1 and N_2 are two random values defining the width of the filter. Hence, by assuming $c_m = 1$ as the first element of the c_n and use an index $K = m - 1$, the equation is transformed as follows,

$$d_{min}^2 = \min_{\substack{c_n=\pm 1,0 \\ k>0}} \frac{4T}{2\pi\rho} \int_{-\pi\rho}^{\pi\rho} |1 - \sum_{n=1}^{K} c_n e^{-i\theta n}|^2 d\theta \tag{1.18}$$

The minimum distance of $d_{min}^2 = 1$ guaranteeing s successful decoding is then realized when $\rho = 0.802$ as shown in (Mazo & Landau, 1988).

1.8 Matched Filters

In literature, the basic definition of a matched filter is formulated so that for any physical waveform $s(t)$, the filter which is matched to it is defined by its impulse response as (Turin, 1960)

$$h(\tau) = ks(\Delta - \tau), \tag{1.19}$$

k and Δ are two random constants.

Various methods exist to derive the matched filter, namely the Lagrangian or the matrix algebra methods. However, the most straightforward procedure is the mean-square one. The common goal between these methods is the maximization of the SNR by the optimal choice of the matched filter.

The mean-square procedure consists of assuming that for a transmitted signal $s(t)$ withstanding a noise signal $n(t)$ in its travel across the channel, results in a received signal $y(t)$ composed of $s(t)$, $n(t)$, or their sum. So the goal of the method is to ensure that the power in $y(\Delta)$ (the received signal at the moment Δ) would be much greater than the average power contained in the noise $n(t)$ at the same moment $t = \Delta$.

Hence, for noise with a power density $(\frac{N_0}{2})$ and a transfer function $G(j2\pi f)$, the output power of the noise would be valued at

$$\frac{N_0}{2} \int_{-\infty}^{\infty} |G(j2\pi f)|^2 df \tag{1.20}$$

Similarly, if $S(j2\pi f)G(j2\pi f)$ is the output signal spectrum, then its inverse Fourier transform at the instant $t = \Delta$ is

$$y_s(\Delta) = \int_{-\infty}^{\infty} S(j2\pi f)G(j2\pi f)e^{j2\pi f\Delta} df \tag{1.21}$$

As a result, the objective is to maximize the following entity.

$$\rho = \frac{[\int_{-\infty}^{\infty} S(j2\pi f)G(j2\pi f)e^{j2\pi f\Delta} df]^2}{\frac{N_0}{2}\int_{-\infty}^{\infty} |G(j2\pi f)|^2 df} \tag{1.22}$$

Using the Cauchy-Schwarz inequality, we obtain

$$\rho \leq \frac{2}{N_0} \int_{-\infty}^{\infty} |S(j2\pi f)|^2 df \tag{1.23}$$

Given that $|S(j2\pi f)|^2$ represents the Energy Spectral Density (ESD) of the signal $s(t)$, the expression of ρ becomes

$$\rho \leq \frac{2E}{N_0} \tag{1.24}$$

Equation (1.24) then holds if the following condition on the two used filters is respected

$$G(j2\pi f) = kS^*(j2ßf)e^{-j2\pi f\Delta} \tag{1.25}$$

It is to be noted that this is the only form of linear filter that maximizes ρ. Alternatively, for a non-White noise with a PSD $|N(j2\pi f)|^2$, the matched filter becomes

$$G(j2\pi f) = \frac{kS^*(j2ßf)e^{-j2\pi f\Delta}}{|N(j2\pi f)|^2}. \tag{1.26}$$

1.8.0.1 Examples of Pulses

Although multiple pulses have been studied in the literature, the most commonly used pulses for radio communication are the Rectangular, Cosine, and Raised Cosine pulses.

• The rectangular pulse is defined as

$$h(t) = \sqrt{\frac{2}{T}} \quad 0 \leq t < T \tag{1.27}$$

This pulse is primarily used in MPSK modulations for its constant envelope but presents the main drawback of its high side lobes.

• The cosine filter, mainly used for its property of reducing the magnitude of the side lobes, has the following pulse shape

$$h(t) = \frac{sin(\pi t)}{T} \quad 0 \leq t < T \tag{1.28}$$

• The Raised cosine filter, primarily known for its configurable bandwidth via its roll-off factor β which determines how much excess the bandwidth occupied by the filter in comparison with the Nyquist limit as shown in Figure 1.11. The filter is defined and customized in the frequency domain as follows.

$$h(t) = \begin{cases} T & 0 \leq |f| \leq \frac{1-\beta}{2T} \\ \frac{T}{2}\left(1 - sin\frac{\pi T}{\beta}(f - \frac{1}{T})\right) & \frac{1-\beta}{2T} < f \leq \frac{1+\beta}{2T} \\ 0 & else \end{cases} \tag{1.29}$$

The Raised cosine filter reduces to the rectangular pulse for $\beta = 0$. This filter suffers from ISI's introduction when sampling errors are encountered in its standard or square root form.

1.8.0.2 Fading Channels

Our focus in this thesis is narrowband fading channels and their transformations. If we consider two Gaussian random variables x and y with zero mean and equal variances σ^2, then the variables $z = \sqrt{x^2 + y^2}$ follow the standard Rayleigh distribution denoted by z as follows (Goldsmith, 2005)

$$f(z) = \frac{z}{\sigma^2} e^{-\frac{z^2}{2\sigma^2}}, \qquad z \geq 0 \tag{1.30}$$

Similarly, the distribution of $t = z^2$ has an exponential envelope with an expression.

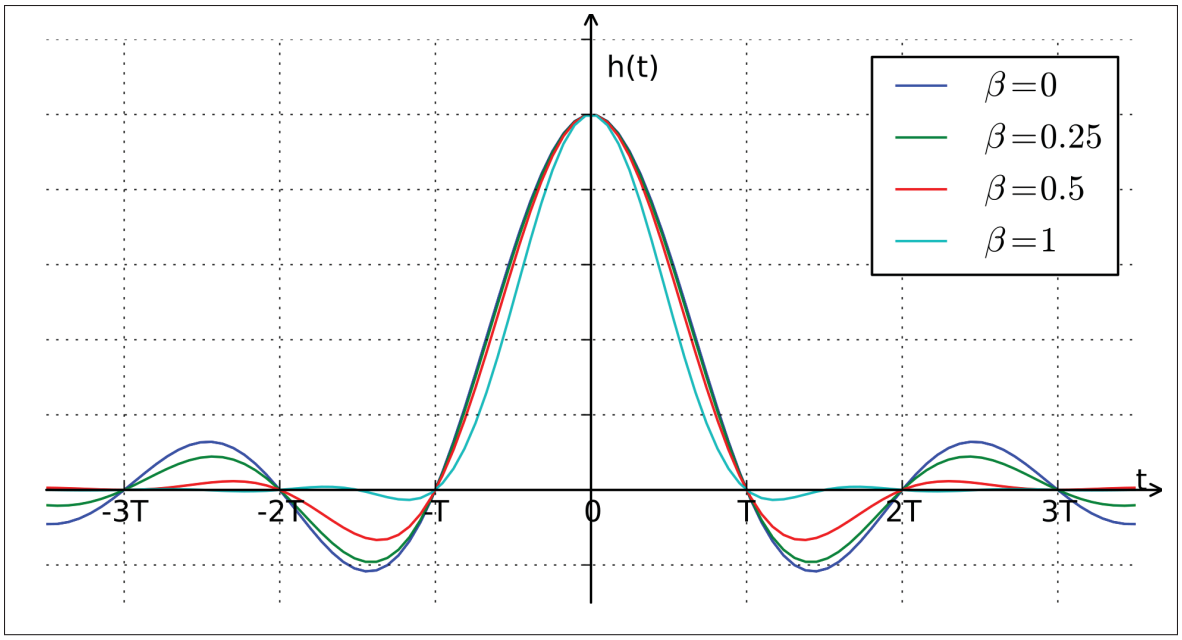

Figure 1.11 Impulse Response of Raised-Cosine Filter with Various Roll-Off Factors.

$$f(t) = \frac{1}{2\sigma^2} e^{-\frac{t}{2\sigma^2}}, \qquad t \geq 0 \tag{1.31}$$

Here, the quadrature on z shifts the mean of the distribution to $2\sigma^2$.

The Rayleigh model does not take the LOS into account; hence adding a LOS component to the channel model transforms it to the Rician model defined by the expression of its envelope as follows.

$$f(z) = \frac{z}{\sigma^2} e^{-\frac{z^2+s^2}{2\sigma^2}} I_0\left(\frac{zs}{\sigma^2}\right), \qquad z \geq 0 \tag{1.32}$$

I_0 is the Bessel function of zero order.

A more generalized channel model is introduced in literature which is built based on statistical properties of fading channels, and that can capture the physical properties of the channel is the Nakagami-m channel, where m is used to parameterize the model that is defined as follows.

$$f(z) = \frac{2mz^{2m-1}}{\Gamma(m)\bar{P}_r^m} e^{-\frac{mz^2}{\bar{P}_r}}, \qquad z \geq 0.5, \tag{1.33}$$

where $\bar{P}_r$ represents the average power at the receiver. The Nakagami-m model reduces to the following particular distributions for different values of m; m=1 $\rightarrow$ Rayleigh fading, m=$\frac{(k+1)^2}{2k+1}$ $\rightarrow$ Rician fading with parameter k, m=∞ $\rightarrow$ Gaussian additive white noise. The parameter that governs the model's behavior makes the fading all the more severe the lower its value. The squared value of a Nakagami-m random variable follows the Gamma distribution, and its summation leads to modified versions of the same distribution, i.e., the gamma distribution, with a change in the weights multiplied by the exponential terms.

CHAPTER 2

A GENERALIZED LOWER BOUND ON THE BIT-ERROR-RATE OF DCSK SYSTEMS OVER MULTIPATH RAYLEIGH FADING CHANNELS

Mohamed DAWA[1] , Georges Kaddoum[1] , Zeeshan Sattar[1]

[1] Department of Electrical Engineering,
École de Technologie Supérieure,
1100 Notre-Dame Ouest, Montréal,
Québec, Canada H3C 1K3

Article published in IEEE Transactions on
Circuits and Systems II: Express Briefs, July 2017.

2.1 Abstract

This paper presents a generalized closed-form expression of the lower bound on the bit error rate (BER) of Differential Chaos-Shift-Keying (DCSK) systems. The analytical expressions are derived for multipath Rayleigh fading channels. Unlike already existing research work, where numerical integration is the only way forward to derive the average BER for DCSK systems, this paper provides a generalized analytical expression of the lower bound on the BER. In this vein, the bounds of the Q-function are used to solve complex integrals of the average BER expression. Furthermore, a theoretical framework is also provided to generalize the derived analytical expression for the Multi-carrier Differential Chaos Shift Keying (MC-DCSK) and the Quadrature Chaos Shift Keying (QCSK) systems. For validation of these results, a detailed comparative study with already existing numerical simulations is also provided. In this study, the analytically derived bound matches the simulation results with a very narrow gap. Therefore, the bound allows the prediction of the actual BER of any chaos-based transmit reference modulation system and its derivatives with a negligible gap.

2.2 Introduction

The DCSK communication system is based on the idea of exploiting a chaotic carrier to spread digital signals over a large bandwidth. The resulting system acts more robust to multipath

fading and detection errors due to its wider bandwidth (Kaddoum, 2016a). The DCSK system is based on a non-coherent detection; hence the deployment of its architecture does not need any complex channel estimator nor a synchronization element (Lau & Tse, 2003). The DCSK system has its own specific limitations (i.e., low data rate, low spectral efficiency, etc.). Thus, to tackle these limitations, many derivatives such as the QCSK, Frequency Modulated-DCSK (FM-DCSK), and MC-DCSK have been proposed (Kolumbán, Kis, Kenedy & Jáko, 1997; Kaddoum, Richardson & Gagnon, 2013a; Yang, Tang, Chen & Jiang, 2016). In (Galias & Maggio, 2001), the QCSK system has been proposed. Its main concept is to double the data rate through orthogonal transmissions. In (Kolumbán *et al.*, 1997), the FM-DCSK system has been introduced using an FM modulator to stabilize the bit energy level of the DCSK system. The MC-DCSK system in (Kaddoum *et al.*, 2013a) has been proposed to enhance the data rate and energy efficiency without significantly increasing the system's complexity. Furthermore, numerous other derivatives of the DCSK communication system have also been proposed recently (Cheng, Wang, Xu & Chen, 2016) (Huang, Wang, Xu & Lau, 2016) (Kaddoum & Soujeri, 2016) (Li, Zhao, He, Wu & Li, 2016).

The existing performance analysis of the aforementioned systems has been done for the Additive White Gaussian Noise (AWGN) using analytical and numerical derivations (Kaddoum *et al.*, 2009). The analytical analysis of the BER performance is not that trivial when multipath Rayleigh fading channels are considered. In (Xia, Tse & Lau, 2004), Y. Xia *et. al* studied the performance of a DCSK system over a multipath Rayleigh fading channel using numerical integration to derive the average BER. In this vein, G. Kaddoum *et. al* used the same methodology to derive the performance of the MC-DCSK system over Rayleigh fading channel (Kaddoum *et al.*, 2013a). In (Kaddoum, Tran, Kong & Atallah, 2016), a Gauss Hermite integration method is applied to find the final BER expression. Furthermore, the authors in (Mandal & Banerjee, 2002) analyzed the DCSK system for an L-paths Rayleigh channel and provided a closed-form expression for the BER just for a high signal-to-noise ratio (SNR) regime.

Although the BER analysis of the DCSK system and its derivatives considering a multipath Rayleigh fading channel is a well-researched topic, none of those previous studies provides a generalized analytical expression. In fact, most of the previous work always considered a numerical integration for their evaluation, using the Monte Carlo method. Others considered the numerical integration over the probability density function (PDF) of the Rayleigh channel or using the histogram method to recover the bit energy distribution and then undertaking a summation to calculate the BER. Though there is some work on the closed-form expression of the BER for high SNR, none of them provides a generalized solution for chaos-based transmit reference systems. In order to solve complex integrals of the average BER expression, the bounds of the Q-function are used. In the literature, the Gaussian Q-function bound has been studied extensively. In (Wu, Lin & Kam, 2011), an exponential lower bound is provided using Jensen's inequality which provides a family of lower bounds for the Gaussian Q-function. Similarly, the Jensen-cotes upper and lower bounds are applied to the Q-function in (Abreu, 2009) in order to develop a new and very tight bound for the Q-function and its related functions. Moreover, a simple, accurate approach is provided in (Chang, Cosman & Milstein, 2011), in which the Q-function is bounded by a single exponential.

In this paper, we propose a new generalized approach to compute the lower bound for the BER performances of the DCSK system or its derivatives over multipath Rayleigh fading channels for the first time. To reach this aim, firstly, the Q- function is bounded using a single exponential term as in (Chang *et al.*, 2011). Since the argument of the exponential term is too complicated to manipulate, an approximation of the exponential term is applied. This approximation aims to simplify the exponential term in order to retrieve a simple polynomial form that can be integrated. In this vein, another approximation is applied to the exponential term of the channel's PDF. Furthermore, the resultant polynomial obtained from the multiplication of the two approximated exponential terms is integrated in order to obtain the lower bound performance. The importance of this work is that the analytically derived bound matches the simulation results with a very tight gap. Therefore, the obtained expression allows the prediction of any chaos-based transmit reference's performance.

This paper is organized as follows: section II covers the widely studied non-coherent chaos based transmit reference modulation schemes. Section III depicts the newly derived bit error rate performances. The simulation and analytical results are examined and discussed in section IV, and conclusive comments are presented in section V.

2.3 On-coherent Chaos-based Modulation Systems

In this section, we briefly present the widely studied DCSK communication scheme and its derivatives to prove the generality of our performance derivation approach.

2.3.1 DCSK Communication Scheme

As shown in Figure 2.1, the DCSK modulation consists of transmitting two sets of chaotic signal samples. Here, one set carries the reference signal while the other one carries the information signal. Depending on the transmitted bit $s_i \in \{+1, -1\}$, the informational set is either the reference signal itself or the inverted version of the reference. Assuming a $2\beta T_c$ period, with β being the spreading factor, and the time chip T_c is assumed equal to one in this paper, the discrete base-band signal of the transmitter, for the i^{th} bit duration, is given by

$$e_{i,k} = \begin{cases} x_{i,k} & \text{for } 1 < \mathrm{k} \leq \beta \\ s_i x_{i,k-\beta} & \text{for } \beta < \mathrm{k} \leq 2\beta, \end{cases} \tag{2.1}$$

where x_k is the k^{th} chaotic sample and $x_{k-\beta}$ is the delayed version of the same reference. In order to recover the transmitted bits, the received signal r_k is correlated with its delayed replica, i.e., $r_{k+\beta}$, and then demodulation is carried out by computing the sign of the output of the correlator.

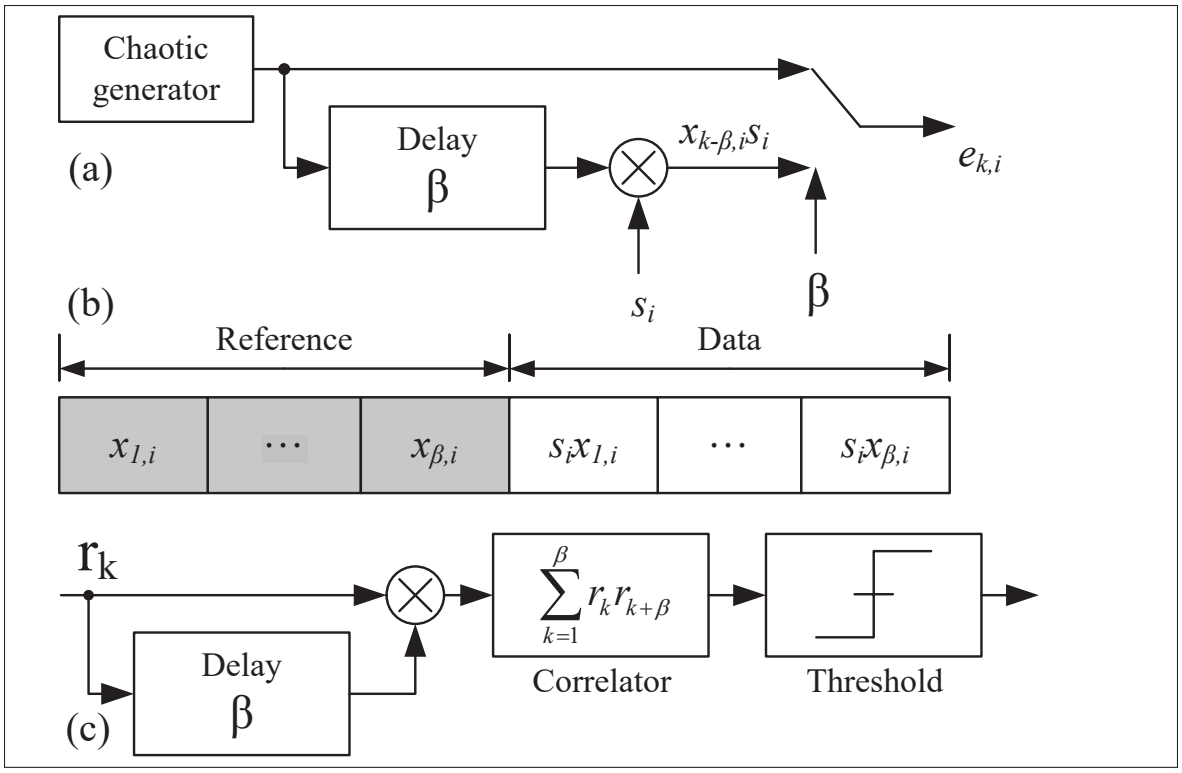

Figure 2.1 Block Diagram of the Structure of the DCSK Communication System (a) Where the DCSK Transmitter (b) Represents the DCSK Frame and (c) is the DCSK Receiver.

2.3.2 Quadrature Chaos Shift Keying

Similarly to the DCSK, the QCSK system is a non-coherent detection scheme that employs the same design as the DCSK, with the exception of transmitting an additional orthogonal waveform at the same time (Galias & Maggio, 2001).

The second waveform is introduced through a Hilbert transform which ensures the orthogonality of the generated chaos sample to the basic reference. The transmitted signal comprises a reference chaotic signal sample transmitted in the first half of the symbol period. In the second half of the period, similarly to the DCSK, the information is transmitted by multiplying two bits of information by the basic reference signal and its orthogonal version. Since there are two orthogonal reference signals, the transmitted signal is as follows

$$e_{i,k} = \begin{cases} x_{i,k} & \text{for } 1 < \mathrm{k} \leq \beta \\ s_i x_{i,k-\beta} + s_{i+1} x_{j,k-\beta} & \text{for } \beta < \mathrm{k} \leq 2\beta, \end{cases} \tag{2.2}$$

where $x_{i,k-\beta}$ is the reference signal and $x_{j,k-\beta}$ is the orthogonal reference generated by the Hilbert filter.

In the receiver, the information-bearing signal is correlated with the basic reference signal and its Hilbert transform to retrieve the information carried by the two transmitted orthogonal signals.

2.3.3 Multi-Carrier DCSK

The MC-DCSK system was first introduced in (Kaddoum *et al.*, 2013a), where they proposed an architecture that further improved the data rate and energy efficiency by using just one reference to transmit a stream of data over different orthogonal frequencies. Therefore, the transmitted signal is given as

$$\begin{aligned} e(t) = x(t)cos(2\pi f_1 t + \phi_1) + \\ \sum_{i=2}^{M} s_i x(t) cos(2\pi f_i t + \phi_i), \end{aligned} \tag{2.3}$$

where $x(t)$ is the chaotic reference, s_i and f_i are respectively the ith data and the carrier frequency of the MC-DCSK system. As shown in equation Equation (2.3), the chaotic reference signal is transmitted on the first carrier while the $M-1$ data signals are transmitted over the other orthogonal remaining frequencies. The reference signal is first recovered from the predefined frequency at the receiver side, then used to decode the transmitted data.

2.3.4 Generalized Bit Error Rate Expressions

The generalized BER expression of the DCSK system and any of its extensions over an AWGN channel is given as follows (Kaddoum *et al.*, 2009, 2013a; Galias & Maggio, 2001)

$$\mathrm{BER}(\gamma_\mathrm{b}) = \mathrm{Q}\Big[\Big(\frac{\mathrm{A}}{\gamma_\mathrm{b}} + \frac{\mathrm{B}}{\gamma_\mathrm{b}^2}\Big)^{\frac{-1}{2}}\Big]. \tag{2.4}$$

Where $\gamma_b = \frac{E_b}{N_0}$ is the SNR with $\frac{E_b}{2}$ being the bit energy and N_0 is the double-sided power spectral density of the additive white Gaussian noise. In addition, A and B are two constants taking different values with respect to the chaos-based transmit reference communication model. For example: $A = 2\sqrt{2}$ and $\mathrm{B} = \sqrt{2}\beta$ for the DCSK system (Kaddoum *et al.*, 2009); $A = \sqrt{2}\frac{M}{(M-1)}$ and $\mathrm{B} = \frac{M^2\beta}{\sqrt{2}(M-1)^2}$ for the MC-DCSK system (Kaddoum *et al.*, 2013a); and $A = 2\sqrt{2}$ and $B = \frac{\beta}{\sqrt{2}}$ for the QCSK system (Galias & Maggio, 2001).

Hence, for an L path quasi-static Rayleigh fading channel with different channel coefficients $\alpha_{l,i}$, and negligible inter-symbol interference (ISI) (i.e., The largest delay spread D_s is much shorter than the reference duration $\frac{Ds}{\beta} << 1$) , the instantaneous SNR γ_b will become equal to $\gamma_b = \sum_{l=0}^{L} |\alpha_{l,i}|^2 \frac{E_b}{N_0}$ in Equation (2.4).

Then, the average BER expression is obtained through the integration of Equation (2.4) over the PDF of the channel gain (Kaddoum *et al.*, 2009, 2013a; Galias & Maggio, 2001).

$$\overline{\mathrm{BER}} = \int_0^\infty \mathrm{Q}\Big[\frac{\mathrm{A}}{\gamma_\mathrm{b}} + \frac{\mathrm{B}}{\gamma_\mathrm{b}^2}\Big]^{\frac{-1}{2}} \mathrm{f}(\gamma_\mathrm{b})\mathrm{d}\gamma_\mathrm{b}, \tag{2.5}$$

where $f(\gamma_b)$ is the PDF of the channel gain.

For dissimilar multipath Rayleigh fading channels, the PDF is the sum of L exponentially distributed variables and is as follows (Goldsmith, 2005)

$$f(\gamma_b) = \sum_{l=1}^{L} \frac{\rho_l}{\gamma_l} e^{-\frac{\gamma_b}{\gamma_l}}, \tag{2.6}$$

where $\gamma_l = E(\gamma_b)$ is the average SNR for the l^{th} path and

$$\rho_l = \prod_{j=1,\ j\neq l}^{l} \frac{\gamma_l}{\gamma_l - \overline{\gamma_j}}.$$

2.4 Bit Error Rate Performances

In this section, the generalized closed-form expression of the BER's lower bound of the DCSK systems is introduced.

Taking into account the expression of the PDF in Equation (2.6) and replacing it into the BER expression in Equation (2.5), the average BER can be expressed as follows

$$\overline{\mathrm{BER}} = \sum_{\mathrm{l}=1}^{\mathrm{L}} \int_0^{\infty} \mathrm{Q}\Big[\frac{\mathrm{A}}{\gamma_{\mathrm{b}}} + \frac{\mathrm{B}}{\gamma_{\mathrm{b}}^2}\Big]^{\frac{-1}{2}} \frac{\rho_{\mathrm{l}}}{\gamma_{\mathrm{l}}} \mathrm{e}^{-\frac{\gamma_{\mathrm{b}}}{\gamma_{\mathrm{l}}}} \mathrm{d}\gamma_{\mathrm{b}}. \tag{2.7}$$

The integral of Equation (2.7) does not have a closed-form expression, and the only way to compute the average BER was by numerical integration (Kaddoum *et al.*, 2009, 2013a; Xia *et al.*, 2004). Hence, the only available solution for Equation (2.7) is to bound Q function first and then solve the resultant integral, leading to the lower bound expression.

In this vein, many studies have shown that the Q function admits an upper and lower bound (Wu *et al.*, 2011; Abreu, 2009; Chang *et al.*, 2011). Thus, the simplest form of the lower and upper bounds for the Q function is proposed in (Chang *et al.*, 2011). Their derivation considered a single-term exponential bound with adaptive parameters (τ and θ). The adaptive parameters are used to control the tightness of the bound. The general form of this bound is given by the following exponential function

$$g(z) = \tau e^{-\theta z^2} \leq Q(z), \quad \text{for } z \geq 0. \tag{2.8}$$

For the function in Equation (2.8) to be a lower bound, two necessary conditions are established in (Chang *et al.*, 2011) and are as follows.

$$\begin{cases} \theta \geq 0 \\ 0 < \tau \leq \sqrt{\frac{2e}{\pi}\frac{\theta-1}{\theta}}. \end{cases} \tag{2.9}$$

By applying the bound to the given general BER formula over a multipath Rayleigh fading channel, the lower bound of the BER expression is as follows

$$\mathrm{LB}(\gamma_\mathrm{b}) = \mathrm{C}\int_0^{\infty} \mathrm{e}^{-2\theta(\frac{\mathrm{A}}{\gamma_\mathrm{b}}+\frac{\mathrm{B}}{\gamma_\mathrm{b}^2})^{-1}} \mathrm{e}^{-\gamma_\mathrm{b}} \mathrm{d}\gamma_\mathrm{b} \leq \overline{\mathrm{BER}}. \tag{2.10}$$

C is a constant that does not depend on the variable γ_b.

$$\mathrm{C} = \sqrt{\frac{2\mathrm{e}}{\pi}\frac{\theta-1}{\theta}} \sum_{\mathrm{l}=1}^{\mathrm{L}} \frac{\rho_\mathrm{l}}{\gamma_\mathrm{l}} \mathrm{e}^{-\frac{1}{\gamma_\mathrm{l}}}.$$

The other challenge here is to integrate the expression in Equation (2.10) since even the new bounding form of the BER is not analytically integrable, and a direct primitive cannot be extracted. To solve this issue, an approximation of the exponential expression ($e^{-2\theta(\frac{A}{\gamma_b}+\frac{B}{\gamma_b^2})^{-1}} e^{-\gamma_b}$) is mandatory. In this context, it is proven in (Bae & Kim, 2009b) that the exponential function is upper bounded as follows

$$e^{z} \leq \frac{1}{1-z}. \tag{2.11}$$

Using this inequality, we can derive a new form of bound, which admits an analytically calculable primitive. Hence, while considering the variable $z = \gamma_b$ as the instantaneous SNR, the exponential terms' approximations are as follows.

$$\begin{aligned} e^{-z} &\leq \frac{1}{1+z}, \\ e^{-2\theta(\frac{A}{z}+\frac{B}{z^2})^{-1}} &\leq \frac{Az+B}{2\,\theta\, z^2 + Az + B}. \end{aligned} \tag{2.12}$$

Replacing the exponential terms in Equation (2.10) with their upper bounds, the expression of the lower bound Y to integrate is derived as follows

$$Y(z) = \frac{(Az + B)}{(1 + z)\left(2\,\theta\, z^2 + Az + B\right)}, \tag{2.13}$$

From the expression in Equation (2.13), an analytical form of the lower bound is easily determined and can be adjusted through the parameter θ.

The integral of Equation (2.13) is obtained through partial-fraction decomposition of the $Y(z)$ polynomial and then integrating it with respect to the variable z. The decomposition is carried as follows

$$Y(z) = \frac{T_1(z)}{(1 + z)} + \frac{T_2(z)}{\left(2\,\theta\, z^2 + Az + B\right)}, \tag{2.14}$$

where $T_1(z)$ and $T_2(z)$ are the polynomials resulting from the partial-fraction decomposition and are as follows

$$\begin{aligned} T_1(z) &= \frac{A - B}{A - B - 2\theta} \\ T_2(z) &= -\frac{2((A - B)z + B)\theta}{A - B - 2\theta}. \end{aligned} \tag{2.15}$$

The integration is carried out using Maple software, and the resulting polynomial form of the lower bound is LB(z).

$$\begin{aligned} LB(z) &= C \int Y(z)dz \\ &= C(C_1P_1(z) + C_2P_2(z) + C_3P_3(z)). \end{aligned} \tag{2.16}$$

Where C_i are constants that depend on the system parameters, i.e., A, B, θ, and are defined as

$$\begin{aligned} C_1 &= A^2 - AB - 4\theta B, \\ C_2 &= \frac{1}{2}(B - A), \\ C_3 &= B - A. \end{aligned}$$

Moreover, $P_i(z)$ are the polynomials that determine the behavior of the bound following the SNR variable.

$$P_1(z) = \frac{\arctan(\frac{4z\theta+A}{\sqrt{8\beta B-A^2}})}{(-2\theta+A-B)\sqrt{8\,\theta B-A^2}},$$
$$P_2(z) = \frac{\ln\left(2\,\theta\,z^2+Az+B\right)}{-2\,\theta+A-B},$$
$$P_3(z) = \frac{\ln\left(1+z\right)}{-2\,\theta+A-B}.$$

Finally, the lower bound of the average BER for the DCSK system and its derivatives over multipath Rayleigh fading channels is given in Equation (2.17).

$$\begin{aligned} LB(\gamma_b) =& \frac{C}{(-2\theta+A-B)}[(A^2-AB-4\theta B)\frac{\arctan(\frac{4\gamma_b\theta+A}{\sqrt{8\theta B-A^2}})}{\sqrt{8\,\theta B-A^2}} \\ &+(B-A)\ln((1+\gamma_b)+\ln(2\theta{\gamma_b}^2+A\gamma_b+B)] \leq \overline{\mathrm{BER}}. \end{aligned} \tag{2.17}$$

2.5 Simulations Results

A comparative analysis with the numerical simulations is presented in this section to validate the tightness of the newly derived bound. At first, we simulate the DCSK system and its derivatives and then plot the derived bounds for the different values of SNR. The Monte Carlo simulation method is applied here for the different system sets. Our model considers three and six taps multipath Rayleigh fading channels, i.e., $L = 3$ and $L = 6$. Figure 2.2 illustrates the simulation and the bound implementation results for the DCSK system. The parameters used for these simulations are: a spreading factor $\beta = 50$, $\theta = 2$ and a multipath Rayleigh fading channel with a number of taps $L = 3$ and $L = 6$. As observed in Figure 2.2, the derived lower bound is very close to the DCSK BER's curve and perfectly limits it from below for the different SNR values. As a result, the closeness between the original DCSK performances and the computed lower bound proves that the study of the DCSK's BER performances can be achieved through the bound itself. Therefore, this solution makes the prediction of the BER performance of the DCSK

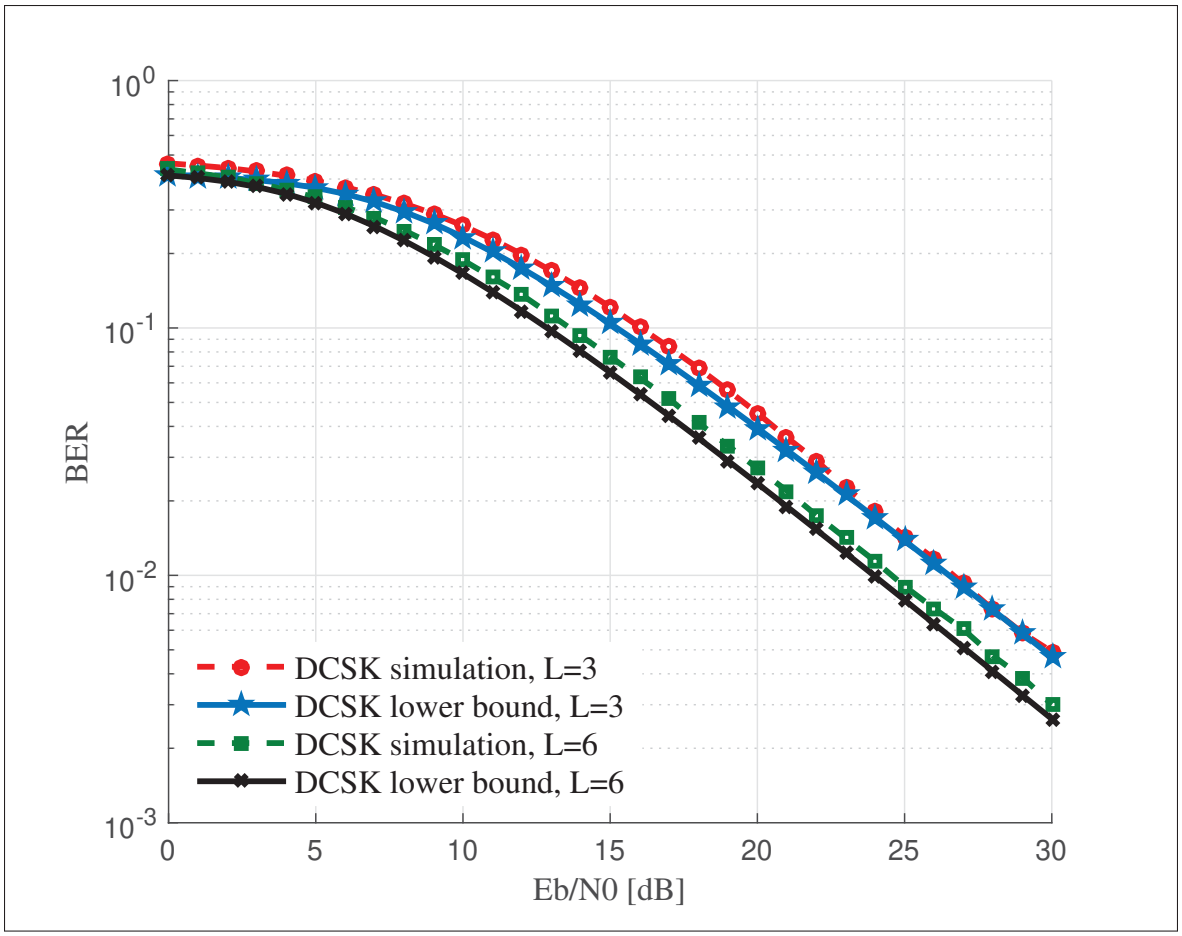

Figure 2.2 Simulation of the BER and its Analytical Lower Bound for the DCSK under Rayleigh Multipath Fading Channel with $L = 3$ and $L = 6$, with a Spreading Factor $\beta = 50$.

system over multipath Rayleigh fading channels possible through the lower bound expression. Similarly, Figure 2.3 illustrates the implementation of the bound for the QCSK system for the same settings as for the DCSK system. It is shown in Figure 2.3 that the lower bound is the same as depicted in the DCSK situation and permits to successfully limit of the BER of this system without a noticeable difference. The only exception is for the water-cliff region of the SNR values, where a tiny difference between the bound and the numerical simulation values can be observed. The difference is still acceptable since the analytical bound converges again toward the numerically simulated curve for high values of SNR.

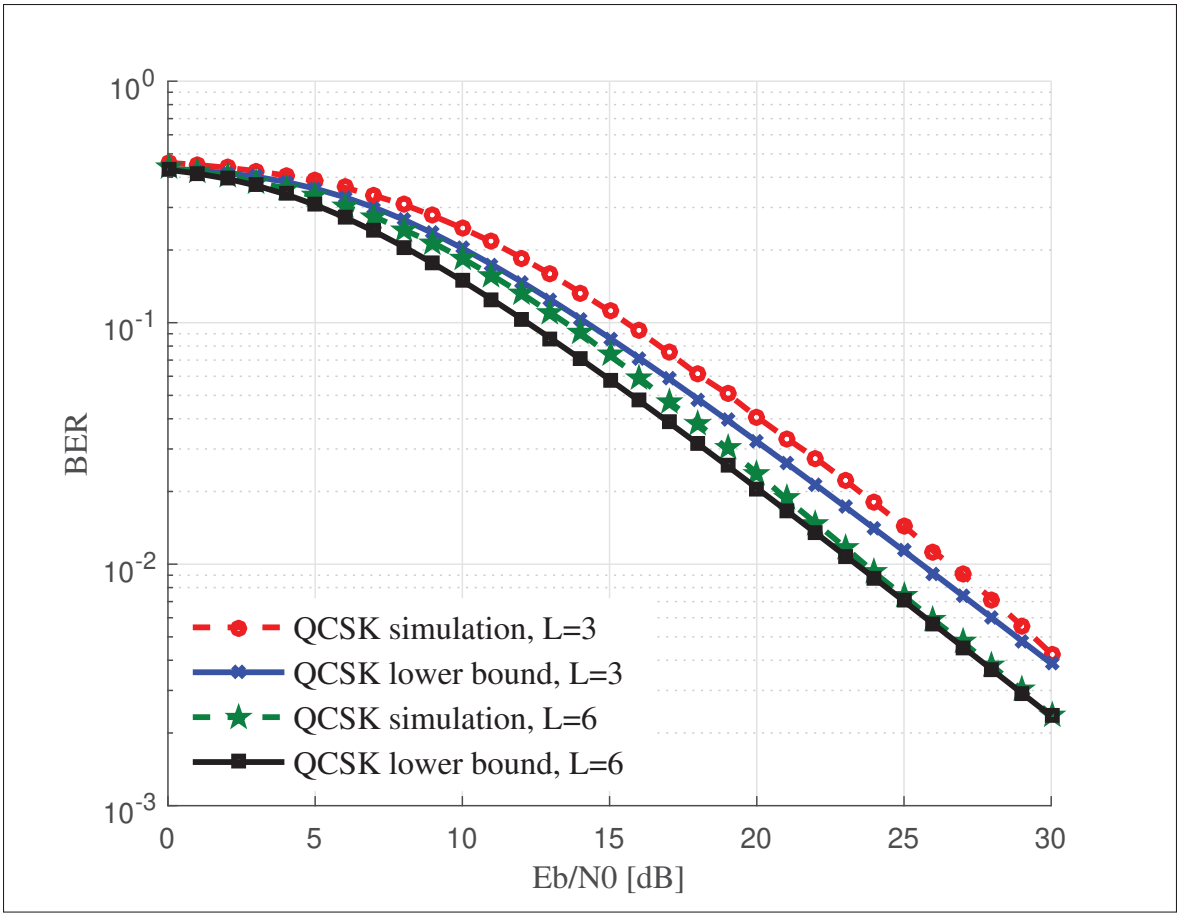

Figure 2.3 Simulation of the BER and its Analytical Lower Bound for the QCSK under Rayleigh Multipath Fading Channel with $L = 3$ and $L = 6$, with a Spreading Factor $\beta = 50$.

Finally, the lower bound is applied to the MC-DCSK for a number of carriers $M = 64$. The Figure 2.4 displays the results of the lower bounds implementation for the different simulation settings. Since we use the same form of approximation, the implementation results for the MC-DCSK are similar to the previously studied cases (DCSK and QCSK). We notice that the maximum difference between the simulation results and the analytical bound's computation is less than 1 dB. As a result, the newly derived analytical expression can be considered an excellent approximation to predict the BER curve's shape and magnitude.

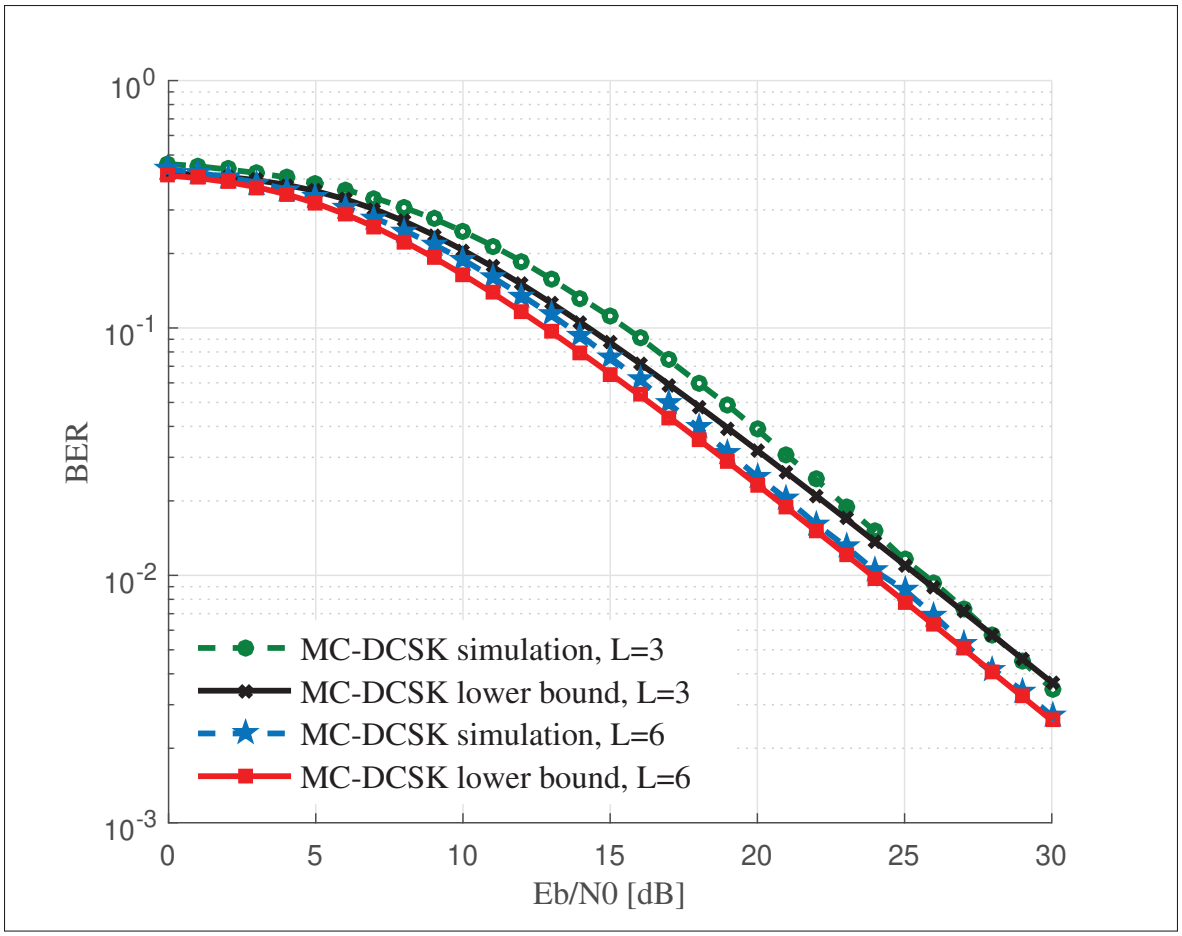

Figure 2.4 Simulation of the BER and its Analytical Lower Bound for the MC-DCSK under Rayleigh Multipath Fading Channel with $L = 3$ and $L = 6$, the Number of Carriers $M = 64$, a Spreading Factor $\beta = 50$.

2.6 Conclusion

In this paper, a closed-form expression of the lower bound on the BER performance of the DCSK and its derivative systems is derived for the first time. A thorough comparative analysis with existing numerical solutions is also provided for validation. The simulation results show that the newly derived bound comes extremely close to the actual BER curve. The only observable difference between the derived closed-form expression and the numerical solutions can be seen in the water-cliff region of the BER curve. Therefore, this bound can be used to predict the DCSK and its other derivatives' performances. Moreover, the approximations we used to derive

the lower bound can be applicable to any other chaotic system's BER performance under the specific conditions discussed in the paper. Finally, future works will focus on deriving new bounds for different channel models and distributions.

CHAPTER 3

A FRAMEWORK FOR THE LOWER BOUND ON THE BER OF DCSK SYSTEMS OVER MULTIPATH NAKAGAMI-M FADING CHANNELS

Mohamed DAWA[1] , Georges Kaddoum[1] , Marijan Herceg[2]

[1] Department of Electrical Engineering,
École de Technologie Supérieure, 1100 Notre-Dame Ouest,
Montréal, Québec, Canada H3C 1K3
[2] Department of Communications, Faculty of Electrical Engineering,
Computer Science and Information Technology, Osijek, Croatia.

Article published in IEEE Transactions on
Circuits and Systems II: Express Briefs , November 2019.

3.1 Abstract

In this paper, a generalized closed-form approach for the evaluation of the lower bound on the BER of differential chaos-shift-keying (DCSK) systems over multipath Nakagami-*m* fading channels is presented. A closed-form lower bound is derived for all configurations of the Nakagami-*m* channel model, which extends to all fading profiles covered by the Nakagami model. In contrast to previous works where very specific models were targeted and only numerical analyses of the DCSK systems were presented, we provide an approach that analytically unifies the performance analysis of DCSK systems over more generalized fading models. A similar analytical development is generalized for Quadrature Chaos Shift Keying (QCSK) and Multi-carrier Differential Chaos Shift Keying (MC-DCSK) systems. A lower bound is applied to the Q-function to extract an exponential expression of the BER. Afterwards, a bound on the exponential function is used to derive a simple polynomial expression which is easily integrable using basic integration techniques for all multipath Nakagami-*m* fading channels. The final expression of the newly derived lower bound is forwarded in terms of the Gaussian hypergeometric functions. Comparative simulations conducted for the different systems under consideration show a tight gap between the BER of the simulated systems and their respective lower bounds.

3.2 Introduction

The use of chaotic signals to propose new modulation schemes has seen great interest lately in the context of 5G and Internet of Things (IoT) communications. The excellent properties of chaotic signals such as broadband spectrum and good inter-correlation/cross-correlation make them excellent candidates for the design of communication schemes for future IoT devices (Kaddoum, 2016a). Differential chaos-shift-keying (DCSK), the most basic non-coherent scheme, is an example of the usage of chaotic signals to mitigate multipath fading with a simple yet efficient scheme (Kolumbán *et al.*, 1996). Many schemes have been proposed to overcome the limitations of DCSK, including its low spectral efficiency and rate division. Quadrature Chaos Shift Keying (QCSK), Frequency Modulated DCSK (FM-DCSK), and Multi-carrier Differential Chaos Shift Keying (MC-DCSK) are examples of the proposed systems (Galias & Maggio, 2001; Kolumbán *et al.*, 1997; Kaddoum, Richardson & Gagnon, 2013d). Precisely, QCSK solves the rate problem in DCSK through orthogonal transmission while FM-DCSK enhances the spectral efficiency using an FM modulator. In MC-DCSK, the spectral efficiency is improved using multiple orthogonal transmissions. Furthermore, schemes exploiting the different degrees of freedom offered by chaos-based communications, like index modulation, have been recently put forward in the literature (Manoharan, Saraff, Kedia & Saroja, 2019; Soujeri, Kaddoum & Herceg, 2018; Herceg *et al.*, 2018; Tan, Xu, Huang & Wang, 2018).

The performance analysis of DCSK and its different derivatives has been analytically derived for the standard Additive White Gaussian Noise (AWGN) channel model in (Tse & Lau, 2003). These expressions are conjointly used with the Probability Density Function (PDF) of a given fading channel to calculate the BER performance of the different DCSK-based systems over the corresponding fading channel (Kaddoum *et al.*, 2009). However, no closed-form expression for the BER performance analysis of DCSK systems over multipath Nakagami-m fading channels is provided in the literature. In (Fang, J. Xu & Chen, 2013), the Moment Generating Function (MGF) of the Nakagami-m channel was used with an approximation to the integral of the Q-function to derive a closed form expression for DCSK cooperative diversity (DCSK-CD) systems which is only accurate for a high number of channel paths. Zhou *et. al* presented in

(Zhou, Wang & Ye, 2010) a general methodology for the BER calculation over fading channels, including Nakagami-m fading, using the non-central F cumulative distribution function (CDF). However, their final expression is not a closed form but rather a numerical integration.

The analytical BER analysis for DCSK and its different derivatives over multipath Nakagami-m fading channels is not extensively studied in the literature due to the lack of mathematical tools that provide a closed-form expression. The BER performance is only provided numerically by integration, summation over the different values of the channel classes, or using partial approximations for very particular conditions. In this vein, we developed in (Dawa, Kaddoum & Sattar, 2018) an approximation for the analytical BER computation that uses the results presented in (Chang *et al.*, 2011) on the Q-function and in (Bae & Kim, 2009b) on the exponential function. The newly introduced approximation, generalized to different derivatives of DCSK, calculates the lower bound on the BER of these systems over multipath Rayleigh fading channels with a negligible gap. Hence, since the methodology was proven to deliver a robust approximation, its application to the Nakagami-m channel model can maintain the same promises. The insights obtained from the outcomes of this paper regarding the closed-form BER's lower bound expression inspire researchers and communication engineers to quickly and simply evaluate the system performance and optimize available parameters aiming to enhance the performance of the DCSK-inspired modulations.

In this paper, we present a general framework for the BER calculation of DCSK and its different derivatives over Nakagami-m fading channels. First, an approximation of the Q-function is used to transform the BER expression into an integral of only exponential functions. Then, the exponential expressions are all approximated using the bound given in (Bae & Kim, 2009a). The final step is a partial decomposition of the polynomial obtained from the previous approximations and its integration with respect to the boundaries of the integral. As a result, this paper further validates our methodology towards analytically analyzing the BER performance of DCSK systems over multipath fading channels.

The organization of this paper is as follows; section II presents the DCSK system and its different derivatives studied here. Section III displays the analytical development of the new lower bound while the simulation results and analysis are shown in section IV. Finally, in section V, the paper is concluded with final comments.

3.3 An Overview of Non-Coherent Chaos Based Transmit Reference Modulation Schemes

A short overview of DCSK and its different derivatives under consideration is presented in this section, as well as the generalized derivation of the new lower bound.

3.3.1 DCSK

DCSK is based on the reference transmit principle for its system model, which means that a transmission period is divided into two slots during which a reference is transmitted first, followed by the transmission of that same reference multiplied by the bipolar information symbol (Kaddoum, 2016a). The reference is a chaotic signal generated using a specific chaotic map. The demodulation is based on the sign of the output of the correlator.

3.3.2 QCSK

QCSK doubles the data rate of DCSK by sending an additional orthogonal reference waveform using the Hilbert transform in the second half period. Two information bits are each multiplied by one of the two orthogonal reference signals (Galias & Maggio, 2001). The detection is based on applying the DCSK detection method on both of the orthogonal waveforms.

3.3.3 MC-DCSK

The communication model is based on transmitting the reference on a basic frequency and then modulating the data part on (M-1) other frequencies from a total of M orthogonal frequencies. The data time slot contains the information bit multiplied by the reference signal, just like in DCSK (Kaddoum *et al.*, 2013d). The detection is based on retrieving the chaotic

reference signal from the first carrier frequency and then using it to decode the remaining (M-1) frequencies.

3.3.4 BER over Multipath Nakagami-m Fading Channels

The BER expression for the three different systems can be generalized as follows

(Galias & Maggio, 2001; Kolumbán *et al.*, 1997; Kaddoum *et al.*, 2013d; Dawa *et al.*, 2018)

$$\mathrm{BER}(\gamma_b) = \mathrm{Q}\left[\left(\frac{A}{\gamma_b} + \frac{B}{\gamma_b^2}\right)^{-\frac{1}{2}}\right]. \tag{3.1}$$

Here $\gamma_b = \sum_{l=0}^{L} |\alpha_{l,i}|^2 \frac{E_b}{N_0}$ is the SNR with E_b being the bit energy and N_0 the double-sided power spectral density of the additive white Gaussian noise. Moreover, $\alpha_{l,i}$ denotes the Nakagami-m channel coefficient for the i^{th} symbol and l^{th} path, and L is the total number of paths. We consider a quasi-static multipath Nakagami-m fading channel where we neglect the inter-symbol interference (ISI) since the maximum delay spread D_s satisfies the following condition, $\frac{D_s}{\beta} << 1$[1].

Finally, A and B are two constants depending on the system under consideration and can take different values with respect to the chaos-based communication model. The configuration of the different values of these constants is given in Table 3.1 (Kolumbán *et al.*, 1997), (Kaddoum *et al.*, 2013d), (Galias & Maggio, 2001).

Table 3.1 Parameters Configuration

	DCSK	QCSK	MC-DCSK
$\{A,B\}$	$2\sqrt{2},\sqrt{2}\beta$	$2\sqrt{2}, \frac{\beta}{\sqrt{2}}$	$\sqrt{2}\frac{M}{(M-1)}, \frac{M^2\beta}{\sqrt{2}(M-1)^2}$

The average BER expression for the three given systems when integrating over all the channel coefficients can be generalized as follows

$$\overline{\mathrm{BER}} = \int_0^{\infty} \mathrm{Q}\left[\left(\frac{A}{\gamma_b} + \frac{B}{\gamma_b^2}\right)^{-\frac{1}{2}}\right] f_s(\gamma_b) d\gamma_b, \tag{3.2}$$

[1] We show in the simulation section the validity of this assumption for low delay spreads.

where $f_s(\gamma_b)$ is the PDF of the sum of Nakagami-m channel gains. For dissimilar multipath Nakagami-m fading channels the PDF is the result of a nested finite weighted sum of Gamma PDFs which is expressed as (Karagiannidis, Sagias & Tsiftsis, 2006)

$$f_s(\gamma_b) = \sum_{i=1}^{L} \sum_{k=1}^{m_i} \Xi_L\left(i, k, \{m_q\}_{q=1}^{L}, \{\eta_q\}_{q=1}^{L}, \{l_q\}_{q=1}^{L-2}\right) \times f_g(\gamma_b, k, \eta_i)\ , \tag{3.3}$$

where $f_g(\gamma_b, k, \eta_i)$ is the PDF of the Gamma distribution with k and η_i denoting the Nakagami-m fading parameters. In $f_s(\gamma_b)$, m_i is the Nakagami-m parameter and i, m_q, η_q, and $_q$ are internal indexes ruling the iteration. The PDF f_g is considered only for integer values of k and is also known as the Erlang distribution which is defined as follows (Coelho, 1998)

$$f_g(\gamma_b, k, \eta_i) = \frac{\gamma_b^{k-1}}{\eta_i^k (k-1)!} e^{-\frac{\gamma_b}{\eta_i}}, \tag{3.4}$$

The weights of the summation terms Ξ_L are expressed in an indexed way as follows (Karagiannidis *et al.*, 2006),

$$\begin{aligned}
\Xi_L(i, k, \{m_q\}_{q=1}^{L}, \{\eta_q\}_{q=1}^{L}, \{l_q\}_{q=1}^{L-2}) &= \sum_{l_1=k}^{m_i} \sum_{l_1=k}^{l_2} \cdots \\
&\sum_{l_{L-2}=k}^{l_{L-3}} \Bigg[\frac{(-1)^{R_L - m_i} \eta_i^k}{\prod_{h=1}^{L} \eta_h^{m_h}} \times \frac{(m_i + m_{1+U(1-i)} - l_1 - 1)!}{(m_{1+U(1-i)} - 1)(m_i - l_1)!} \\
&\times \left(\frac{1}{\eta_i} - \frac{1}{\eta_{1+U(1-i)}}\right)^{l_1 - m_i - m_{1+U(1-i)}} \\
&\times \frac{(l_{L-2} + m_{L-1+U(L-1-i)} - k - 1)!}{(m_{L-1+U(L-1-i)} - 1)!(l_{L-2} - k)!} \\
&\times \left(\frac{1}{\eta_i} - \frac{1}{\eta_{L-1+U(L-1-i)}}\right)^{k - l_{L-2} + m_{L-1+U(L-1-i)}} \\
&\quad \times \prod_{s=1}^{L-3} \frac{(l_s + m_{s+1+U(s+1-i)} - l_{s+1} - 1)!}{(m_{s+1+U(s+1-i)} - 1)!(l_s - l_{s+1})!} \\
&\quad \times \left(\frac{1}{\eta_i} - \frac{1}{\eta_{s+1+U(s+1-i)}}\right)^{l_{s+1} - l_s + m_{s+1+U(s+1-i)}} \Bigg],
\end{aligned} \tag{3.5}$$

with $R_L \triangleq \sum_{i=1}^{L} m_i$, and $U(x \geq 0) = 1$ is the step function.

3.4 New Lower Bound On the BER

The lower bound on the BER is presented in this section. Substituting Equation (3.3), Equation (3.4) and Equation (3.5) into Equation (3.2), the average BER expression becomes

$$\begin{aligned}\overline{\mathrm{BER}} = &\sum_{i=1}^{L}\sum_{k=1}^{m_i} \Xi_L(i,k,\{m_q\}_{q=1}^{L},\{\eta_q\}_{q=1}^{L},\{l_q\}_{q=1}^{L-2}) \\ &\times \int_0^{\infty} \mathrm{Q}\left[\left(\frac{A}{\gamma_b}+\frac{B}{\gamma_b^2}\right)^{-\frac{1}{2}}\right] \frac{\gamma_b^{k-1}}{\eta_i^k(k-1)!} e^{(-\frac{\gamma_b}{\eta_i})} d\gamma_b.\end{aligned} \tag{3.6}$$

Since the integral term in Equation (3.6) does not have a closed-form solution due to the complicated module of the Q function, we instead use an exponential lower bound on the Q function to ease this expression. Despite the existence of multiple lower bounds on the Q function, we choose the simple yet very versatile expression given in (Chang *et al.*, 2011), where a single exponential term bounds the Q function both in upper and lower limits and can be tuned using the bound's parameters. The bound is expressed as follows

$$g(z) = \tau e^{-\theta z^2} \leq Q(z), \text{ for } z \geq 0. \tag{3.7}$$

The following conditions should be respected in order to use Equation (3.7) as a lower bound,

$$\theta > 1 \text{ and } 0 < \tau \leq \sqrt{\frac{2e}{\pi}}\frac{\sqrt{\theta-1}}{\theta}. \tag{3.8}$$

Therefore Equation (3.6) is lower bounded by

$$\begin{aligned}\mathrm{BER_{LB}} &= \tau \sum_{i=1}^{L} \sum_{k=1}^{m_i} \Xi_L(i,k,\{m_q\}_{q=1}^{L},\{\eta_q\}_{q=1}^{L},\{l_q\}_{q=1}^{L-2}) \\ &\quad \frac{1}{\eta_i^k (k-1)!} \times \left[\int_0^{\infty} \underbrace{\gamma_b^{k-1} e^{-\theta\left(\frac{A}{\gamma_b}+\frac{B}{\gamma_b^2}\right)^{-1}} e^{\left(-\frac{\gamma_b}{\eta_i}\right)}}_{\mathrm{I}(\gamma_b)} d\gamma_b \right] \\ &< \overline{\mathrm{BER}}.\end{aligned} \tag{3.9}$$

Here, for a good control over the magnitude of the bound given certain values of θ, τ is set to $\sqrt{\frac{2e}{\pi}}\frac{\sqrt{\theta-1}}{\theta}$. The terms before the integral are just weights, and the problem lies in the integral, which, despite the usage of the lower bound on the Q-function, is still not directly solvable. Thus, we use the following bound on the exponential function (Bae & Kim, 2009a)

$$e^{x} \leq \frac{1}{1-x}. \tag{3.10}$$

Although the approximation is very simple and lacks precision for high values of x, it is still very effective given the range of SNR considered for communication systems. Approximating the exponential terms in Equation (3.9) using Equation (3.10) yields

$$e^{-\frac{\gamma_b}{\eta_i}} \leq \frac{\eta_i}{\eta_i+\gamma_b} \text{ and } e^{-\theta\left(\frac{A}{\gamma_b}+\frac{B}{\gamma_b^2}\right)^{-1}} \leq \frac{A\gamma_b + B}{\theta\,{\gamma_b}^2 + A\gamma_b + B}. \tag{3.11}$$

From Equation (3.11), the expression $I(\gamma_b)$ to integrate is given as follows

$$I(\gamma_b) = \frac{\eta_i \gamma_b^{k-1}\,(A\gamma_b + B)}{(\eta_i+\gamma_b)\left(\theta\,{\gamma_b}^2 + A\gamma_b + B\right)}. \tag{3.12}$$

Integrating Equation (3.12) is straightforward since a partial-fraction decomposition permits the split of $I(\gamma_b)$ into different integrable fractions (Horowitz, 1971). The partial-fraction decomposition is carried out by firstly separating the denominator into two fractions and then assuming a hypothetical general polynomial which matches the original nominator while having a degree of k+1. The second step is a polynomial redevelopment of the newly separated fractions

and finally a match of coefficients with the equivalent hypothetical general form, which gives the following expression

$$I(\gamma_b) = \frac{T_1(\gamma_b)}{\eta_i + \gamma_b} + \frac{T_2(\gamma_b)}{\theta\,{\gamma_b}^2 + A\gamma_b + B} + T_3(\gamma_b), \tag{3.13}$$

with $T_i(\gamma_b)$, $i = \{1, .., 3\}$, are the polynomials resulting from the partial-fraction decomposition, given as follows

$$\begin{aligned} T_1(\gamma_b) &= \frac{(A\eta_i - B)\gamma_b^k}{\theta\eta_i^2 - A\eta_i + B}, \\ T_2(\gamma_b) &= -\frac{\eta_i\theta(\eta_i\theta\gamma_b^{k+1} + B\gamma_b^k)}{\theta\eta_i^2 - A\eta_i + B}, \\ T_3(\gamma_b) &= \gamma_b^{k-1}. \end{aligned} \tag{3.14}$$

Subsequently, the integration of $I(\gamma_b)$ results in the following polynomial form for the lower bound given in Equation (3.9)

$$\begin{aligned} \mathrm{BER}_{\mathrm{LB}}(\gamma_{\mathrm{b}}) =& R\Big(C_1P_1(\gamma_b) + C_2P_2(\gamma_b) + C_3P_3(\gamma_b) \\ &+ C_4P_4(\gamma_b)\Big), \end{aligned} \tag{3.15}$$

where R is the nested sum of weights defined as

$$R = \tau \sum_{i=1}^{L} \sum_{k=1}^{m_i} \Xi_L(i, k, \{m_q\}_{q=1}^{L}, \{\eta_q\}_{q=1}^{L}, \{l_q\}_{q=1}^{L-2}) \frac{1}{\eta_i^k (k-1)!}. \tag{3.16}$$

Also, $P_i(\gamma_b), i = \{1, .., 4\}$, are the functions resulting from the integration of $I(\gamma_b)$ and C_i are the constant weights resulting from the integrations and are expressed in terms of the parameters of the systems, the lower bound, and the fading channel i.e, A, B, θ, k, m_i and η_i. The constants

C_i are given as follows (Gradshteyn & Ryzhik, 2014)

$$C_1 = \frac{(A\eta_i - B)}{\theta\eta_i^2 - A\eta_i + B}, \tag{3.17}$$

$$C_2 = -\frac{\eta_i B\theta}{\theta\eta_i^2 - A\eta_i + B}, \tag{3.18}$$

$$C_3 = -\frac{\eta_i^2\theta^2}{\theta\eta_i^2 - A\eta_i + B}, \tag{3.19}$$

$$C_4 = \frac{1}{k}, \tag{3.20}$$

and the polynomials $P_i(\gamma_b)$ are given in as

$$P_1(\gamma_b) = \frac{{\gamma_b}^{k+1}}{\eta_i\, k + \eta_i}.{}_2F_1\left(1, k+1, k+2, -\frac{\gamma_b}{\eta_i}\right), \tag{3.21}$$

$$\begin{aligned} P_2(\gamma_b) = \frac{2^{-k}}{k\sqrt{B^2 - 4\theta\eta_i}}\Bigg[& \left(\frac{\theta\gamma_b}{-\sqrt{A^2 - 4\theta B} + A + 2\theta\gamma_b}\right)^{-k} \\ & \times {}_2F_1\left(-k, -k, 1-k, -\frac{A - \sqrt{A^2 - 4\theta B}}{A + 2\gamma_b\theta - \sqrt{A^2 - 4\theta B}}\right) - \\ & \left(\frac{\theta\gamma_b}{\sqrt{A^2 - 4\theta B} + A + 2\theta\gamma_b}\right)^{-k} \\ & \times {}_2F_1\left(-k, -k, 1-k, -\frac{A + \sqrt{A^2 - 4\theta B}}{A + 2\gamma_b\theta + \sqrt{A^2 - 4\theta B}}\right)\Bigg], \end{aligned} \tag{3.22}$$

$$P_4(\gamma_b) = \gamma_b^k. \tag{3.23}$$

Where ${}_2F_1$ is the Gaussian hypergeometric function. It is noted here that the expression of $P_3(\gamma_b)$ can be obtained from $P_2(\gamma_b)$ by replacing k with k+1. As a result, the final form of the lower bound is obtained in Equation (3.24) at the top of the next page.

3.5 Simulations and Analysis

The simulation results are presented in this section for DCSK, QCSK, and MC-DCSK which are all simulated using the Monte-Carlo method and where the number of multipath

$$\mathrm{BER_{LB}}(\gamma_b) = \sqrt{\frac{2e}{\pi}}\frac{\sqrt{\theta-1}}{\theta}\sum_{i=1}^{L}\sum_{k=1}^{m_i}\frac{1}{\eta_i^k(k-1)!}\Xi_L(i,k,\{m_q\}_{q=1}^{L},\{\eta_q\}_{q=1}^{L},\{l_q\}_{q=1}^{L-2})\left[\frac{{\gamma_b}^{k+1}(A\eta_i-B)}{\eta_i(\theta\eta_i^2-A\eta_i+B)(k+1)}\cdot{}_2F_1\left(1,k+1,k+2,-\frac{\gamma_b}{\eta_i}\right)\right.$$
$$-\frac{2^{-k}\eta_i\theta}{(\theta\eta_i^2-A\eta_i+B)\sqrt{B^2-4\theta\eta_i}}\left[\frac{B}{k}\left(\left(\frac{\theta\gamma_b}{-\sqrt{A^2-4\theta B}+A+2\theta\gamma_b}\right)^{-k}\times{}_2F_1\left(-k,-k,1-k,-\frac{A-\sqrt{A^2-4\theta B}}{A+2\gamma_b\theta-\sqrt{A^2-4\theta B}}\right)\right.\right.$$
$$\left.-\left(\frac{\theta\gamma_b}{\sqrt{A^2-4\theta B}+A+2\theta\gamma_b}\right)^{-k}\times{}_2F_1\left(-k,-k,1-k,-\frac{A+\sqrt{A^2-4\theta B}}{A+2\gamma_b\theta+\sqrt{A^2-4\theta B}}\right)\right)+\frac{\eta_i\theta}{2(k+1)}\left(\left(\frac{\theta\gamma_b}{-\sqrt{A^2-4\theta B}+A+2\theta\gamma_b}\right)^{-(k+1)}\right.$$
$$\times{}_2F_1\left(-k-1,-k-1,-k,-\frac{A-\sqrt{A^2-4\theta B}}{A+2\gamma_b\theta-\sqrt{A^2-4\theta B}}\right)-\left(\frac{\theta\gamma_b}{\sqrt{A^2-4\theta B}+A+2\theta\gamma_b}\right)^{-(k+1)}$$
$$\left.\left.\left.\times{}_2F_1\left(-k-1,-k-1,-k,-\frac{A+\sqrt{A^2-4\theta B}}{A+2\gamma_b\theta+\sqrt{A^2-4\theta B}}\right)\right)\right]+\frac{\gamma_b^k}{k}\right] \tag{24}$$

Nakagami-m channel taps considered is $L = 3$ and the channel parameter m takes different values, $m = \{0.5, 1, 2, 3\}$. The parameter θ takes the values detailed in Table 3.2

Table 3.2 Bound's parameter configuration

	m=0.5	m=1	m=2	m=3
θ	1.2	1.95	4	7.35

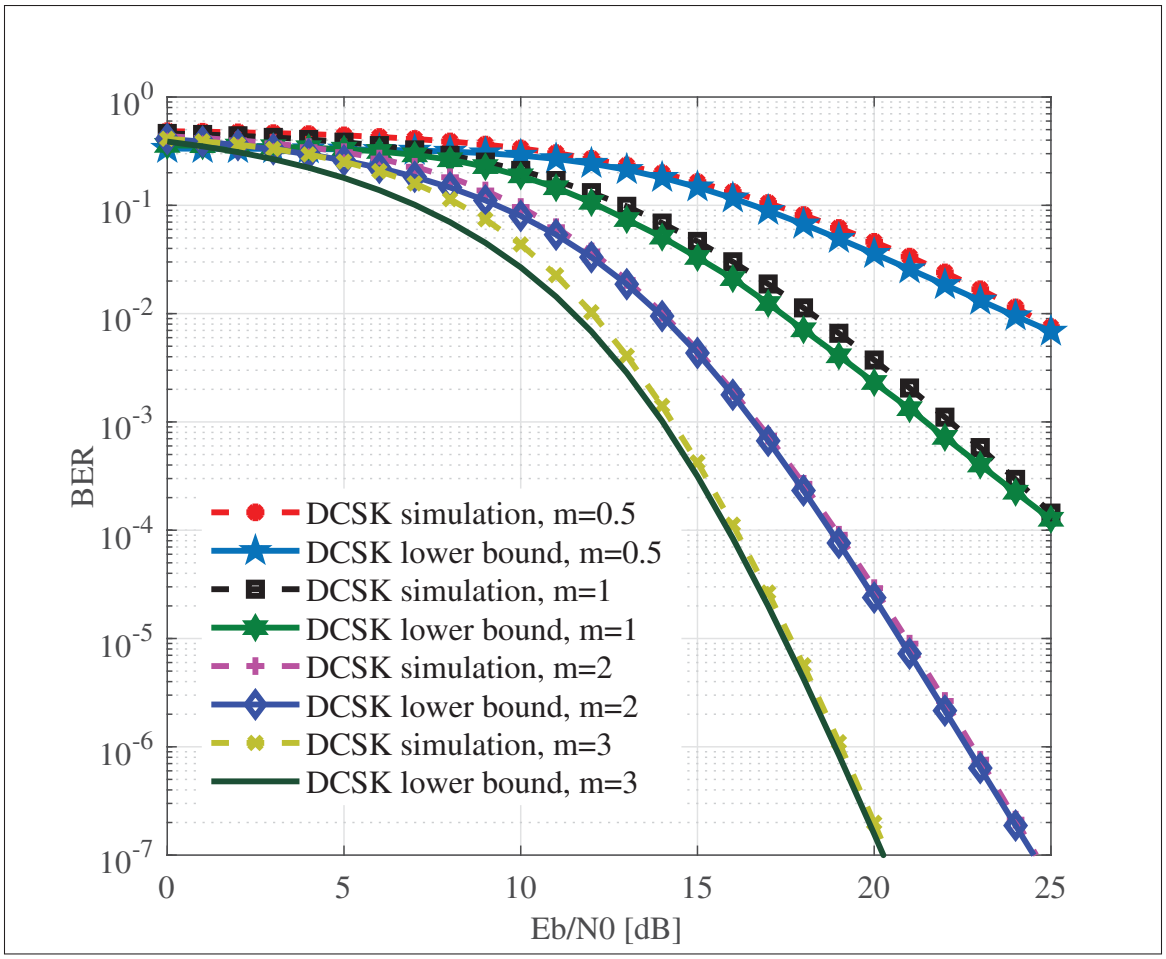

Figure 3.1 BER Simulation Versus the Analytical Lower Bound for DCSK Over Multipath Nakagami-m Fading, with $L = 3$, $m = \{0.5, 1, 2, 3\}$, D_s=20%β, and with a Spreading Factor of $\beta = 50$.

Figure 3.1 displays the analytical derivations and the simulation results for DCSK. The channel effect varies following m with better BER results for higher values of m, where a gain of 12 dB can be observed between the curves of $m = 0.5$ and $m = 3$ for a BER of 10^{-2}. Nonetheless, we can clearly observe that the derived lower bound accurately characterizes the numerical simulation curves. Thus, the newly derived bound provides a novel very powerful closed-form expression for the study of DCSK performances over multipath Nakagami-m fading channels.

The same performance is observed in Figure 3.2 for QCSK where the lower bound offers the same results as in the DCSK case, and where the convergence is still preserved with a negligible gap, i.e., lower than 0.5 dB, for all values of m.

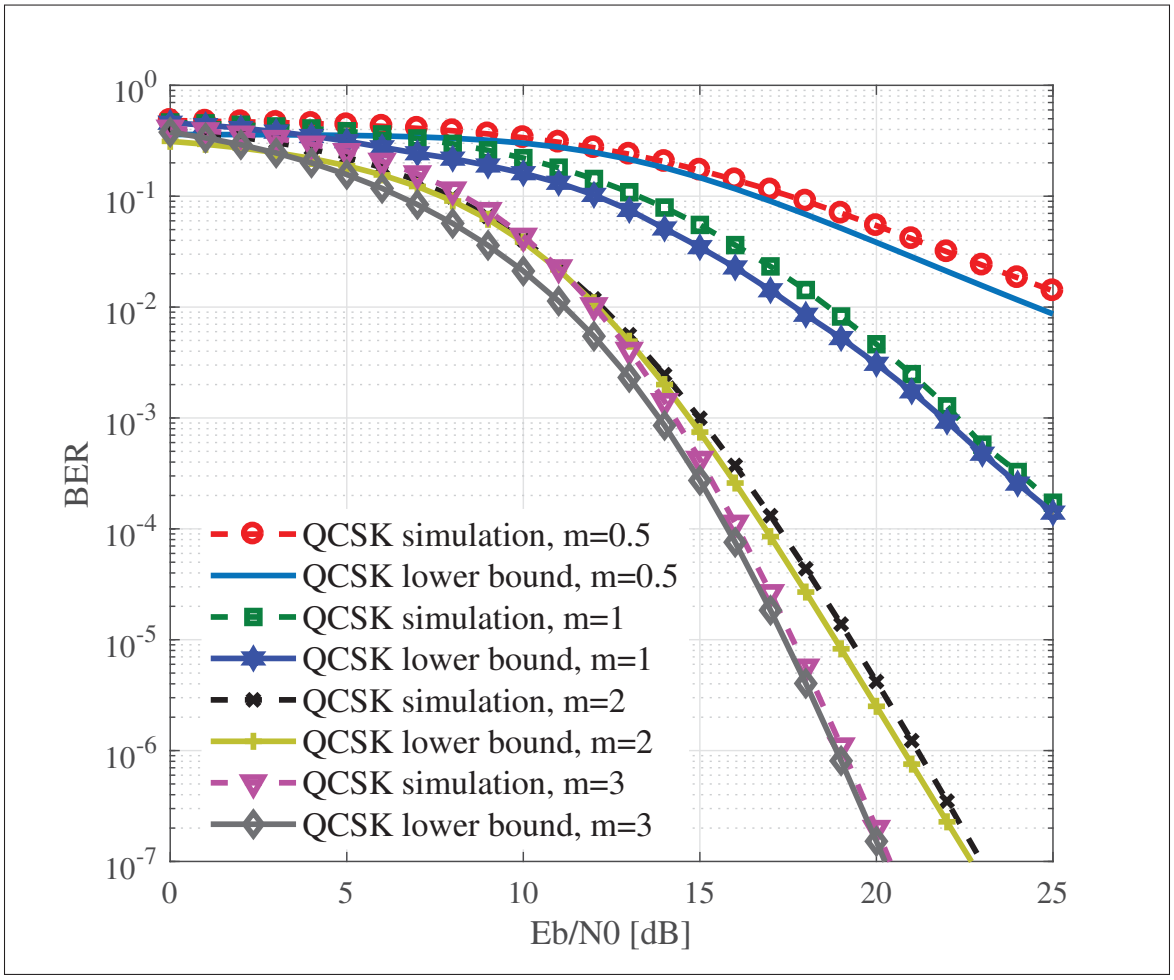

Figure 3.2 BER Simulation Versus the Analytical Lower Bound for QCSK over Multipath Nakagami-m Fading, with $L = 3$, $m = \{0.5, 1, 2, 3\}$, D_s=20%β, and with a Spreading Factor of $\beta = 50$.

Similarly, for the MC-DCSK system, the results shown in Figure 3.3 show the same trend as for DCSK and QCSK. Particularly, we can notice that the match is extremely tight for $m = 2$ which was also the case for DCSK and QCSK. The negligible differences observed in the water-cliff region are likely caused by the approximation on the exponential terms, which can be subject to precision errors. It is observed that the fading effect is much more noticeable for low

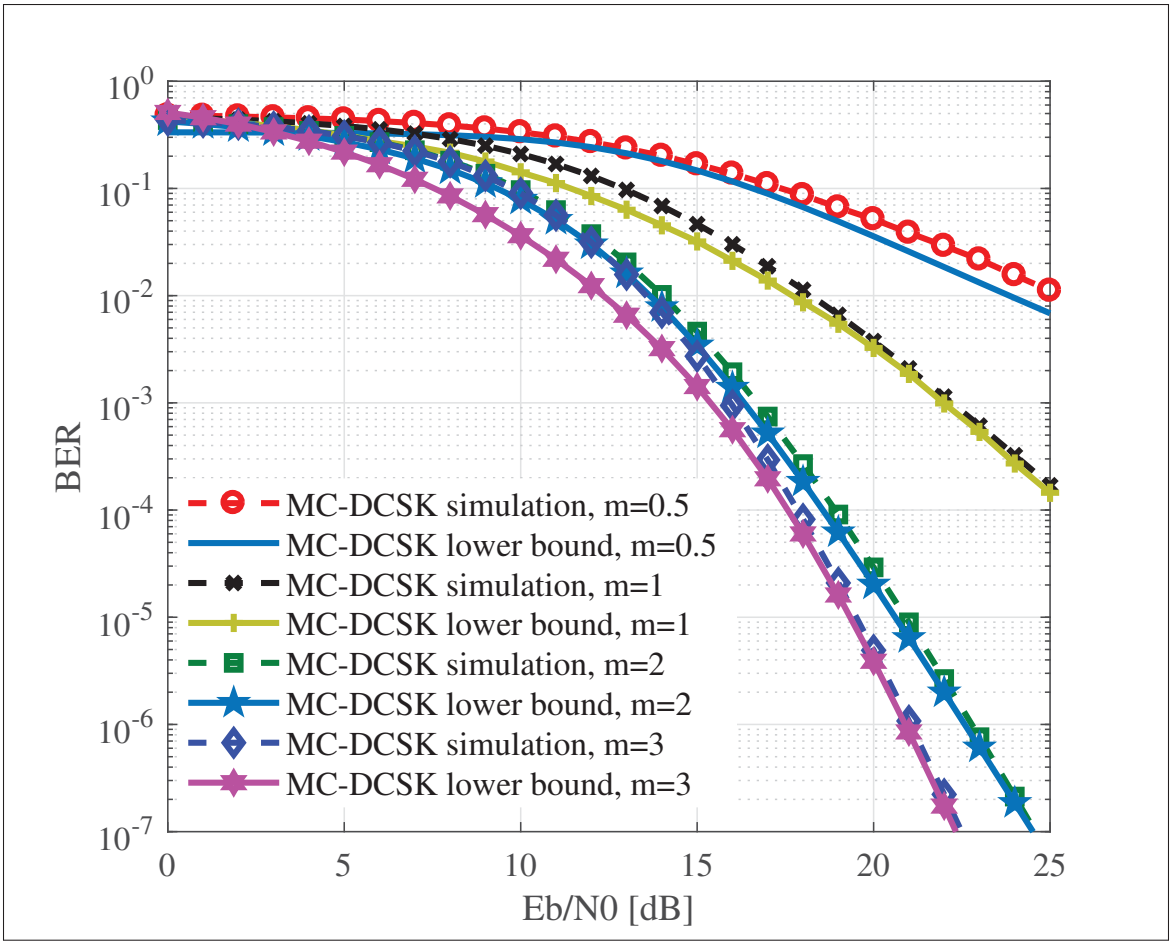

Figure 3.3 BER Simulation Versus the Analytical Lower Bound for MC-DCSK over Multipath Nakagami-m Fading, with $L = 3$, $M = 64$, $m = \{0.5, 1, 2, 3\}$, D_s=20%β, and with a Spreading Factor of $\beta = 50$.

values of m when the gap reaches its maximum of about 0.5 dB. Additionally, we can notice that QCSK outperforms both DCSK and MC-DCSK for $m = 2$, thus providing a better alternative in case this channel configuration is considered. Moreover, both DCSK and QCSK provide a better performance than MC-DCSK (about 2 dB) for $m = 3$. This is caused by the extra interference caused by the multi-carriers considered for MC-DCSK.

The results of these simulations offer a very valuable understanding on the optimization of the DCSK-based systems' parameters in order to enhance their performance in conjunction with rapidly and easily computing them. Moreover, these results come to confirm several

assumptions such as the resistance of DCSK systems to delay spread (for values much lower than the spreading factor) and to multipath fading which is observable through the different curves in Figs. 1-3.

3.6 Conclusion

A new generalized approach for the derivation of the lower bound on the BER of DCSK systems over multipath Nakagami-*m* fading channels is provided in this paper. For the first time, a lower bound in the form of a polynomial expression embedding the Gaussian hypergeometric function is derived and shown to match the simulation results. Therefore, the performance of the DCSK derivatives over multipath Nakagami-*m* channel model can now be predicted using the novel approach presented in this paper. Furthermore, the methodology presented in this paper can be generalized to other fading models for analytical analysis of the BER performances of DCSK systems. Finally, the closed-form expression obtained in this work provides excellent insights on improving chaos-based systems' design over Nakagami-*m* related fading channels and can eventually be used for designing new systems with better fading and delay spread resistances.

CHAPTER 4

DESIGN AND ANALYSIS OF MULTI-USER FASTER-THAN-NYQUIST-DCSK COMMUNICATION SYSTEMS OVER MULTIPATH FADING CHANNELS

Mohamed DAWA[1] , Marijan Herceg[2] , Georges Kaddoum[3]

[1,3] Department of Electrical Engineering,
École de Technologie Supérieure, 1100 Notre-Dame Ouest,
Montréal, Québec, Canada H3C 1K3
[2] Department of Communications, Faculty of Electrical Engineering,
Computer Science and Information Technology, Osijek, Croatia.

Article published in MDPI Sensors , September 2022.

4.1 abstract

In this paper, we present a new multi-user chaos-based communication system using Faster-than-Nyquist sampling to achieve higher data rates and lower energy consumption. The newly designed system, designated Multi-user Faster Than Nyquist Differential Chaos Shift Keying (MU- FTN-DCSK), uses the traditional structure of Differential Chaos Shift Keying (DCSK) communication systems in combination with a filtering system that goes below the Nyquist limit for data sampling. The system is designed to simultaneously enable transmissions from multiple users through multiple sampling rates resulting in semi-orthogonal transmissions. The design, performance analysis, and experimental results of the MU-FTN-DCSK system are presented to demonstrate the utility of the newly proposed system in enabling multi-user communications and enhancing the spectral efficiency of the basic DCSK design without the addition of new blocks. The MU-FTN-DCSK system presented in this paper demonstrates spectral gains for one user of up to 23% and a combined gain of 25% for four ($U = 4$) users. In this paper, we present a proof of concept demonstrating a new degree of freedom in the design of Chaos-based communication systems and their improvement in providing wireless transmissions without complicated signal processing tools or advanced hardware designs.

keywords Chaos-based communication systems, Differential Chaos Shift Keying, Faster-Than-Nyquist, Interference, Multi-user, Sampling rate.

4.2 Introduction

Higher data rates and energy efficiency are the core goals when designing new chaos-based communication systems. These goals originate from different aspects, like introducing the new communication standards (4G&5G) and the new challenges related to spectrum distribution to enable massive numbers of devices to access the network. Chaos-based systems, used as spread spectrum communication systems, were proven to be a great candidate for communications of IoT devices that constitute a considerable portion of the newly introduced standards (Kaddoum, 2016a).

In this vein, among the significant motives for improving chaos-based systems is the inherent limitations of non-coherent chaos-based systems and the rapid development of new methods that can profit the design of new highly performing chaos-based schemes. In the literature, the non-coherent scheme called Differential Chaos Shift Keying (DCSK) (Dawa *et al.*, 2018) has received significant attention in developing new chaos-based schemes, given its simple detection structure and its proven ability to mitigate the effect of fading channels (Dawa, Kaddoum & Herceg, 2019). It is also one of the most adaptive schemes and has been extensively studied over the last two decades and has seen numerous upgrades in its basic symbol structure. In this sense, various signal processing approaches have been developed to improve its data rate, spectral efficiency, transmit energy efficiency, and Bit-Error-Rate (BER). Among the most notable emerging modulation schemes, index modulation has been primarily explored, given its potential to encode data more optimally and, therefore, ameliorate the performances of DCSK systems. Index modulation (IM) was first studied for Orthogonal Frequency Division Multiplexing (OFDM) in (Başar, Aygölü, Panayırcı & Poor, 2013), where it was shown that IM could be used for more than just the transmit antennas of MIMO systems. IM was then applied to DCSK and Short Reference DCSK (SR-DCSK) using Walsh codes in (Xu & Wang, 2016), which showed that the application of Code-Index Modulation (CIM) results in a considerable performance enhancement. Walsh codes are combined with a natural number-based mapping method in (Xu, Huang & Wang, 2017) to improve the data rate of the simple Code-Index Modulation DCSK (CIM-DCSK) while using the same resources. A combination of multiple

modulation techniques, such as OFDM, vector modulation, and index modulation, has been proposed to improve the data rate and spectral efficiency of chaos-based systems. The data rate was addressed in (Ma, Cai, Fang, Chen & Chen, 2020) with the introduction of superposition coding to Pulse-Position-Modulation DCSK (PPM-DCSK) to enhance multi-user download rates. Permutation index differential chaos shift keying (PI-DCSK) and differential permutation index differential chaos shift keying (DPI-DCSK) modulations were presented in (Herceg, Kaddoum, Vranješ & Soujeri, 2018) and (Liu *et al.*, 2021), where a permutation is used to encode additional data with a list of codes referring to a series of chaotic references. Sparse codes were used similarly to achieve higher spectral efficiency for the Multi-carrier DCSK systems in (Chen, Zhang, Wu, Wang & Xu, 2020). In (Que, Quyen & Hoang, 2021), time-reversal transform is combined with the DCSK design to improve the BER and spectral performances given a land mobile satellite channel model. According to (Adame & Salau, 2022), optimal finger selection based on a genetic algorithm can be used to enhance the performance of the MMSE receiver. Orthogonal chaotic generators (OCG) were combined with Walsh codes in (Zhang, Zhao & Zhang, 2020a) to enable multi-user transmissions and achieve higher spectral efficiency than the DCSK systems. General Carrier Indexing (GCI), which uses carrier indexing in a more general and arbitrary form to reduce the number of indexes required for carriers and data bits, was used in (Cheng, Chen, Liu & Xiao, 2019) to provide higher spectral efficiency than conventional index-based DCSK systems. Combining M-ary modulation with index modulation and multi-carrier transforms in (Cai *et al.*, 2019) increased data rate but at the expense of much higher complexity. Amplitude Phase Shift Keying (APSK) was applied instead of Quadrature Amplitude modulation (QAM) to the DCSK scheme in (Fan, Xu, Wang & Zhang, 2020) in order to enhance the Peak-to-Average Power Ratio (PAPR) and the robustness against channel estimation errors. The authors in (Liu, Zhang, Wu & Jiang, 2020c) used M-ary phase shift keying (MPSK) in combination with parallelly concatenated index modulation. They integrated it with carrier interferometry (CI) codes into the OFDM-DCSK to reach a satisfactory quality of service (QoS) and low PAPR for all users. Precoding was used in (Chen, Zhang, Wang & Wu, 2021) to encode the data of Multi-Carrier M-ary Chaotic Vector Cyclic Shift Keying (MC-M-CVCSK) to combat the noise and interferences caused by the channel.

Meanwhile, one of the emerging and most efficient signal processing techniques for improving communication systems' throughput is Faster than Nyquist (FTN), which defies the limit set by Nyquist for inter-symbol spacing, thus resulting in data rate improvements. The approach has been extensively studied for a possible time and frequency domains superpositions (Anderson *et al.*, 2013). In (Mazo, 1975), the FTN approach is proven to provide an increased data rate of 23% when the symbol spacing is at a specific limit, named the Mazo limit, where the reduction in the spacing between symbols does not affect the BER performance. The reduction can be applied in time and frequency, providing two degrees of freedom for enhancing the performance of communication systems. FTN signaling has been studied extensively, especially for optimal detection of signal-spacings lower than the Mazo-limit (Zavjalov, Ovsyannikova, Lavrenyuk & Volvenko, 2019). While traditional detection algorithms, like the Maximum Likelihood Sequence Estimation (MLSE) and Viterbi algorithm, provide decent performance for a limited decrease in sampling rates, their detection optimality is limited to a short increase of symbol rate. In addition, they induce an additional computational complexity for high-order constellations. New algorithms have been proposed to tackle the computation time issue. For instance, in (Bedeer, Ahmed & Yanikomeroglu, 2017), to achieve a sub-optimal detection while maintaining a polynomial solving time, the sequence estimation is based on the semidefinite relaxation (SDR) technique to achieve a sub-optimal detection. In (Li, Yuan, Bai & Benvenuto, 2020a), output-retainable convolutional codes (ORCCs) were used for channel memorization to reduce the decoding complexity. A new approach based on a deep learning-assisted sum-product detection algorithm (DL-SPA) was presented in (Liu, Li, Xie & Yuan, 2019) for faster detection convergence.

Moreover, lately, the key research goals on FTN-based modulations focus on reaching higher orders of magnitude in the frequency domain, designing optimal filters in the time domain, Inter-Symbol-interference (ISI) and Inter-Carrier-Interference (ICI) reduction, and the elaboration of a general FTN theory. A comparative analysis of Frequency-domain equalization (FDE) and time-domain equalization (TDE) was carried out in (Li *et al.*, 2020b) where it was shown that TDE outperforms FDE, especially for ISI elimination; however, this comes at the

cost of increased complexity. In (Petitpied, Tajan, Chevalier, Ferré & Traverso, 2020), FDE was improved using Expectation Propagation (EP) to achieve a performance similar to that of the Bahl Cocke Jelinek and Raviv (BCJR) receiver (Bahl, Cocke, Jelinek & Raviv, 1974) with less complexity. However, all related FTN works introduce additional algorithmic or hardware-related computation requirements. So far, no simple yet efficient modulation scheme has been introduced in the literature. More complexity is expected to be introduced going forward with the research on a generalized FTN theory and its optimal detection. The main goal of this paper is to introduce a design that combines the architectural simplicity of DCSK and the benefits of a transform that enables a spectral gain, namely, FTN. Accordingly, the spectrum would be used less, depending on the level of the filtering rate, ranging from a maximum value at Nyquist rate ($\rho = 1$) to zero ($\rho = 0$), for which no spacing would be introduced between symbols. This would enable spectral gains ranging from zero to 100% depending on the BER requirements.

This paper introduces a novel multi-user FTN-based DCSK system where a combination of FTN filtering and non-coherent detection allows better usage of the available spectrum for the DCSK systems. Moreover, the new system enables multi-user access using the same mechanism that enables spectral efficiency gain, i.e., FTN sampling. The MU- FTN-DCSK enables multi-user access via different sampling rates with a gain in spectral efficiency for all the users simultaneously transmitting within the FTN regime. The BER results prove the system's capabilities for various sampling rates and spreading factors. The contributions of this paper are listed as follows:

1. Designing the Multi-user Faster-Than-Nyquist system that enables access for users with different sampling rates, all transmitting in an FTN regime.
2. Derivation of the theoretical BER expression for the proposed system over multipath Rayleigh Fading channels.
3. Performance analysis of the designed system, via monte-Carlo simulation, over the AWGN and Rayleigh fading channels for different system parameters and configurations.

The rest paper is structured as follows. In section 4.3, the MU-FTN-DCSK system is presented. Section 4.4 derives the BER expressions of the system. In section 4.5, the simulation results of the MU-FTN-DCSK system are presented along with their analysis. The paper is concluded in section 4.6, where we highlight the most important findings related to the newly introduced system.

4.3 System Design

The FTN-DCSK system combines a sinc filter functioning at a sub-Nyquist sampling rate with the basic transmit-receive DCSK design. The system is described in this section, where the schematic and mathematical representations of the transmitted signals are provided. The FTN prospect reflects on the possibility of enabling filtering on sub-Nyquist rates, which reduces the separation between successive transmissions to less than the minimum distance guaranteeing orthogonality. The belief proceeding FTN was that such reduction would be disastrous on signal transmission following the theorems of Shannon and Nyquist for optimal filter design and sampling. It is only through the work of T.Mazo (Mazo, 1975) that this belief was questioned, where in his work, he proved that a 401Hz/bit/s was sufficient for a sub-Nyquist filter to guarantee the same Euclidean distance offered by an ideal Sinc filter in regular orthogonal transmissions. As a result, with FTN, compared to a regular orthogonal pulse with a separation period T, the Mazo limit is $\rho = 0.802T$.

Moreover, the DCSK system is based on transmitting a chaotic sequence (reference) of length β and its product with the data signal in two successive time slots. The detection is based on differential detection, where the incoming signal is delayed by β. Then the product of the two sequences in the different time slots is taken, followed by a summation over the duration. Finally, the sign is taken to determine the transmitted data symbol.

4.3.1 FTN-DCSK

The FTN-DCSK system is constructed using a Sinc filter with a sub-Nyquist sampling rate to encode the chaotic sequence at the output of the DCSK system, as shown in the block diagram in Figure 4.1 (a). We use the normalized Chebychev map for chaos generation

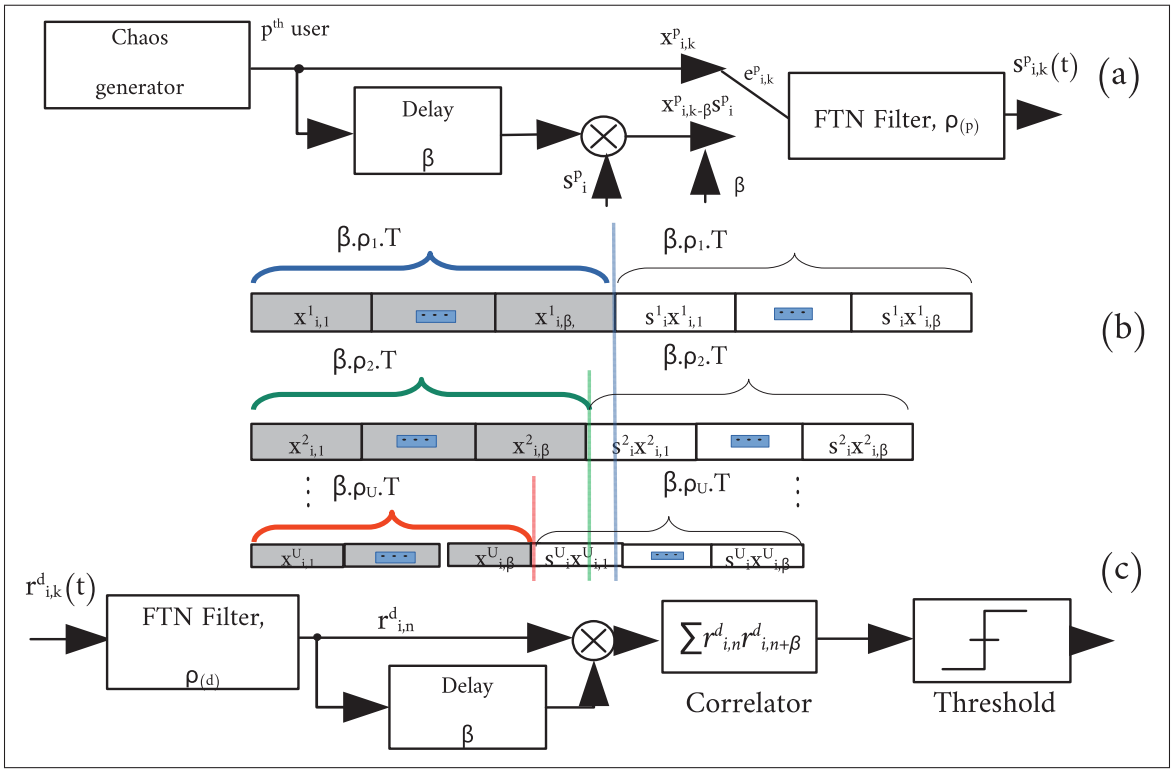

Figure 4.1 Block diagram of the MU-FTN-DCSK Communication System, (a) Random p^{th} User's Transmitter, (b) Frame Shapes for Different Users with Different Sampling Parameters, (c) Receiver Structure for the Desired User.

$$e^p_{i,k} = \begin{cases} x^p_{i,k} & \text{for } 2i\beta + 1 < k \leq (2i\beta + 1)\beta \\ b^p_i x^p_{i,k-\beta} & \text{for } (2i\beta + 1)\beta < k \leq (i+1)2\beta, \end{cases} \tag{4.1}$$

where $x^p_{i,k}$ is the i^{th} state for i^{th} symbol and k is the index of chaotic sample, for the p^{th} user, with a spreading factor β for the reference and data bearing signals, and the $b^p_i \in [-1, 1]$ are the data bits. We use a normalized Sinc filter $g^k_{\rho_{(p)}}$ to encode the chaotic sequences with a different

sampling parameter $\rho_{(p)}$ for every user, expressed as

$$g^{k}_{\rho_{(p)}}(t) = \sqrt{\rho_{(p)}} sinc(t - k.\rho_{(p)}.T), \tag{4.2}$$

where k is the chaotic sample being encoded, ρ_p is the sampling parameter for p^{th} user, and T is the typical Nyquist period. The multiplication by the sampling parameter's square root is for normalizing the filters at both ends of the transmission. As a result, the continuous-time transmitted signal $s^{p}_{i,k}$(t), for the p^{th} user, has the following form

$$s^{p}_{i,k}(t) = e^{p}_{i,k} g^{k}_{\rho_{(p)}}(t). \tag{4.3}$$

For detection, the Sinc filter is first applied at the receiver, followed by the DCSK detection scheme. The multi-user system design is shown in Figure 4.1, where a different FTN sampling parameter is used for each user. The detection is based on selecting the desired user's signal by passing the combined signal, summed in the channel, through the filter with the designated sampling parameter ρ_d, followed by the delay loop and the product and summation blocks.

The index d is used to separate the symbol of the desired user from the rest of the users transmitting in the same channel. Hence, the received signal $r^{d}_{i,k}(t)$ during 2β samples, for the desired user with a sampling parameter $\rho_{(d)}$, corresponding to the k^{th} sinc pulse of the i^{th} transmitted symbol, is expressed as

$$\mathrm{r^{d}_{i,k}(t)} = \sum_{l=1}^{L} \alpha^{d}_{i,l} s^{d}_{i,k-\tau_{i,l}}(t) + \sum_{k'=-\infty}^{\infty} \sum_{p=1}^{U-1} \sum_{l'=1}^{L} \alpha^{p}_{i',l'} s^{p}_{i',k'-\tau_{i',l'}}(t) + W(t), \;\; i' = \lfloor \frac{k'}{2\beta} \rfloor, \tag{4.4}$$

where U is the total number of users, $\alpha^{p}_{i',l'}$ is the p^{th} user's channel coefficient over the l'^{th} channel tap, and $l = \{1, .., L\}$, $\tau_{i',l'}$ is the $(l')^{th}$ channel tap delay for the $(i')^{th}$ symbol. Similarly, $\alpha^{d}_{i,l}$ is the desired user's channel coefficient over the l^{th} channel tap, $l = \{1, .., L\}$, $\tau_{i,l}$ is the l^{th} channel tap delay for the i^{th} symbol, $\lfloor . \rfloor$ is the floor operator, and W is the noise signal.

The detection is based on applying the matched filter to the received signal $r^d_{i,k}(t)$ in order to retrieve the different $e^d_{i,k}$ samples and is expressed as

$$r^d_{i,n} = \langle r^d_{i,k}(t), g^n_{\rho_{(d)}}(t)\rangle. \tag{4.5}$$

$\langle,\rangle$ is the dot product.

For filters with different sampling factors $\rho_{(d)}$ at reception for the desired user and $\rho_{(p)}$ for any random user with a different sampling parameter, the detection matrix is derived as follows,

$$\begin{aligned} G^p_{k,n} =& \langle g^k_{\rho_{(p)}}(t), g^n_{\rho_{(d)}}(t)\rangle \\ =& \int_{-\infty}^{\infty} g^k_{\rho_{(p)}}(t).\overline{g^n_{\rho_{(d)}}(t)}, \end{aligned} \tag{4.6}$$

by applying The Plancherel transform for integral substitution, we obtain

$$\begin{aligned} G^p_{k,n} &= \int_{-\infty}^{\infty} e^{-j\omega k\rho_{(p)}.T} G_T(\omega).\overline{e^{-j\omega n\rho_{(d)}.T} G_T(\omega)}d\omega \\ &= \int_{-\infty}^{\infty} e^{-j\omega(k\rho_{(p)}-n\rho_{(d)}).T} |G_T(\omega)|^2 d\omega, \end{aligned} \tag{4.7}$$

where $G_T(\omega)$ is the Fourier transform of the regular sinc filter. The Fourier transform is applied again with a variable change $\theta = \omega T$, which gives

$$\begin{aligned} G^p_{k,n} =& \frac{1}{2\pi}\int_{-\pi}^{\pi} e^{-j\theta(k\rho_{(p)}-n\rho_{(d)})} d\theta \\ =& \sqrt{\rho_{(p)}\rho_{(d)}}sinc(k\rho_{(p)} - n\rho_{(d)}). \end{aligned} \tag{4.8}$$

For the same sampling parameter $\rho_{(d)}$ in transmission and reception, the dot product of the two vectors obtained at the output of the matched filters, as shown in (Ringh, 2013), is expressed as,

$$\langle g^k_{\rho_{(d)}}(t), g^n_{\rho_{(d)}}(t)\rangle = \rho_{(d)}sinc(\rho_{(d)}(k-n)). \tag{4.9}$$

We consider a dissimilar multipath Rayleigh channel model with L paths and a PDF expressed as

$$f(\alpha_{i,l}^{p}) = \frac{\alpha_{i,l}^{p} e^{-\alpha_{i,l}^{p\,2}/\sigma^2}}{\sigma^2}, \qquad \alpha_{i,l}^{p} > 0, \tag{4.10}$$

where $\alpha_{i,l}^{p}$ is the channel gain and σ is its standard deviation. The overall energy over a symbol duration is

$$\sum_{l=1}^{L} E(\alpha_{i,l}^{p}) = 1,$$

Here $E(\alpha_{i,l}^{p})$ is the energy level for the l^{th} path for both cases of similar and dissimilar power distribution over the channel paths.

The following assumptions are considered for transmission: (1) the coefficients of the channel $\alpha_{i,l}^{p}$ are independent and identically distributed (iid); (2) the bit energy is constant over the symbol duration of length 2β; (3) the delay spread of the channel D_s is neglected for the same reason, ensuring that the channel introduces no ISI, i.e., $D_s << \beta$.

4.3.2 Spectral Efficiency

For a single user, the length of an MU-FTN-DCSK symbol is given as $(2\beta\rho_{(d)}T)$. Hence, we obtain the percentage of spectral gain S_e expressed as,

$$S_e = 2\beta T \left(\frac{1}{\rho_{(d)} 2\beta T} - \frac{1}{2\beta T} \right) \times 100. \tag{4.11}$$

The spectral gain is then simplified to the following expression

$$S_e = \left(\frac{1 - \rho_{(d)}}{\rho_{(d)}} \right) \times 100. \tag{4.12}$$

For the total spectral gain for U users, we sum over the total number of users as follows

$$S_e = \sum_{p=1}^{U} \left(\frac{1 - \rho_{(p)}}{\rho_{(p)}} \right) \times 100. \tag{4.13}$$

Given this expression, we know that the system's spectral efficiency depends on the total number of users and their individual sampling parameters. Therefore, to reach a maximal spectral efficiency, one would have to increase the number of users to the maximum while trying to minimize their sampling parameters concerning the desired BER performance.

4.4 Performance Analysis

This section derives the BER expression for the proposed MU-FTN-DCSK system over multipath Rayleigh fading channels. Following the design presented in Figure 4.1, the Probability Density Function (PDF) of the received signal follows an exponential distribution expressed as

$$f(\gamma_{i,l}^{p}) = \sum_{l=1}^{L} \frac{\tau_{i,l}^{p}}{\bar{\gamma}_{i,l}^{p}} e^{-\frac{\gamma_{i,l}^{p}}{\bar{\gamma}_{i,l}^{p}}}, \tag{4.14}$$

where $\gamma_{i,l}^{p}$ is the channel gain, $\bar{\gamma}_{i,l}^{p}$ is its averaged value, and $\tau_{i,l}^{p}$ being the weight for the i^{th} symbol duration over the l^{th} path and is expressed as

$$\tau_{i,l}^{p} = \prod_{j=1,\ j\neq l}^{l} \frac{\gamma_l}{\gamma_l - \overline{\gamma_j}}. \tag{4.15}$$

Hence, considering (Ringh, 2013, Eq.3.3), the result in (4.8), and the normalized filters for different users, the received signal $r_{i,n}^{d}$ post filtering during the first β samples i.e., the n^{th} sample of the reference signal, for the desired user with a sampling parameter $\rho_{(d)}$ is expressed as :

$$\begin{aligned} \mathrm{r}_{\mathrm{i,n}}^{\mathrm{d}} = & \sum_{k=-2}^{\beta+2} \sum_{l=1}^{L} \alpha_{i,l}^{d} x_{i,k-\tau_{i,l}}^{d} \rho_{(d)} sinc(\rho_{(d)}(k-n)) + \sum_{k'=-\infty}^{\infty} \sum_{p=1}^{U-1} \sum_{l'=1}^{L} \alpha_{i',l'}^{p} x_{i',k'-\tau_{i',l'}}^{p} \\ & \times \sqrt{\rho_{(p)}\rho_{(d)}} sinc(k'\rho_{(p)} - n\rho_{(d)}) + W_n. \end{aligned} \tag{4.16}$$

W_n is the noise signal received during the same i^{th} symbol duration. It is assumed that only two samples prior to and after the desired signal can influence it, and thus the value of $k = \{-2, \beta + 2\}$. Similarly, the value of $k' \in \{-\infty, \infty\}$ is used to express the 2β samples transmitted by any other random user asynchronously. The operator $\lfloor . \rfloor$ in (4.4) expresses the sampling of 2β sample at the moment of detection.
Similarly, the data-bearing signal, received during the second β samples is expressed by multiplying the signal of the desired user form (4.16) by the data bits s_i^d.

Due to the asynchronous nature of the system, both the reference and data-bearing signals only assume the chaos in the expression of other users' signals so that generality is not lost.. The assumption does not impact the derivation of the BER expression from a statistical perspective since $E|e_{i,k}^p| = 1$. Hence, the decision variable for the desired user's i^{th} transmitted symbol for the MU-FTN-DCSK system is derived as,

$$\begin{aligned} D_i &= \sum_{n=1}^{\beta} r_{i,n}^d * r_{i,n+\beta}^d \\ &= \sum_{n=1}^{\beta} \Bigg(\sum_{k=-2}^{\beta+2} \sum_{l=1}^{L} \alpha_{i,l}^d x_{i,k-\tau_{i,l}}^d \rho_{(d)} sinc(\rho_{(d)}(k-n)) + \sum_{p=1}^{U-1} \sum_{l_1'=1}^{L} \sum_{k'=-\infty}^{\infty} \alpha_{i',l_1'}^p x_{i',k'-\tau_{i',l_1'}}^p \sqrt{\rho_{(p)}\rho_{(d)}} \\ &\quad \times sinc(k\rho_{(p)} - n\rho_{(d)}) + W_n \Bigg) \times \Bigg(\sum_{k=-2}^{\beta+2} \sum_{l'=1}^{L} \alpha_{i,l'}^d s_i^d x_{i,k-\tau_{i,l'}}^d \rho_{(d)} sinc(\rho_{(d)}(k-n)) \\ &\quad + \sum_{p'=1}^{U-1} \sum_{l_2'=1}^{L} \sum_{k'=-\infty}^{\infty} \alpha_{i',l_2'}^{p'} x_{i',k'-\tau_{i',l_2'}}^{p'} \times \sqrt{\rho_{(p')}\rho_{(d)}} sinc(k\rho_{(p')} - n\rho_{(d)}) + W_{n+\beta} \Bigg), \end{aligned} \tag{4.17}$$

The desired signal is then the product of the chaotic terms having the index of the desired user d and the filter with the desired user's sampling parameter $\rho_{(d)}$, resulting in the following signal

$$U_i = \sum_{n=1}^{\beta} \sum_{k=-2}^{\beta+2} \sum_{l=1}^{L} s_i^d (\alpha_{i,l}^d)^2 (x_{i,k-\tau_{i,l}}^d)^2 \rho_{(d)}^2 \times sinc^2(\rho_{(d)}(k-n)), \tag{4.18}$$

The cross-product of the chaotic terms in (4.17) results in interferences expressed as

$$
\begin{aligned}
I_i = & \sum_{n=1}^{\beta} \sum_{k=-2}^{\beta+2} \sum_{k'=-\infty, k' \neq k}^{\infty} \Bigg(\sum_{l=1}^{L} \sum_{l'=1}^{L} s_i^d \alpha_{i,l}^d \alpha_{i,l'}^d x_{i,k-\tau_{i,l}}^d x_{i,k'-\tau_{i,l'}}^d \rho_{(d)}^2 sinc(\rho_{(d)}(k-n)) \\
& \times sinc(\rho_{(d)}(k'-n)) \Bigg\} ISI \\
& + \sum_{l=1}^{L} \sum_{l'=1}^{L} \sum_{p=1}^{U-1} \alpha_{i,l}^d (1+s_i^d) \alpha_{i',l_1'}^p \sqrt{\rho_{(p)}} \times \rho_{(d)}^{3/2} x_{i,k-\tau_{i,l}}^d x_{i',k'-\tau_{i',l'}}^p sinc(\rho_{(d)}(k-n)) \\
& \times sinc(k'\rho_{(p)} - n\rho_{(d)}) + \sum_{p=1}^{U-1} \sum_{p'=1}^{U-1} \sum_{l_1'=1}^{L} \sum_{l_2'=1}^{L} \alpha_{i_1',l_1'}^p \alpha_{i_2',l_2'}^{p'} \sqrt{\rho_{(p)}\rho_{(p')}} \rho_{(d)} \\
& \times x_{i_1',k'-\tau_{i_1',l_1'}}^p x_{i_2',k'-\tau_{i_2',l_2'}}^{p'} sinc(k\rho_{(p)} - n\rho_{(d)}) \times sinc(k\rho_{(p')} - n\rho_{(d)}) \Bigg) \Bigg\} IUI
\end{aligned}
\tag{4.19}
$$

The first term in (4.19) is the ISI, which occurs because of the reduced distances between samples due to the nature of the FTN filter. The remaining part is the inter-user interference (IUI) for different chaos generators and sampling parameters. The noise term is expressed as

$$
\begin{aligned}
N_i = & \sum_{n=1}^{\beta} \Bigg(W_{n-\beta} \Bigg(\sum_{k=-2}^{\beta+2} \sum_{l=1}^{L} \alpha_{i,l}^d x_{i,k-\tau_{i,l}}^d \rho_{(d)} \times sinc(\rho_{(d)}(k-n)) + \sum_{p=1}^{U-1} \sum_{k'=-\infty}^{\infty} \sum_{l_1'=1}^{L} \alpha_{i',l_1'}^p s_{i'}^p \\
& \times \sqrt{\rho_{(p)}\rho_{(d)}} x_{i',k'-\tau_{i',l_1'}}^p sinc(k\rho_{(p)} - n\rho_{(d)}) \Bigg) \\
& + W_n \Bigg(\sum_{k=-2}^{\beta+2} \sum_{l=1}^{L} \alpha_{i,l}^d s_i^d x_{i,k-\tau_{i,l}}^d \rho_{(d)} sinc(\rho_{(d)}(k-n)) + \sum_{p'=1}^{U-1} \sum_{k'=-\infty}^{\infty} \sum_{l_2'=1}^{L} \alpha_{i',l_2'}^{p'} s_{i'}^{p'} x_{i',k'-\tau_{i',l_2'}}^{p'} \\
& \times \sqrt{\rho_{(p')}\rho_{(d)}} sinc(k\rho_{(p')} - n\rho_{(d)}) \Bigg) + W_n W_{n-\beta} \Bigg).
\end{aligned}
\tag{4.20}
$$

In this paper, it is assumed that the sum of β chaotic samples is equal to,

$$
E_b = 2 \sum_{k=1}^{\beta} x_{i,k}^2 \tag{4.21}
$$

Hence, the mean value of the desired signal is given as

$$E = \frac{1}{2}\rho_{(d)}^2 \frac{E_b}{\beta} \sum_{n=}^{\beta} \sum_{k=-2}^{\beta+2} \sum_{l=1}^{L} (\alpha_{i,l}^d)^2 sinc^2(\rho_{(d)}(k-n)). \tag{4.22}$$

Since the chaotic sequences are generated with zero mean ($E(x_{i,k}) = 0$) and using (4.21), the variance of the individual chaotic chips is given as,

$$var(x_{i,k}^2) = \frac{E_b^2}{4\beta} \tag{4.23}$$

Hence, the variances of the interference terms in (4.19) can be split as the ISI, with variance V_{I_1}, the interference to the desired user, with variance V_{I_2}, and the interference among all other users, with variance V_{I_3} as

$$\begin{aligned}
V_{I_{i_1}} =& \frac{E_b^2}{4\beta^2} \sum_{n=1}^{\beta} \sum_{k=-2}^{\beta+2} \sum_{k'=-\infty}^{\infty} \sum_{l=1}^{L} \sum_{l'=1}^{L} (\alpha_{i,l}^d \alpha_{i,l'}^d)^2 \\
& \times \rho_{(d)}^4 sinc^2(\rho_{(d)}(k-n)) sinc^2(\rho_{(d)}(k'-n) \\
V_{I_{i_2}} =& \frac{E_b^2}{2\beta^2} \sum_{p=1,p\neq d}^{U} \sum_{n=1}^{\beta} \sum_{k=-2}^{\beta+2} \sum_{k'=-\infty}^{\infty} \sum_{l=1}^{L} \sum_{l'=1}^{L} (\alpha_{i,l}^d \alpha_{i',l'}^p)^2 \rho_{(p)} \\
& \times \rho_{(d)}^3 sinc^2(\rho_{(d)}(k-n)) sinc^2(k'\rho_{(p)} - n\rho_{(d)}) \\
V_{I_{i_3}} =& \frac{E_b^2}{4\beta^2} \sum_{p=1}^{U} \sum_{p'=1,p'\neq p}^{U} \sum_{n=1}^{\beta} \sum_{k=-2}^{\beta+2} \sum_{k'=-\infty}^{\infty} \sum_{l=1}^{L} \sum_{l'=1}^{L} (\alpha_{i,l}^p \alpha_{i',l'}^{p'})^2 \\
& \times \rho_{(p)}\rho_{(p')}\rho_{(d)}^2 sinc^2(k\rho_{(p)} - n\rho_{(d)}) \times sinc^2(k'\rho_{(p')} - n\rho_{(d)}).
\end{aligned} \tag{4.24}$$

The noise variance is equally affected by the sinc filter at the reception. The result shown in (Ringh, 2013, Eq.3.3) is valid for our case since the noise is only affected by the filter of the

desired user at detection. As a result, the power of the noise is reduced by a factor of $G_{k,n}$ for the sampling parameter $\rho_{(d)}$ as :

$$\begin{aligned} Cov(w_k, w_n) =& \sigma^2 G_{k,n} \\ =& \sigma^2 \rho_{(d)} sinc(\rho_{(d)}(k-n)), \end{aligned} \tag{4.25}$$

where σ is the standard deviation of the noise. Henceforth, for noise with a double-sided power spectral density N_0, the variance of the noise terms is expressed as

$$\begin{aligned} V_{N_i} =& \frac{N_0 E_b}{2\beta} \sum_{n=1}^{\beta} \sum_{k=-2}^{\beta+2} \Bigg(\sum_{k'=-\infty}^{\infty} \sum_{l=1}^{L} (\alpha_{i,l}^{d})^2 \rho_{(d)}^3 sinc(\rho_{(d)}(k-n)) sinc^2(\rho_{(d)}(k'-n)) \\ &+ \frac{N_0 E_b}{2\beta} \sum_{p=1}^{U-1} \sum_{n=1}^{\beta} \sum_{k'=-\infty}^{\infty} \sum_{l=1}^{L} (\alpha_{i,l}^{p})^2 \rho_{(p)} \rho_{(d)}^2 sinc(\rho_{(d)}(k-n)) sinc^2(k' \rho_{(p)} - n\rho_{(d)}) \\ &+ \frac{N_0^2}{4} \sum_{n=1}^{\beta} \rho_{(d)}^2 sinc^2(\rho_{(d)}(k-n)) \Bigg). \end{aligned} \tag{4.26}$$

For non-coherent chaos-based communications in regular Nyquist transmissions, the covariance is often neglected while expressing variances, given the low cross-correlation between chaotic sequences when time delayed or for different chaos generators,

$$x_{(i,t)} . (x_{(j,t)})^T \approx 0 \qquad i \neq j. \tag{4.27}$$

However, in sub-Nyquist transmissions with the introduction of the *sinc* terms, as seen in the derivation of the variances and the expectation, covariances are introduced in the formulation of the BER expression. Here, we explore the different covariances that may occur in this scenario of multi-user chaos-based transmission below the Nyquist rate.

For the Chebychev map (Geisel & Fairen, 1984), we know that the joint PDF of two chaotic variables x_0 and x_1, time delayed by t, is expressed as

$$f(x_0, x_1; t) = \pi^{-1}(1 - x_0)^{-\frac{1}{2}}\delta(x_1 - T_{k^t}(x_0)), \tag{4.28}$$

where T_{k^t} is the Chebychev polynomial for a variable x expressed as

$$T_{k^t}(x) = \cos(k.\arccos(\mathrm{x})), \tag{4.29}$$

where cos is the cosine function and δ is the delta function.

The variance of a sum of dependent random variables X_i with weights a_i is known as(Papoulis, 1984),

$$var(\sum_{i=1}^{n} a_i X_i) = \sum_{i=1}^{n} a_i^2 var(X_i) + 2\sum_{i=1}^{n}\sum_{j=i+1}^{n} a_i a_j cov(X_i, X_j), \tag{4.30}$$

and the covariance is given as

$$cov(X_i, X_j) = E(X_i.X_j) - E(X_i)E(X_j). \tag{4.31}$$

Given that the chaotic sequences are generated with zero mean (E(X_i)=0), the covariance of two FTN-filtered chaotic sequences is derived as

$$\begin{aligned} Cov(X_i, X_j) &= E(X_i.X_j) \\ &= E(\int_{-\infty}^{\infty}\int_{-\infty}^{\infty} x_i.x_j.G_T^i(t)G_T^j(s)dtds) \\ &= \int_{-\infty}^{\infty}\int_{-\infty}^{\infty} E(x_i.x_j).G_T^i(t)G_T^j(s)dtds, \end{aligned} \tag{4.32}$$

where $G_T^i(t)G_T^j(s)$ are two sub-Nyquist filters from two random users with different sampling rates. We use the joint PDF of two chaotic variables to compute the expectation $E(x_i.x_j)$

$$\begin{aligned} E(x_i.x_j) &= \int_{-\infty}^{\infty}\int_{-\infty}^{\infty} x_i.x_j.f_{x_ix_j}(x_i, x_j)dx_i.dx_j \\ &= \int_{-\infty}^{\infty}\int_{-\infty}^{\infty} x_i.x_j.\pi^{-1}(1-x_i^2)^{-\frac{1}{2}}\delta(x_j - x_i)dx_i.dx_j \\ &= (\frac{E_b}{\beta})^2\int_{-1}^{1}\pi^{-1}(1-x_i^2)^{-\frac{1}{2}} \\ &= \frac{E_b^2}{2\beta^2} \end{aligned} \tag{4.33}$$

As a result, by injecting the expectation into (4.32) and using the results from (4.7), the new covariance introduced by the FTN regime is expressed in terms of the detection matrix $G_{k,n}$ as follows

$$Cov(X_i, X_j) = \frac{E_b^2}{2\beta^2}\sum_{n=1}^{\beta}\sum_{k=-2}^{\beta+2} G_{k,n}. \tag{4.34}$$

This covariance occurs even in the absence of noise and for single-user cases and is strictly inherent to the nature of the filters used for transmission/reception.

Finally, the overall BER expression of the MU-FTN-DCSK system over an AWGN channel is expressed identically to DCSK as

$$BER(SNR) = \frac{1}{2} erfc(\frac{2\sum Var}{E^2}) \tag{4.35}$$

Hence, using the derived expressions of expectation and variances, the BER expression over the AWGN channel can be obtained by assuming unitary channel coefficients, i.e., $\alpha_{i,l} = 1, \quad \forall\, i, l$. Thus, the BER performance over multipath Rayleigh fading channels is expressed as

$$BER(\gamma) = \int_{\gamma=-\infty}^{\infty} \frac{1}{2} erfc(\frac{2\sum Var}{E^2}) f(\gamma) d\gamma. \tag{4.36}$$

4.5 Numerical Analysis and Results

This section presents the MU-FTN-DCSK system's simulation results over AWGN and multipath Rayleigh fading channels. For the Rayleigh channel, we consider an $L = 3$ multipath channel model with power levels of $\{P_1 = \frac{7}{10}, P_2 = \frac{2}{10}, P_3 = \frac{1}{10}\}$, with $P_i, i = 1, ..3$ being the variance of the channel gains $\alpha_{i,l}$. Due to the high computation time dedicated to the sinc filter at transmission, since a continuous-time signal is simulated with many points for processing, the transmitter is implemented in C++ to use the multi-thread and multi-processor features. For this purpose, the *Intel* MKL library is used to implement the filter and other vector manipulations. Moreover, a comparison with state-of-the-art modulations is carried out to establish the proposed system's relative performances.

4.5.1 BER Analysis

Figure 4.2 presents BER results for different numbers of users over the AWGN channel. The parameters used for the simulations are $\beta = 150$, $\rho_{(p)} = \{0.9, 0.8, 0.7, 0.6\}$ where the main user always takes the value of $\rho_{(d)} = 0.9$. We can notice the tiny gap for a single user transmitting at a sub-Nyquist rate ($\rho_{(d)} = 0.9$) in comparison with normal Nyquist transmissions ($\rho_{(d)} = 1$), labeled as the normal DCSK, due to the ISI introduced by the sinc filter functioning in the sub-Nyquist regime. For $U = 1$, the ISI introduced by the matched filters results in an approximate 1dB loss of BER but with a gain of 10% of the bandwidth. This means that slightly raising the energy for transmission, in order to compensate for the 1dB, would allow a gain of 10% in bandwidth usage in both the reference and the data sequences. The analytical results match the simulation results proving the validity of the new covariance derived in (4.34).

The same observation is perceived when the number of users is increased. We notice that up to three users with different sampling parameters can be accepted in the system with an acceptable BER for noisy environments. In the setting used for the simulations that lead to these results with sampling parameters $\rho_{(p)} = \{0.9, 0.8, 0.7\}$, we obtain a slot of length $(0.6\times\beta)$ of extra bandwidth. As a comparison, for U=4 users, the BER performance offered by the MU-FTN-DCSK over an AWGN channel matches that of the regular DCSK over the Nakagami-m fading for a channel parameter $m = 0.5$ (Dawa *et al.*, 2019) due to the severe interference caused by the simultaneous transmissions of all users in the sub-Nyquist regime. Nonetheless, the bandwidth gain here is 2β if we sum the individual gains from different users transmitting at a sub-Nyquist rate in both the reference and data signals. An optimization in the choice of the spreading factor would improve these results since it can significantly contribute to the reduction of ISI.

In this sense, Figure 4.3 provides insights into the impact of the spreading factor relative to the BER performances of the MU-FTN-DCSK system for an SNR=25dB. The sampling parameter takes the values $\rho_{(p)} = \{0.9, 0.8, 0.7, 0.6, 0.5\}$ with $\rho_{(d)} = 0.9$ for the desired user. As observed in this figure, increasing β positively impacts the system's capability to reduce the

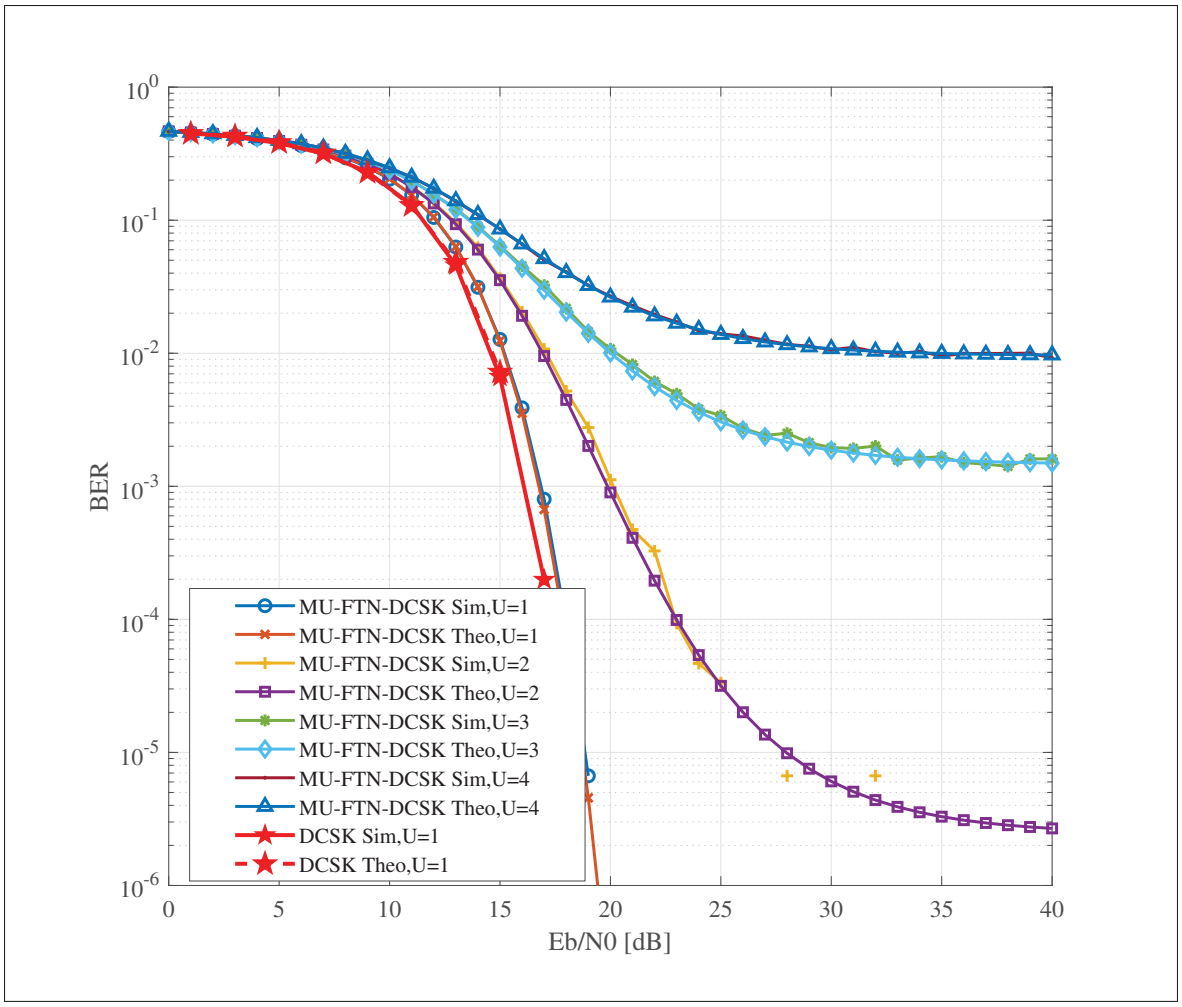

Figure 4.2 BER performance of MU-FTN-DCSK over AWGN Channel with Different Number of Users U=$\{1, 2, 3, 4\}$, $\beta = 150$, $\rho_{(d)} = 0.9$, $\rho_{(p)} = \{0.8, 0.7, 0.6\}$

ISI for a certain range before reaching a plateau of BER performances centered around certain values depending on the number of users under consideration. Notably, after these specific values, higher BER values are observed. However, the value of β is also limited by the desired data rate, which creates a trade-off.

The BER performance of the MU-FTN-DCSK over multipath Rayleigh fading channels with dissimilar channel gains is presented in Figure 4.4. We can notice from the BER performance of a single user that the degradation caused by the ISI is comparable in magnitude to the

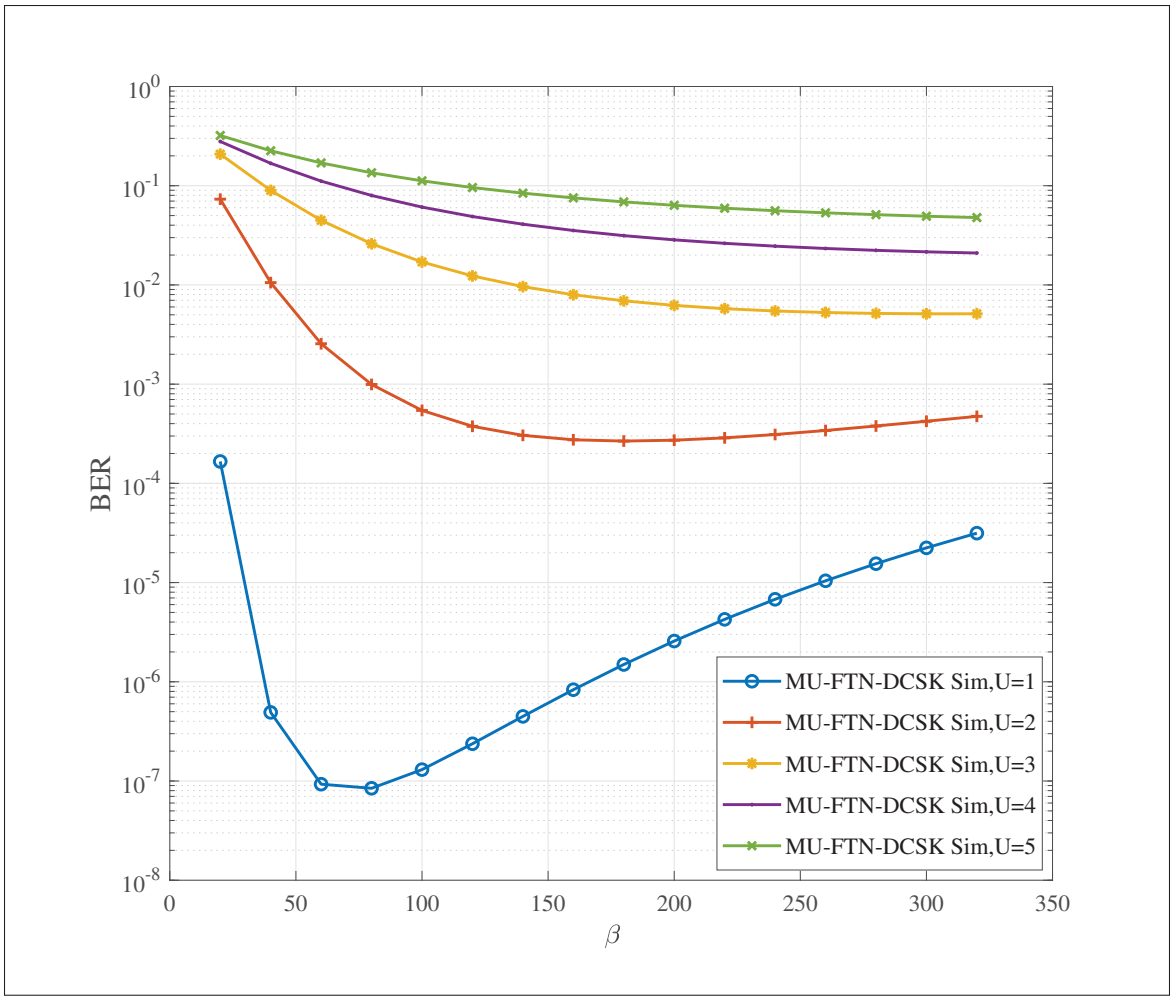

Figure 4.3 BER performance of MU-FTN-DCSK over AWGN Channel for Different Spreading Factors and Number of Users U={1, 2, 3, 4}, $\beta = 150$, $\rho_{(d)} = 0.9$, $\rho_{(p)} = \{0.8, 0.7, 0.6, 0.5\}$, and SNR=25dB

degradation for the AWGN situation. However, now the impact of the floor introduced by the extra Chaos-Chaos interference on the BER, derived in (4.34), is more apparent, regardless of the number of users in the system. Nonetheless, it can be seen that such high ISI has a nearly identical impact on the BER for the number of users superior to two. Moreover, the BER performances in this figure confirm the system's capability to combat multipath loss.

The impact of the sampling rate on the BER performances over AWGN and multipath Rayleigh fading channels is presented for different numbers of users up to a maximum $U =$

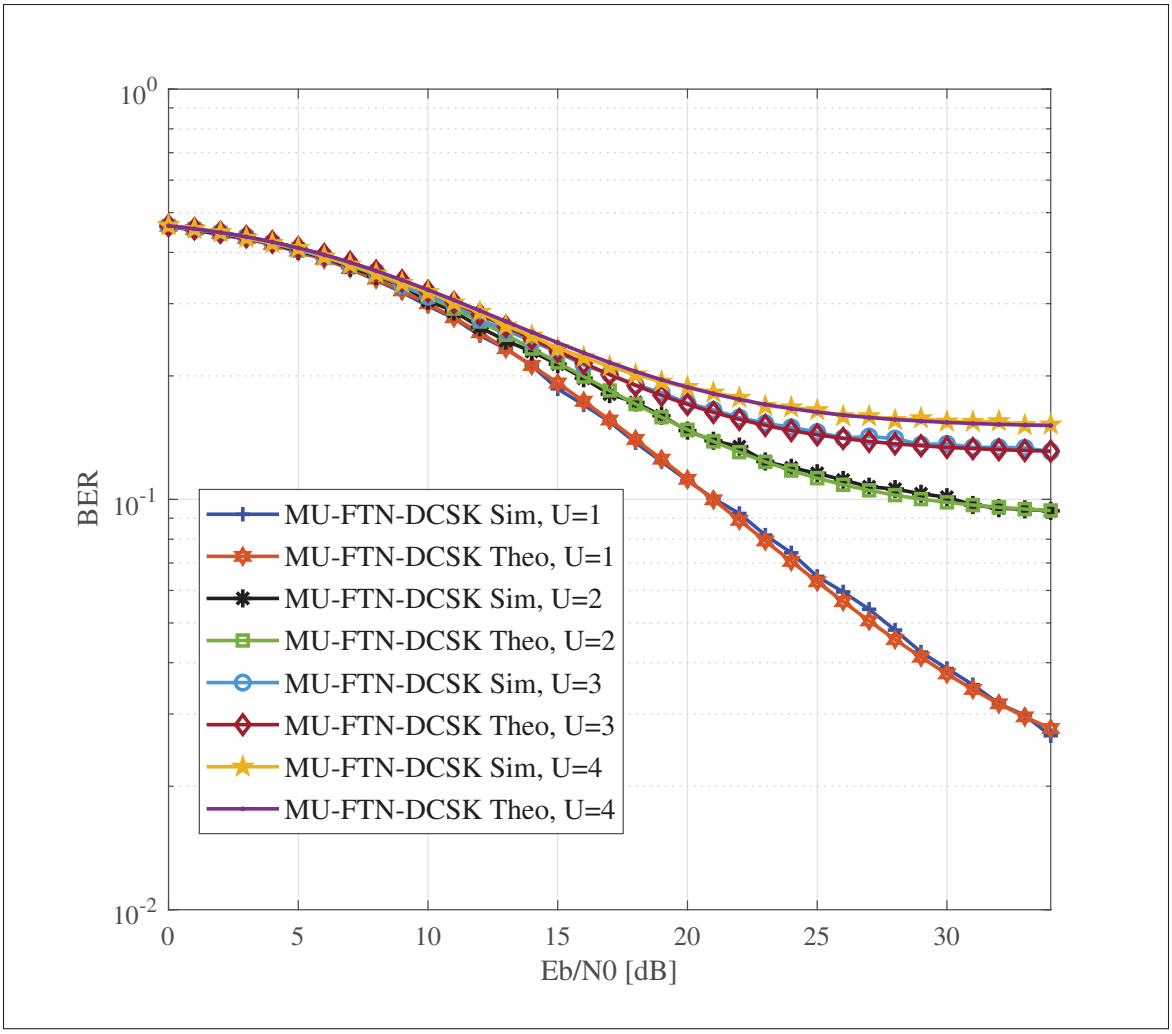

Figure 4.4 BER performance of MU-FTN-DCSK over Rayleigh Channel for a Dissimilar Power Distribution, U={1, 2, 3, 4}, $\beta = 150$, $\rho_{(d)} = 0.9$, $\rho_{(p)} = \{0.8, 0.7, 0.6\}$

9 in Figure 4.5 and Figure 4.6, respectively. An SNR of 30 and a sampling parameter ρ of [0.05, .., 0.95] are used for the primary user, while the other user's sampling parameters are switched in the same range of values, but different from the desired user's sampling parameters in order to enable detection. It is interesting to notice that for a single user, in the high SNR regime, the reduction in sampling rate to half the Nyquist limit ($\rho = 0.5$) does not hinder the MU-FTN-DCSK from having a successful transmission with a good BER performance, especially for the AWGN channel. The same observation can be applied for up to three users in

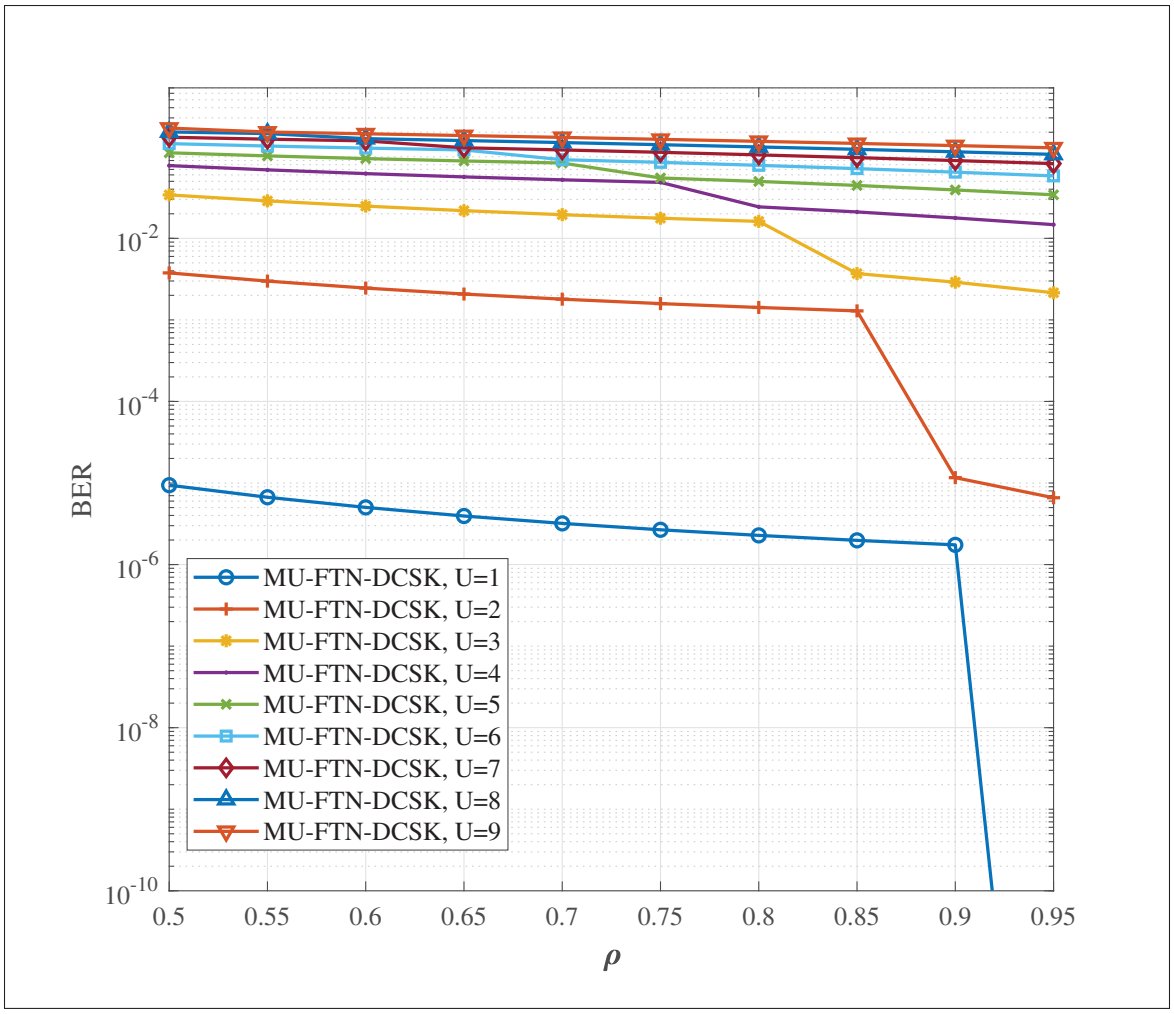

Figure 4.5 BER performance for Different Sampling Rates and Number of Users Over the AWGN Channel, U={1, ...9}, $\beta = 100$, $\rho_{(p)} = \{0.95, 0.9, ..0.5\}$, SNR=30dB.

the system with relatively close sampling rates but for reduced spectral efficiency. As a result, the ISI, despite impacting the system's performance considerably even in the absence of noise, does not prevent a successful transmission, even with a substantial decrease in sampling rates. Therefore, the combination of DCSK with FTN seems very promising in improving the spectral efficiency if the detection can be improved.

The BER performance of the MU-FTN-DCSK system is dictated by the extra interference between the chaotic signals, which does not exist in traditional chaos-based systems. The

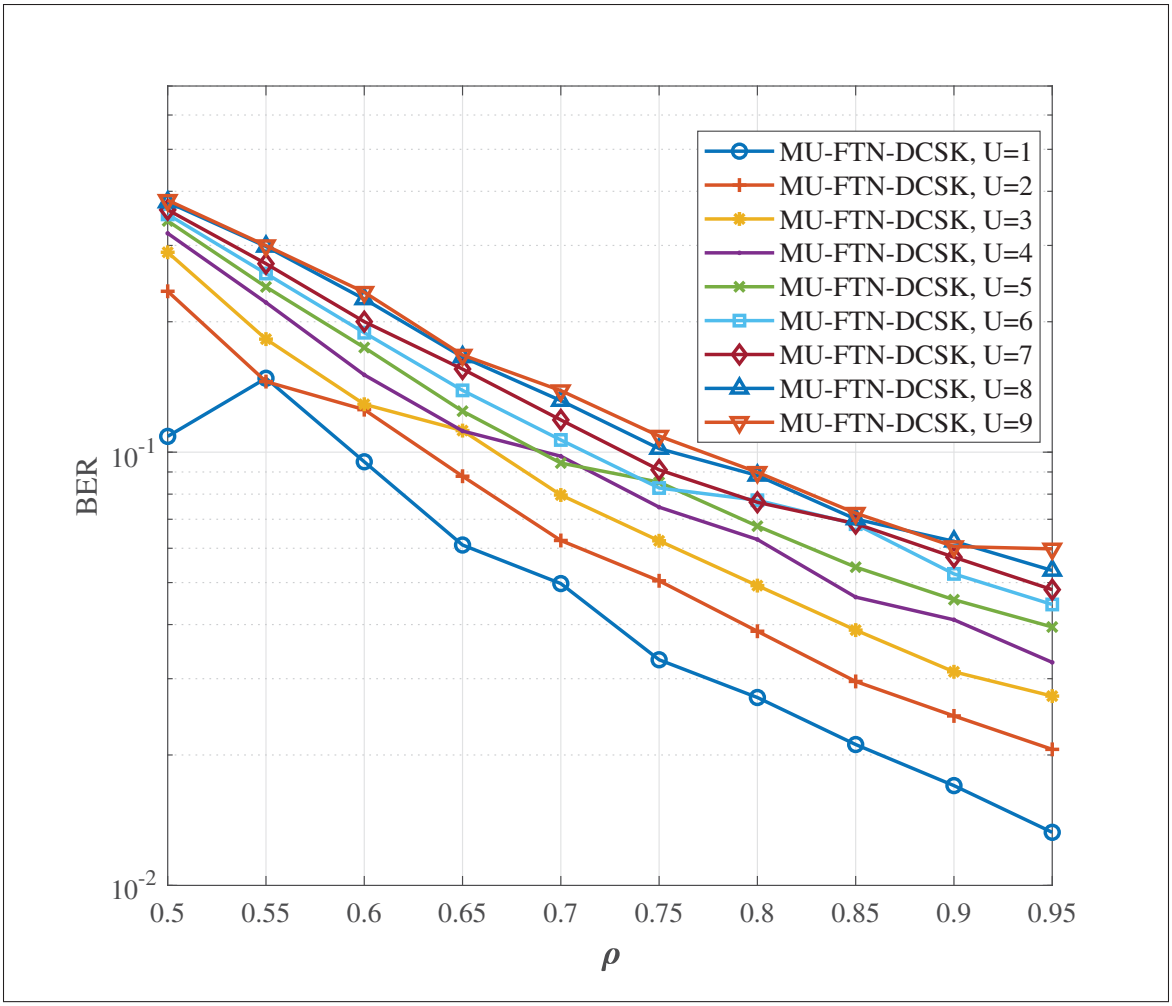

Figure 4.6 BER Performance for Different Sampling Rates and Number of Users Over the Dissimilar Multipath Rayleigh Fading Channel, U={1, ...9}, $\beta = 100$, $\rho_{(p)} = \{0.95, 0.9, ..0.5\}$, SNR=30dB.

chaos-chaos interference is caused solely by the functioning of the sub-Nyquist filters in a similar manner to the ISI. The impact of this new form of interference can be seen in Figure 4.7, where a noise-free channel ($N_0 = 0$) is considered for the transmission. As seen here, the chaos-chaos interference results in a performance floor that establishes the best BER performance that can be obtained for a given number of users. The new form of interference depends on the filter and its sampling rate and is also cumulative to the group of users in the system.

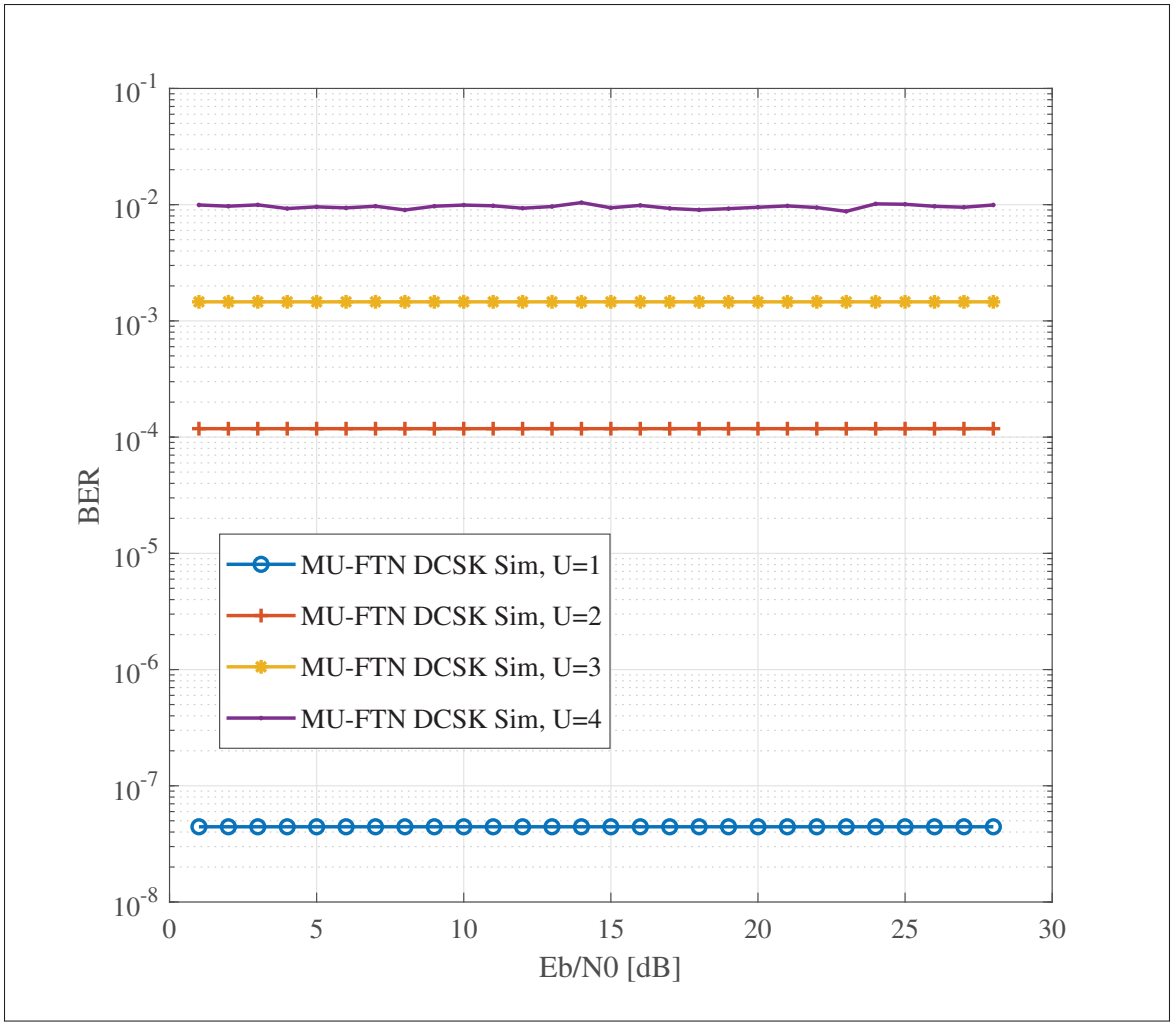

Figure 4.7 BER performance of MU-FTN-DCSK for a Noiseless Channel.

The introduction of the custom-selected sampling rates to enable FTN and multi-user transmission results in an additional feature presented by the MU-FTN-DCSK in terms of security. Indeed, the probability of detection goes to zero if the appropriate sampling rate is not used as presented in Figure 4.8. Using a sampling rate different from the desired users' rate enables perfect secrecy, as seen in the simulation results in Figure 4.8 for $\rho_{(d)} \neq 0.9$. This intuitively comes down to the fact that the use of an erroneous sampling rate subsequently alters the capability of detection of the basic DCSK design, given that the value of β changes by the

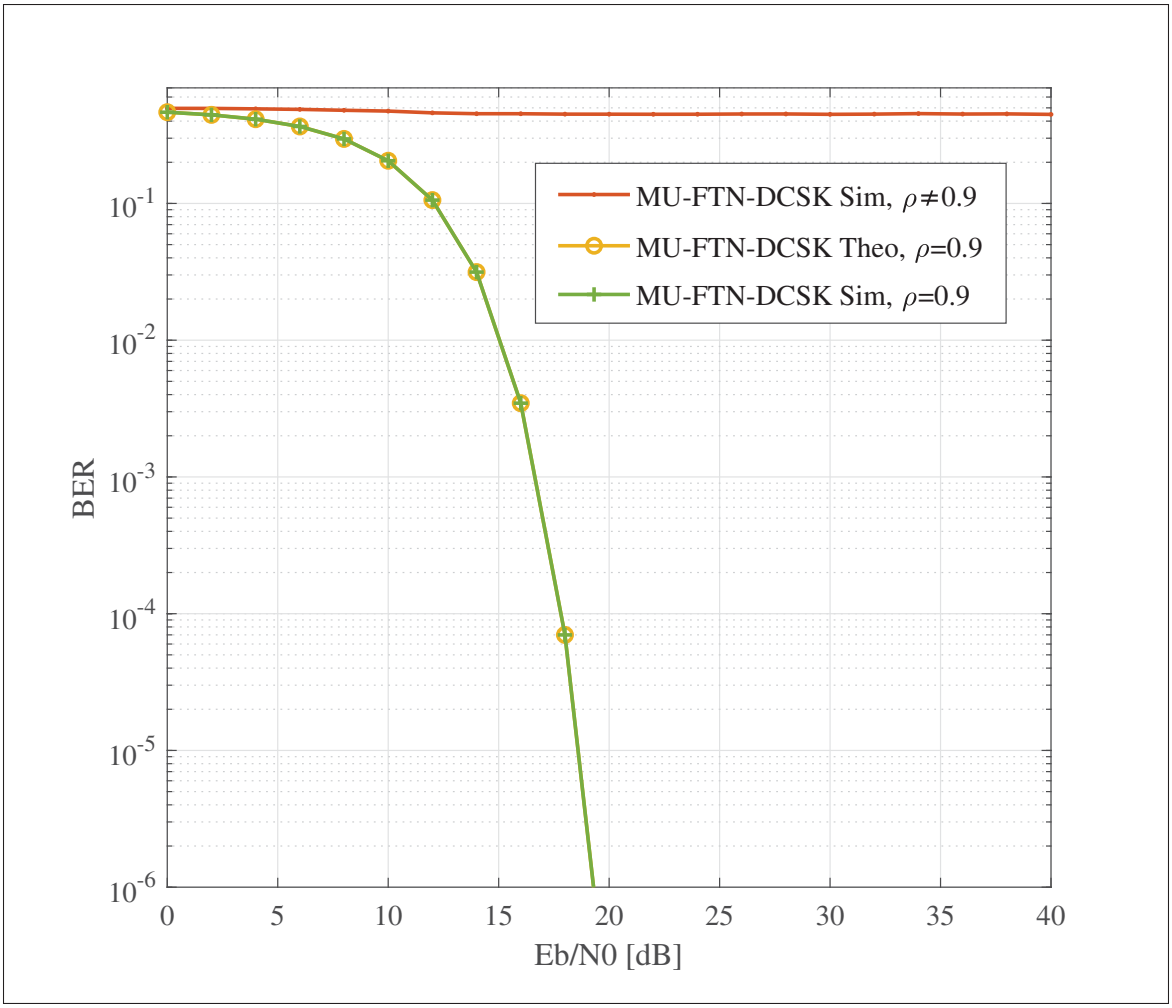

Figure 4.8 BER Performances of MU-FTN-DCSK for a Faulty Sampling Rate.

change of the sampling rate. Hence, MU-FTN-DCSK can be seen as an improved version of DCSK in terms of security since it requires an extra parameter for successful detection.

4.5.2 Performance Comparison

The MU-FTN-DCSK system is compared to newly introduced DCSK-based schemes in order to evaluate its effectiveness as a newly proposed design. In terms of BER performances, the system lags due to the impact of the interferences caused by the functioning of the filter in the FTN regime. For instance, for a multipath Rayleigh fading channel, a difference of 5dB is

observed in comparison with the CIM-MC-M-DCSK MISO-SWIPT system (Cai *et al.*, 2021a). However, the complexity is greatly reduced since the latter system uses many additional signal processing transforms to accomplish the given gain. The table below gives a detailed comparison of the complexity of the two systems. Moreover, the BER performance of MU-FTN-DCSK is comparable to the performance of the GCI-DCSK SWIPT for the AWGN and Rayleigh fading channels. The MU-FTN-DCSK also presents an overall better BER relative to the spreading factor for the single-user scenario.

Table 4.1 Complexity Comparison

Modulation	MU-FTN-DCSK	CIM MC-M-DCSK MISO-SWIPT
Blocks	matched filters	matched filters serial to parallel bit/symbol converter code index modulation Hilbert filter code index modulation Walsh codes

In the addition to the lesser complexity, the MU-FTN-DCSK offers a better spectral efficiency given the same configuration as the CIM-MC-M-DCSK MISO-SWIPT system. For example, for the CIM-MC-M-DCSK MISO-SWIPT system and for a number of antennas N=1 and a modulation order M=2, the spectral efficiency is lower than that of the MU-FTN-DCSK system for any value of the sampling parameter meeting the condition $\rho_{(p)} < 0.65$. In addition, the accumulative spectral efficiency gained from all users transmitting in the FTN regime can be higher than systems having very advanced designs. Furthermore, the results above indicate that using FTN in combination with additional signal processing methods can result in much higher spectral efficiency gains.

4.6 Conclusion and Recommendation

A multi-user Faster than Nyquist DCSK system, where we use transmission/reception filters below the Nyquist required limit to enable a gain in spectral efficiency as well as simultaneous access for multiple users, was presented in this paper. FTN, in combination with DCSK, enables the enhancement of the latter in terms of bandwidth usage, which is one of the main drawbacks of traditional DCSK designs. The newly proposed system enables multi-user access without the addition of complicated blocks or new procedures. Using different sampling rates in FTN is a simple yet very effective design showing promising results. Moreover, several new algorithms have been proposed for optimal FTN detection, which can be added to this conceptual system for improved performance and may even be able to rival coherent chaos-based systems like Chaos Shift Keying (CSK). The performance analysis of the newly proposed system has shown a possible multiple-access of up to three users with good BER results even without additional transmission power or a high spreading factor. Besides, it presents the same resistance to multipath fading as the traditional DCSK systems while going below the Nyquist rate and for multiple users. The newly designed system allows a gain in bandwidth between 10% and 200% of the DCSK reference size, assuming up to four users ($U = 4$), and can go beyond if a better detection algorithm is introduced. One user's gain can vary depending on the sampling parameter value, from 24% at the Mazo limit up to 40% when $\rho = 0.6$. The main challenge encountered during this study was the use of lower sampling rates, as this increases the level of ISI. Moreover, adding new users results in higher levels of IUI which restricts the number of users in the system. The limitation in the number of users or the minimum sampling rates to consider was shown here to be related to the new form of interference between chaos signals that happens to originate from the usage of the filters on non-orthogonal transmissions. Hence, future works will be directed towards improving the detection algorithm in order to eliminate interference and the possibility of applying both time and frequency FTN transmissions. In addition, MIMI-OFDM might be a possible approach in improving BER performances of the current design while keeping the design simple.

CONCLUSION AND RECOMMENDATIONS

5.1 Conclusion

This thesis studies non-coherent chaos-based schemes regarding BER performances and the means to provide better designs that serve as communication schemes for IoT network devices. Mainly targeting low-complexity IoT devices, we study the chaos-based schemes from a theoretical perspective to establish performance benchmarks specifically in terms of BER. Moreover, we tackle the issue of resource limitation and the need for a convenient communication model that suits such requirements.

We reach the first objective in chapters 2 and 3, where we formulate a new theoretical approach to calculating the BER expressions for several non-coherent chaos-based modulations over multipath fading channels.

In chapter 2, we considered the multipath Rayleigh fading for modeling the communication channel. Since the BER of modulations like DCSK, QCSK, and MC-DCSK is established by integrating the product of the BER expression of these systems over the AWGN channel by the PDF of the fading channel, we contribute to the body of literature by proposing a new methodology of derivation to the aforementioned integral. Hitherto, the integral under consideration was deemed theoretically unsolvable since it combines the error function (*erfc*) with a complex argument to the PDF of the channel, resulting in an expression for which no straightforward anti-derivative can be derived. We proposed to replace the *erfc* with an equivalent exponential term. The exponential term is afterward lower bounded using a traditional lower bound to the exponential function. Hence, the product of the newly proposed lower bound with the PDF of the channel led to an anti-derivative and to the theoretical resolution of the integral. Our simulations of the systems under consideration match the newly proposed lower bound with very tiny gaps for a different number of paths of the multipath Rayleigh fading channel.

Chapter 3 extended the work described in chapter 2, where we explored a more generalized model for the fading channel. Using the methodology developed in chapter 2, we replaced the PDF of the channel and considered the Nakagami-m model instead. The same derivation steps were followed, resulting in a new purely analytical expression of the BER of multiple non-coherent chaos-based schemes. The new BER expressions were tested against the previous BER results obtained via numerical integration and simulation of the systems, and a good match was found. Besides confirming the validity of the methodology of derivation for a more complex channel model, the analysis provided insights on the potential use of such lower bounds in the study of non-coherent chaos-based modulations and the now possible easy implementation of such performance measurement metrics on low complexity devices.

Chapter 4 was dedicated to improving the most critical aspect of non-coherent chaos-based schemes, which is using reference sequences to enable non-coherent detection. We proposed a new design based on exploiting the FTN signaling to enable faster transmissions. Although the design consisted of only combining the basic DCSK schemes with a matched filter functioning in the FTN regime, it proved to be an efficient modulation in terms of spectral efficiency and data-rate. The use of FTN enabled multiple access for users transmitting at different sampling rates resulting in a new form of orthogonality. Up to 3 or 4 users were shown to simultaneously transmit their data using the FTN-DCSK system model while guaranteeing a successful detection but at the cost of transmitting at a high SNR. We have also shown that the number of users depends on the level of acceptable ISI and the desired BER performances offered by the system since the asynchronous access from different users, all transmitting at FTN rates, resulted in additional forms of inter-user interferences. Nonetheless, the MU-FTN-DCSK design offers promising spectral efficiency performances that only depend on the allowed reduction in the sampling rates. The model can also be seen as a great candidate for low-complexity IoT devices such as sensors, guaranteeing by such, the security offered by the use of the chaotic waveform,

the multi-user access, and a gain in spectral efficiency without additional blocks that would burden the implementation on such devices.

5.2 Future Works

The future of chaos-based communications for IoT applications revolves around designing low-complexity systems with improved security since advanced security protocols and methods cannot be applied to devices with limited resources.

5.2.1 Improved FTN Detection

The use of the FTN filter coupled with the basic DCSK design without any additional blocks is undoubtedly simple yet not optimal. The ISI introduced by the non-orthogonality of the transmitted waveforms cannot be eliminated using the simple non-coherent scheme alone. Few advanced detection algorithms, such as the BCJR, can be implemented in order to combat the newly introduced ISI. In (Prlja & Anderson, 2012), the M-BCJR is demonstrated to eliminate the severe levels of ISI introduced by the FTN filters, hence combining it with the design provided in chapter 4 would lead to an improved BER performance. The BCJR was shown to offer an approximate 4dB of BER improvement, making its application to the FTN-DCSK result in a BER performance superior to the regular DCSK for up to 2 users and, as a result, immediate multiple access with up to 30% of spectral efficiency. Therefore, the following possible topics for future works are envisioned:

- Introduce the BCJR algorithm in combination with the FTN-DCSK for improved detection.
- Provide a simplified BER expression describing the system performances over the multipath fading channels. This can be done by solving the sums introduced in chapter 4 for the BER derivation.
- Provide a new approach to eliminating chaos-chaos ISI introduced by the FTN filtering.

5.2.2 Synchronization of Multiple Chaotic Maps

Using multiple chaotic maps can enhance the data rate by a factor of M, representing the number of deployed maps. Indeed, if multiple maps transmit multiple overlapping streams through the channel and each decoupled from the other maps, then the data rate can be multiplied multiple times. In addition, the level of privacy should be very high since any attack on the ongoing communication must decode the different maps to retrieve the message. This can be very challenging if multiple chaotic map signals are routed through the radio channel. Multiple maps can only be combined if they can be separated and successfully synchronized at the receiver side. The last work of T.L.Caroll in (Carroll & Byers, 2016) is a promising approach toward multiple chaotic map synchronization. The proposed approach is to subdivide the chaotic signal into multiple sub-streams that are non-chaotic. The resulting sub-streams are then transmitted separately and reconstructed in the receiver using a Viterbi decoder. The level of privacy is thus enhanced since the differently transmitted sub-streams are independent, as a result minimizing the probability of interception. A similar approach can be applied to multiple chaotic maps streams for higher privacy and also a higher data rate. The biggest challenge would be the possibility of separating the different maps' signals at the receiver. For future work on this theme, the following approaches can be considered,

- Modeling the transmission of multiple chaotic maps issued from the same attractor, like Lorenz's, via the multi-dimensional equations.
- Apply the approach provided in (Carroll & Byers, 2016) for synchronizing the chaotic streams.
- Propose a separation algorithm to differentiate the source of the incoming signals in the receiver and their respective chaotic generators.

5.2.3 FTN-OFDM DCSK

The use of OFDM has been applied, taking into consideration the Nyquist limit. However, with the introduction of FTN, the application can be reviewed as shown in (Zhou *et al.*, 2017) where combining OFDM and FTN is possible without compromising the system performance; as such, using FTN-OFDM would make it Non-Orthogonal (FTN-NOFDM). With DCSK and its natural capability to combat interferences, it would allow for a new high-performing system with important gains in terms of spectral efficiency. With a Mazo limit of = 0.8 the gain is about 24% in terms of spectral efficiency, hence, its generalization to the OFDM context would ensure a similar gain on every sub-carrier and an overall gain of $24\% \times Number\ of\ carriers$. The already existing approaches to the optimization of OFDM can then be applied in order to tackle the interference issues resulting from the introduction of FTN. The following approach might be considered for the design and study of this system.

- Simulate the BPSK scenario for an FTN-NOFDM system to isolate the performance achieved by the system in an optimal scenario.
- Replace the BPSK carriers with DCSK references and apply the DCSK detection algorithm.
- Study the new system's performances for different channel models with the possibility of changing the design to accommodate additional blocks that may enhance its performances.

AUTHOR'S PUBLICATIONS

During this Ph.D. research, the author contributed to the following published and submitted research articles.

M. Dawa, M.Herceg, and G. Kaddoum , Design and analysis of Multi-user Faster-Than-Nyquist-DCSK communication systems over multipath fading channels, MDPI Sensors, Sept. 2022.

M. Dawa, G. Kaddoum and M.Herceg, A Framework for the Lower Bound on the BER of DCSK Systems over multipath Nakagami-m Fading Channels, IEEE Transactions on Circuits and Systems II: Express Briefs, vol. 67, no. 10, pp. 1859 - 1863, Oct. 2020.

M. Dawa, G. Kaddoum and Z. Sattar, A Generalized Lower Bound on the Bit Error Rate of DCSK Systems Over multipath Rayleigh Fading Channels, IEEE Transactions on Circuits and Systems II: Express Briefs, vol. 65, no. 3, pp. 321-325, March 2018.

BIBLIOGRAPHY

(2015). *SECURITY IN THE INTERNET OF THINGS: Lessons from the Past for the Connected Future*.

3GPP. (2017). *Study on Scenarios and Requirements for Next Generation Access Technologies, (Report n∘38.913).*

802.15.4-2015, I. S. (2016). IEEE Standard for Low-Rate Wireless Networks. *IEEE Std 802.15.4-2015 (Revision of IEEE Std 802.15.4-2011)*, 1-709. doi: 10.1109/IEEESTD.2016.7460875.

Abdullah, H. N. (2012). Design of high data rate FM-QCSK chaotic communication system. *Journal of Wireless Networking and Communications*, 2(4), 49–54.

Abraham-Frois, G. (1998). *Non-linear dynamics and endogenous cycles*. Springer Science & Business Media.

Abreu, G. T. F. D. (2009). Jensen-cotes upper and lower bounds on the Gaussian Q-function and related functions. *IEEE Trans. Commun.*, 57(11), 3328-3338. doi: 10.1109/T-COMM.2009.11.080479.

Adame, B. O. & Salau, A. O. (2022). Genetic Algorithm Based Optimum Finger Selection for Adaptive Minimum Mean Square Error Rake Receivers Discrete Sequence-CDMA Ultra-Wide Band Systems. *Wirel. Pers. Commun.*, 123(2), 1537–1551. doi: 10.1007/s11277-021-09199-0.

Al-Fuqaha, A., Guizani, M., Mohammadi, M., Aledhari, M. & Ayyash, M. (2015). Internet of Things: A Survey on Enabling Technologies, Protocols, and Applications. *IEEE Communications Surveys Tutorials*, 17(4), 2347-2376. doi: 10.1109/COMST.2015.2444095.

Anderson, J. B., Rusek, F. & Öwall, V. (2013). Faster-Than-Nyquist Signaling. *Proceedings of the IEEE*, 101(8), 1817-1830. doi: 10.1109/JPROC.2012.2233451.

Andrews, J. G., Buzzi, S., Choi, W., Hanly, S. V., Lozano, A., Soong, A. C. & Zhang, J. C. (2014). What will 5G be? *IEEE Journal on selected areas in communications*, 32(6), 1065–1082.

Arnold, L. & Wihstutz, V. (1986). Lyapunov exponents: a survey. In *Lyapunov Exponents* (pp. 1–26). Springer.

Bae, J. G. & Kim, S.-H. (2009a). On a generalization of an upper bound for the exponential function. *J. of Math. Anal. and Applicat.*, 353(1), 1 - 7.

Bae, J. G. & Kim, S.-H. (2009b). On a generalization of an upper bound for the exponential function. *J. of Math. Anal. and Applicat.*, 353(1), 1 - 7. doi: http://dx.doi.org/10.1016/j.jmaa.2008.03.034.

Bahl, L., Cocke, J., Jelinek, F. & Raviv, J. (1974). Optimal decoding of linear codes for minimizing symbol error rate. *IEEE Trans. on Inf. Theory*, 20(2), 284-287. doi: 10.1109/TIT.1974.1055186.

Başar, E., Aygölü, , Panayırcı, E. & Poor, H. V. (2013). Orthogonal Frequency Division Multiplexing With Index Modulation. *IEEE Trans. on Signal Process.*, 61(22), 5536-5549.

Bedeer, E., Ahmed, M. H. & Yanikomeroglu, H. (2017). Low-Complexity Detection of High-Order QAM Faster-Than-Nyquist Signaling. *IEEE Access*, 5, 14579-14588. doi: 10.1109/ACCESS.2017.2719628.

Benchaabene, Y., Boujnah, N. & Zarai, F. (2017). 5G Cellular: Survey on Some Challenging Techniques. *2017 18th International Conference on Parallel and Distributed Computing, Applications and Technologies (PDCAT)*, pp. 348-353. doi: 10.1109/PDCAT.2017.00064.

Cai, G. & Song, Y. (2020). Closed-Form BER Expressions of M-Ary DCSK Systems Over Multipath Rayleigh Fading Channels. *IEEE Communications Letters*, 24(6), 1192-1196. doi: 10.1109/LCOMM.2020.2981060.

Cai, G., Fang, Y., Wen, J., Mumtaz, S., Song, Y. & Frascolla, V. (2019). Multi-Carrier M-ary DCSK System With Code Index Modulation: An Efficient Solution for Chaotic Communications. *IEEE J. of Select. Topics in Signal Process.*, 13(6), 1375–1386.

Cai, G., Fang, Y., Chen, P., Han, G., Cai, G. & Song, Y. (2021a). Design of an MISO-SWIPT-Aided Code-Index Modulated Multi-Carrier M-DCSK System for e-Health IoT. *IEEE Journal on Selected Areas in Communications*, 39(2), 311-324. doi: 10.1109/JSAC.2020.3020603.

Cai, X., Xu, W., Hong, S. & Wang, L. (2021b). Discrete W Transform Based Index-Keying M-Ary DCSK for Non-Coherent Chaotic Communications. *IEEE Communications Letters*, 25(9), 3104-3108. doi: 10.1109/LCOMM.2021.3095075.

Carroll, T. & Byers, J. (2016). Grid-based partitioning for comparing attractors. *Physical Review E*, 93(4), 042206.

Chang, S.-H., Cosman, P. C. & Milstein, L. B. (2011). Chernoff-type bounds for the Gaussian error function. *IEEE Trans. on Commun.*, 59(11), 2939–2944.

Chen, H., Chen, P., Fang, Y., Chen, F. & Kong, L. (2022). Parallel Differential Chaotic Shift Keying With Code Index Modulation for Wireless Communication. *IEEE Transactions on Communications*, 70(8), 5113-5127. doi: 10.1109/TCOMM.2022.3187158.

Chen, L., Xu, W. & Wang, L. (2008). Performance of improved FM-DCSK system based on differential-coding method. *Communications, Circuits and Systems, 2008. ICCCAS 2008. International Conference on*, pp. 1224–1227.

Chen, S., Wang, L. & Chen, G. (2010). Data-aided timing synchronization for FM-DCSK UWB communication systems. *IEEE Transactions on Industrial Electronics*, 57(5), 1538–1545.

Chen, Z., Zhang, L., Wu, Z., Wang, L. & Xu, W. (2020). Reliable and Efficient Sparse Code Spreading Aided MC-DCSK Transceiver Design for Multiuser Transmissions. *IEEE Trans. on Commun.*, 1-1.

Chen, Z., Zhang, L., Wang, W. & Wu, Z. (2021). A Pre-Coded Multi-Carrier M-ary Chaotic Vector Cyclic Shift Keying Transceiver for Reliable Communications. *IEEE Trans. Wireless Commun.*, 1-1. doi: 10.1109/TWC.2021.3100620.

Cheng, G., Wang, L., Xu, W. & Chen, G. (2016). Carrier Index Differential Chaos Shift Keying Modulation. *IEEE Trans. Circuits Syst. II, Exp. Briefs: Exp. Briefs*, PP(99), 1-1. doi: 10.1109/TCSII.2016.2613093.

Cheng, G., Chen, X., Liu, W. & Xiao, W. (2019). GCI-DCSK: Generalized Carrier Index Differential Chaos Shift Keying Modulation. *IEEE Commun. Lett.*, 23(11), 2012-2016. doi: 10.1109/LCOMM.2019.2933827.

Coelho, C. A. (1998). The generalized integer Gamma distribution—a basis for distributions in multivariate statistics. *J. of Multivariate Anal.*, 64(1), 86–102.

Dawa, M., Kaddoum, G. & Sattar, Z. (2018). A Generalized Lower Bound on the Bit Error Rate of DCSK Systems Over Multi-Path Rayleigh Fading Channels. *IEEE Trans. on Circuits and Sys. II: Exp. Briefs*, 65(3), 321-325. doi: 10.1109/TCSII.2017.2733381.

Dawa, M., Kaddoum, G. & Herceg, M. (2019). A framework for the lower bound on the BER of DCSK systems over multi-path Nakagami-m fading channels. *EEE Trans. on Circuits and Sys. II: Exp. Briefs*, 67(10), 1859–1863.

Devaney, R. L., Keen, L. & Alligood, K. T. (1989). *Chaos and fractals: The mathematics behind the computer graphics*. American Mathematical Soc.

Dutta, A. & Hammad, E. (2020). 5G Security Challenges and Opportunities: A System Approach. *2020 IEEE 3rd 5G World Forum (5GWF)*, pp. 109-114. doi: 10.1109/5GWF49715.2020.9221122.

Fan, T., Xu, W., Wang, L. & Zhang, L. (2020). A New APSK-Based M-Ary Differential Chaos Shift Keying Modulation System. *IEEE Commun. Lett.*, 24(12), 2701-2704. doi: 10.1109/LCOMM.2020.3019105.

Fang, Y., J. Xu, L. W. & Chen, G. (2013). Performance of MIMO relay DCSK-CD systems over Nakagami fading channels. *IEEE Trans. on Circuits and Syst. I: Reg. Papers*, 60, 757-767.

Galias, Z. & Maggio, G. M. (2001). Quadrature chaos-shift keying: theory and performance analysis. *IEEE Trans. Circuits Syst. I: Fundam. Theory Appl.*, 48(12), 1510-1519. doi: 10.1109/TCSI.2001.972858.

Ge, X., Cheng, H., Guizani, M. & Han, T. (2014). 5G wireless backhaul networks: challenges and research advances. *IEEE Network*, 28(6), 6–11.

Geisel, T. & Fairen, V. (1984). Statistical properties of chaos in Chebyshev maps. *Physics Letters A*, 105(6), 263 - 266.

Goldsmith, A. (2005). *Wireless communications*. Cambridge university press.

Gradshteyn, I. S. & Ryzhik, I. M. (2014). *Table of integrals, series, and products*. Academic press.

Herceg, M., Kaddoum, G., Vranješ, D. & Soujeri, E. (2018). Permutation Index DCSK Modulation Technique for Secure Multiuser High-Data-Rate Communication Systems. *IEEE Trans. Veh. Technol.*, 67(4), 2997-3011. doi: 10.1109/TVT.2017.2774108.

Herceg, M., Vranješ, D., Kaddoum, G. & Soujeri, E. (2018). Commutation Code Index DCSK modulation technique for high-data-rate communication systems. *IEEE Trans. on Circuits and Sys. II: Exp. Briefs*.

Hilborn, R. C., Coppersmith, S., Mallinckrodt, A. J., McKay, S. et al. (1994). Chaos and nonlinear dynamics: an introduction for scientists and engineers. *Computers in Physics*, 8(6), 689–689.

Hirzallah, M., Krunz, M., Kecicioglu, B. & Hamzeh, B. (2021). 5G New Radio Unlicensed: Challenges and Evaluation. *IEEE Transactions on Cognitive Communications and Networking*, 7(3), 689-701. doi: 10.1109/TCCN.2020.3041851.

Horowitz, E. (1971). Algorithms for partial fraction decomposition and rational function integration. *Proc. of the second ACM Symp. on Symbolic and algebraic manipulation*, pp. 441–457.

Huang, T., Wang, L., Xu, W. & Lau, F. C. M. (2016). Multilevel code-shifted differential-chaos-shift-keying system. *IET Commun.*, 10(10), 1189-1195. doi: 10.1049/iet-com.2015.1109.

Ishihara, T. & Sugiura, S. (2018). Faster-Than-Nyquist Signaling with Differential Encoding and Non Coherent Detection. *2018 IEEE International Conference on Acoustics, Speech and Signal Processing (ICASSP)*, pp. 3734-3738. doi: 10.1109/ICASSP.2018.8462455.

ITU-R, 2015. (2015). *IMT Vision–Framework and overall objectives of the future development of IMT for 2020 and beyond.*

Kaddoum, G. (2016a). Wireless Chaos-Based Communication Systems: A Comprehensive Survey. *IEEE Access*, 4, 2621-2648. doi: 10.1109/ACCESS.2016.2572730.

Kaddoum, G. & Soujeri, E. (2016). NR-DCSK: A Noise Reduction Differential Chaos Shift Keying System. *IEEE Trans. Circuits Syst. II, Exp. Briefs: Exp. Briefs*, 63(7), 648-652. doi: 10.1109/TCSII.2016.2532041.

Kaddoum, G., Richardson, F. & Gagnon, F. (2013a). Design and Analysis of a Multi-Carrier Differential Chaos Shift Keying Communication System. *IEEE Trans. Commun.*, 61(8), 3281-3291.

Kaddoum, G., Tran, H. V., Kong, L. & Atallah, M. (2016). Design of Simultaneous Wireless Information and Power Transfer Scheme for Short Reference DCSK Communication Systems. *IEEE Trans. Commun.*, PP(99), 1-1. doi: 10.1109/TCOMM.2016.2619707.

Kaddoum, G. (2016b). Design and Performance Analysis of a Multiuser OFDM Based Differential Chaos Shift Keying Communication System. *IEEE Trans. on Communications*, 64(1), 249-260. doi: 10.1109/TCOMM.2015.2502259.

Kaddoum, G., Chargé, P. & Roviras, D. (2009). A generalized methodology for bit-error-rate prediction in correlation-based communication schemes using chaos. *IEEE Commun. Lett.*, 13(8), 567–569. doi: http://dx.doi.org/10.1109/LCOMM.2009.090715.

Kaddoum, G., Richardson, F., Adouni, S., Gagnon, F. & Thibeault, C. (2013b). Multi-User Multi-Carrier Differential Chaos Shift Keying Communication System. *CoRR*, abs/1303.2552. Retrieved from: http://arxiv.org/abs/1303.2552.

Kaddoum, G., Richardson, F.-D., Adouni, S., Gagnon, F. & Thibeault, C. (2013c). Multi-user multi-carrier differential chaos shift keying communication system. *Wireless Communications and Mobile Computing Conference (IWCMC), 2013 9th International*, pp. 1798–1802.

Kaddoum, G., Richardson, F.-D. & Gagnon, F. (2013d). Design and analysis of a multi-carrier differential chaos shift keying communication system. *IEEE Trans. on Commun.*, 61(8), 3281–3291.

Karagiannidis, G. K., Sagias, N. C. & Tsiftsis, T. A. (2006). Closed-form statistics for the sum of squared Nakagami-m variates and its applications. *IEEE Trans. on Commun.*, 54(8), 1353–1359.

Khan, R., Khan, S. U., Zaheer, R. & Khan, S. (2012). Future internet: the internet of things architecture, possible applications and key challenges. *Frontiers of Information Technology (FIT), 2012 10th International Conference on*, pp. 257–260.

Kirchgraber, U. & Stoffer, D. (1989). On the definition of chaos. *ZAMM-Journal of Applied Mathematics and Mechanics/Zeitschrift für Angewandte Mathematik und Mechanik*, 69(7), 175–185.

Kolumbán, G., Kis, G., Kenedy, M. P. & Jáko, Z. (1997). FM-DCSK: a new and robust solution to chaos communications. *Proc. Int. Symp. on nonlinear theory and its applications*, pp. 117-120.

Kolumbán, G., Kis, G., Jákó, Z. & Kennedy, M. P. (1998). FM-DCSK: A Robust Modulation Scheme for Chaotic Communications. *IEICE Trans. Fundamentals of Electronics, Communications and Computer*, 89, 1798-1802.

Kolumbán, G., Vizvári, B., Schwarz, W. & Abel, A. (1996). Differential chaos shift keying: A robust coding for chaos communication. *Proc. NDES*, 96, 87–92.

Kramer, G. (2008). *Topics in Multi-User Information Theory*.

Lau, F. C. M. & Tse, C. K. (2003). *Chaos-Based Digital communication systems*. Springer-Verlag.

Lau, F. C., Cheong, K. Y. & Tse, C. (2002). A permutation-based multiple access DCSK system. *Proc. International Symposium on Nonlinear Theory and Its Applications, Xi'an, China*, pp. 511–514.

Li, H., Dai, X. & Xu, P. (2004). A CDMA based multiple-access scheme for DCSK. *Proceedings of the IEEE 6th Circuits and Systems Symposium on Emerging Technologies: Frontiers of Mobile and Wireless Communication (IEEE Cat. No.04EX710)*, 1, 313-316 Vol.1. doi: 10.1109/CASSET.2004.1322985.

Li, S., Zhao, Y., He, L., Wu, Z. & Li, Y. (2016, Jan). Design and performance analysis of a GFDM-DCSK communication system. *2016 13th IEEE Annu. Consumer Commun. Networking Conf. (CCNC)*, pp. 802-803. doi: 10.1109/CCNC.2016.7444885.

Li, S., Yuan, J., Bai, B. & Benvenuto, N. (2020a). Code-Based Channel Shortening for Faster-Than-Nyquist Signaling: Reduced-Complexity Detection and Code Design. *IEEE Trans. Commun.*, 68(7), 3996-4011. doi: 10.1109/TCOMM.2020.2988922.

Li, S., Yuan, W., Yuan, J., Bai, B., Wing Kwan Ng, D. & Hanzo, L. (2020b). Time-Domain vs. Frequency-Domain Equalization for FTN Signaling. *IEEE Trans. Veh. Technol.*, 69(8), 9174-9179. doi: 10.1109/TVT.2020.3000074.

Litvinenko, A. & Aboltins, A. (2016). Selection and performance analysis of chaotic spreading sequences for DS-CDMA systems. *2016 Advances in Wireless and Optical Communications (RTUWO)*, pp. 38-45. doi: 10.1109/RTUWO.2016.7821852.

Liu, B., Li, S., Xie, Y. & Yuan, J. (2019). Deep Learning Assisted Sum-Product Detection Algorithm for Faster-than-Nyquist Signaling. *2019 IEEE Inform. Theory Workshop (ITW)*, pp. 1-5. doi: 10.1109/ITW44776.2019.8989271.

Liu, S., Chen, P. & Chen, G. (2021). Differential Permutation Index DCSK Modulation for Chaotic Communication System. *IEEE Communications Letters*, 25(6), 2029-2033. doi: 10.1109/LCOMM.2021.3061675.

Liu, Z., Zhang, L. & Chen, Z. (2018). Low PAPR OFDM-Based DCSK Design With Carrier Interferometry Spreading Codes. *IEEE Communications Letters*, 22(8), 1588-1591. doi: 10.1109/LCOMM.2018.2842196.

Liu, Z., Zhang, L., Wu, Z. & Bian, J. (2019). Carrier Interferometry Code Index Modulation Aided OFDM-Based DCSK Communications. *2019 IEEE 90th Vehicular Technology Conference (VTC2019-Fall)*, pp. 1-5. doi: 10.1109/VTCFall.2019.8891582.

Liu, Z., Zhang, L. & Wu, Z. (2020a). Reliable and Secure Pre-Coding OFDM-DCSK Design for Practical Cognitive Radio Systems With the Carrier Frequency Offset. *IEEE Transactions on Cognitive Communications and Networking*, 6(1), 189-200. doi: 10.1109/TCCN.2019.2959332.

Liu, Z., Zhang, L., Wu, Z. & Bian, J. (2020b). A Secure and Robust Frequency and Time Diversity Aided OFDM–DCSK Modulation System Not Requiring Channel State Information. *IEEE Transactions on Communications*, 68(3), 1684-1697. doi: 10.1109/TCOMM.2019.2951512.

Liu, Z., Zhang, L., Wu, Z. & Jiang, Y. (2020c). Energy Efficient Parallel Concatenated Index Modulation and M-ary PSK Aided OFDM-DCSK Communications With QoS Consideration. *IEEE Trans. Veh. Technol.*, 69(9), 9469-9482. doi: 10.1109/TVT.2020.3002067.

Lu, Q., Li, S., Bai, B. & Yuan, J. (2022). Spatially-Coupled Faster-than-Nyquist Signaling: A Joint Solution to Detection and Code Design. *IEEE Transactions on Communications*.

Ma, H., Cai, G., Fang, Y., Chen, P. & Chen, G. (2020). Design of a Superposition Coding PPM-DCSK System for Downlink Multi-User Transmission. *IEEE Trans. on Veh. Technol.*, 69(2), 1666-1678. doi: 10.1109/TVT.2019.2958418.

Maali, A., Boukhelifa, A., Mesloub, A., Sadoudi, S. & Benssalah, M. (2019). An Enhanced Pulse Position Modulation (PPM) for Both IR-UWB and DCC-UWB Communication. *2019 13th European Conference on Antennas and Propagation (EuCAP)*, pp. 1-5.

Mandal, S. & Banerjee, S. (2002). Performance of differential chaos shift keying communication over multipath fading channels. *Trans. IEICE*, 1-10.

Manoharan, S., Saraff, N., Kedia, A. & Saroja, K. L. (2019). NR-DCSK-Based MIMO Chaotic Communication System. In *Wireless Commun. Networks and Internet of Things* (pp. 207–215). Springer.

Mazo, J. E. (1975). Faster-than-Nyquist signaling. *The Bell System Technical Journal*, 54(8), 1451–1462.

Mazo, J. E. & Landau, H. J. (1988). On the minimum distance problem for faster-than-Nyquist signaling. *IEEE Transactions on Information Theory*, 34(6), 1420–1427.

Miao, M., Wang, L. & Chen, G. (2022). Performance and Capacity Analysis of MDCSK-BICM for Impulsive Noise in PLC. *IEEE Transactions on Power Delivery*, 37(4), 3164-3175. doi: 10.1109/TPWRD.2021.3124561.

Mobini, M. & Zahabi, M. R. (2019). Multivariable optimisation approach for power allocation in OFDM-DCSK system. *IET Communications*, 13(13), 1869–1876.

Munirathinam, R., Aboltins, A., Pikulins, D. & Grizans, J. (2021). Chaotic Non-Coherent Pulse Position Modulation Based Ultra- Wideband Communication System. *2021 IEEE Microwave Theory and Techniques in Wireless Communications (MTTW)*, pp. 1-6. doi: 10.1109/MTTW53539.2021.9607075.

Otayf, N. & Abbas, M. (2022). A Comparative Analysis of Energy Consumption in Wireless Sensor Networks. In *Pervasive Computing and Social Networking* (pp. 113–126). Springer.

Painuly, S., Sharma, S. & Matta, P. (2021). Future Trends and Challenges in Next Generation Smart Application of 5G-IoT. *2021 5th International Conference on Computing Methodologies and Communication (ICCMC)*, pp. 354-357. doi: 10.1109/ICCMC51019.2021.9418471.

Papoulis, A. (1984). *Probability, Random Variables, and Stochastic Processes, 2nd ed.* mcgraw.

Pecora, L. M., Carroll, T. L., Johnson, G. A., Mar, D. J. & Heagy, J. F. (1997). Fundamentals of synchronization in chaotic systems, concepts, and applications. *Chaos: An Interdisciplinary Journal of Nonlinear Science*, 7(4), 520–543.

Petitpied, T., Tajan, R., Chevalier, P., Ferré, G. & Traverso, S. (2020). A Frequency-Domain EP-based Receiver for Faster-Than-Nyquist Signaling. *2020 IEEE 21st Int. Workshop on Signal Process. Advances in Wireless Commun. (SPAWC)*, pp. 1-5. doi: 10.1109/SPAWC48557.2020.9154339.

Prlja, A. & Anderson, J. B. (2012). Reduced-Complexity Receivers for Strongly Narrowband Intersymbol Interference Introduced by Faster-than-Nyquist Signaling. *IEEE Transactions on Communications*, 60(9), 2591-2601. doi: 10.1109/TCOMM.2012.070912.110296.

Que, D. T., Quyen, N. X. & Hoang, T. M. (2021). Performance of Improved-DCSK system over land mobile satellite channel under effect of time-reversed chaotic sequences. *Physical Communication*, 47, 101342. doi: https://doi.org/10.1016/j.phycom.2021.101342.

Ringh, E. (2013). Low complexity algorithm for faster-than-Nyquist signaling: using coding to avoid an NP-hard problem. *Master of Science thesis, Stockholm, Sweden: Royal Institute of Technology*.

Silva, C. P. & Young, A. M. (2000). Introduction to chaos-based communications and signal processing. *Aerospace Conference Proceedings, 2000 IEEE*, 1, 279–299.

Soujeri, E., Kaddoum, G. & Herceg, M. (2018). Design of an initial condition-index chaos shift keying modulation. *Electronics Letters*, 54(7), 447–449.

Tan, Y., Xu, W., Huang, T. & Wang, L. (2018). A multilevel code shifted differential chaos shift keying scheme with code index modulation. *IEEE Trans. on Circuits and Sys. II: Exp. Briefs*, 65(11), 1743–1747.

Tse, C. & Lau, F. (2003). Chaos-based digital communication systems. *Operating Principles, Analysis Methods and Performance Evaluation (Springer Verlag, Berlin, 2004)*.

Turin, G. (1960). An introduction to matched filters. *IRE Transactions on Information Theory*, 6(3), 311-329. doi: 10.1109/TIT.1960.1057571.

Wang, C., Hao, L., Wang, B., Zhang, J. & Lei, Y. (2019). Performance Analysis for Nonlinear MU-OFDM-DCSK Communication Systems. *2019 IEEE 10th Annual Ubiquitous Computing, Electronics Mobile Communication Conference (UEMCON)*, pp. 1010-1014. doi: 10.1109/UEMCON47517.2019.8993039.

Wu, M., Lin, X. & Kam, P. Y. (2011, May). New Exponential Lower Bounds on the Gaussian Q-Function via Jensen's Inequality. *Vehicular Technology Conference (VTC Spring), 2011 IEEE 73rd*, pp. 1-5. doi: 10.1109/VETECS.2011.5956392.

Wu, M., Lu, T.-J., Ling, F.-Y., Sun, J. & Du, H.-Y. (2010). Research on the architecture of Internet of things. *Advanced Computer Theory and Engineering (ICACTE), 2010 3rd International Conference on*, 5, V5–484.

Xia, Y., Tse, C. K. & Lau, F. C. M. (2004). Performance of differential chaos-shift-keying digital communication systems over a multipath fading channel with delay spread. *IEEE Trans. Circuits Syst. II, Exp. Briefs*, 51(12), 680-684. doi: 10.1109/TCSII.2004.838329.

Xu, W. & Wang, L. (2016). CIM-DCSK: A Differential Chaos Shift Keying scheme with code-index modulation. *2016 16th Int. Symposium on Commun. and Inform. Technol. (ISCIT)*, pp. 100-104. doi: 10.1109/ISCIT.2016.7751600.

Xu, W., Huang, T. & Wang, L. (2017). Code-Shifted Differential Chaos Shift Keying With Code Index Modulation for High Data Rate Transmission. *IEEE Trans. Commun.*, 65(10), 4285-4294. doi: 10.1109/TCOMM.2017.2725261.

Yang, H., Tang, W. K. S., Chen, G. & Jiang, G. P. (2016). System Design and Performance Analysis of Orthogonal Multi-Level Differential Chaos Shift Keying Modulation Scheme. *IEEE Trans. Circuits Syst. I, Reg. Papers*, 63(1), 146-156. doi: 10.1109/TCSI.2015.2510622.

Yatsukova, K., Ovsyannikova, A., Makarov, S. & Cu, N. D. (2022). BER Performance Improvement for M-ary FTN Signals due to Reduction of Analysis Interval of Decision Feedback Detection Algorithm. *2022 International Conference on Electrical Engineering and Photonics (EExPolytech)*, pp. 183-186. doi: 10.1109/EExPolytech56308.2022.9950962.

Yinbiao, S., Lee, K., Lanctot, P., Jianbin, F., Hao, H., Chow, B. & Desbenoit, J.-P. (2014). Internet of things: wireless sensor networks. *White Paper, International Electrotechnical Commission, http://www. iec. ch*, 11.

Zavjalov, S., Prokhorov, V. & Chudnov, A. (2022). Comparison of Spectral Efficiency of FTN -Signaling with Coherent and Noncoherent Detection. *2022 International Conference on Electrical Engineering and Photonics (EExPolytech)*, pp. 166-169. doi: 10.1109/EExPolytech56308.2022.9950789.

Zavjalov, S. V., Ovsyannikova, A. S., Lavrenyuk, I. I. & Volvenko, S. V. (2019). The efficiency of detection algorithms for optimal FTN signals. In *Internet of Things, Smart Spaces, and Next Generation Networks and Systems* (pp. 670–680). Springer.

Zhai, X., Song, G., Xiao, L., Liu, G., Ishikawa, N. & Jiang, T. (2022). Error Probability Analysis for Time-Varying Chaos Unitary Matrix-Based Differential MIMO System. *IEEE Wireless Communications Letters*, 11(7), 1399-1403. doi: 10.1109/LWC.2022.3170873.

Zhang, G., Cui, N. & Zhang, T. (2015). Novel chaos secure communication system based on Walsh code. *Journal of Electrical and Computer Engineering*, 2015.

Zhang, G., Zhao, C. & Zhang, T. (2020a). Performance analysis of MISO-MU-OHE-DCSK system over Rayleigh fading channels. *AEU - Int. J. of Electron. and Commun.*, 115, 153048. doi: https://doi.org/10.1016/j.aeue.2019.153048.

Zhang, H., Zhang, L., Jiang, Y. & Wu, Z. (2022). Reliable and Secure Deep Learning-Based OFDM-DCSK Transceiver Design Without Delivery of Reference Chaotic Sequences. *IEEE Transactions on Vehicular Technology*, 71(8), 8059-8074. doi: 10.1109/TVT.2022.3175968.

Zhang, L., Zhang, H., Jiang, Y. & Wu, Z. (2020b). Intelligent and Reliable Deep Learning LSTM Neural Networks-Based OFDM-DCSK Demodulation Design. *IEEE Transactions on Vehicular Technology*, 69(12), 16163-16167. doi: 10.1109/TVT.2020.3022043.

Zhang, X., Shi, Y. & Chen, G. (2013). Some properties of coupled-expanding maps in compact sets. *Proceedings of the American Mathematical Society*, 141(2), 585–595.

Zhou, J., Qiao, Y., Yang, Z., Cheng, Q., Wang, Q., Guo, M. & Tang, X. (2017). Capacity limit for faster-than-Nyquist non-orthogonal frequency-division multiplexing signaling. *Scientific reports*, 7(1), 1–11.

Zhou, Z., Wang, J. & Ye, Y. (2010). Exact BER analysis of differential chaos shift keying communication system in fading channels. *Wireless personal commun.*, 53(2), 299–310.